UCRL-51862

MULTIPHONON RELAXATION AND EXCITATION TRANSFER IN RARE-EARTH DOPED GLASSES

Clyde B. Layne
(Ph. D. Thesis)

July 31, 1975

Prepared for U.S. Energy Research & Development Administration under contract No. W-7405-Eng-48

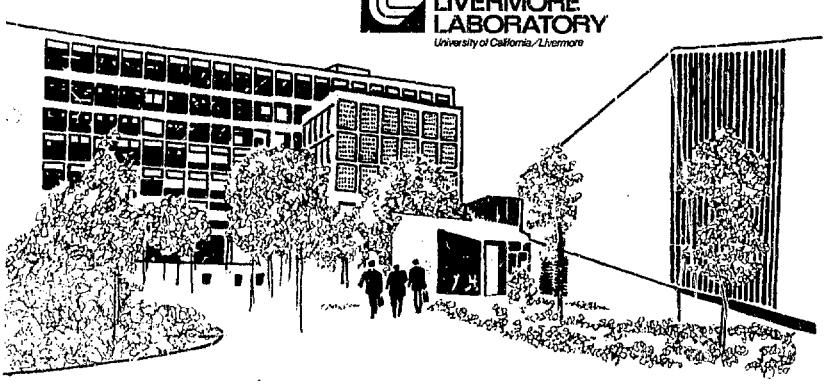

Printed in the United States of America
Available from
National Technical Information Service
U.S. Department of Commerce
5285 Port Royal Road
Springfield, Virginia 22151
Price: Printed Copy $___*; Microfiche $2.25

*Pages	NTIS Selling Price
1-50	$4.00
51-150	$5.45
151-325	$7.60
326-500	$10.60
501-1000	$13.60

LAWRENCE LIVERMORE LABORATORY
University of California / Livermore, California / 94550

UCRL-51862

MULTIPHONON RELAXATION AND EXCITATION TRANSFER IN RARE-EARTH DOPED GLASSES

Clyde B. Layne

(Ph. D. Thesis)

MS. date: July 31, 1975

· Table of Contents ·

Chapter I: Introduction

Ions of the rare-earth elements retain their discrete electronic energy levels when incorporated into crystalline or glassy host materials. This characteristic accounts for the paramagnetic behavior of rare earths and also makes them useful for solid state lasers. The properties of rare-earth ions in crystals are well understood after many years of investigation using solid state physics techniques which exploit the symmetry of the lattice.[1] Today glass is the most important solid state laser material, and many of the details of rare-earth ions in amorphous materials are not well known. Nonradiative relaxation of excited states of rare-earth ions in glasses and the transfer of excitation between these ions have been investigated in this work. The results of this study bring the knowledge of rare-earth ions in glass environments closer to the level of understanding of crystals.

The Nd doped glass laser was developed in 1961 by E. Snitzer,[2] and has since become the most common solid state laser. Efforts are now underway to use the output from a large Nd:glass laser to initiate thermonuclear reactions in small fuel pellets.[3] Lasers for this purpose must produce thousands of joules of 1.06-μm radiation in less than a nanosecond. Given the low efficiency (~0.1%) with which Nd:glass converts input energy (in the form of electricity to drive flashlamps) into laser energy output, any improvements in Nd:glass laser performance can greatly reduce the cost and difficulty of laser fusion experiments. A better understanding of the physics of rare-earth ions in glass matrices will provide guidance for possible improvements in the laser host materials.

The distinguishing feature of glasses is the lack of ordered arrangement of the component molecules. This disorder rules out the straightforward application of the concepts and theories developed for rare-earth ions in crystals. In the course of this work, a conceptual context was developed with which to approach the problems of relaxation and energy transfer. Some of the ideas of solid state physics were abandoned and others were modified to fit the glass environment. The concept of a phonon in a disordered glass lattice led to a reformulation of the theory of multiphonon relaxation developed for crystals. Energy transfer measurements were interpreted with the aid of theories derived for crystals, taking into consideration the distribution of rare-earth sites in the glass.

This paper is divided into two parts, the first dealing with multiphonon relaxation. The theory of multiphonon decay of rare-earth ions in glasses is derived with more attention to details than the original formulations of this theory for crystals. The structure of glasses is reviewed in order to understand the coupling of the ion to the glass lattice, and a molecular model of high energy vibrations in glasses is found to be appropriate for multiphonon rate calculations. The details of the ion-lattice coupling strength are not known, but the form of the perturbation calculation gives the dependence of multiphonon rates on phonon energies, on energy gap between levels, and on glass temperature. One section of the first chapter is devoted to a discussion of multiphonon decay to a single vibrational mode. Although this process is shown to be unimportant in glasses, the unique properties of relaxation to a single highly excited vibration may be

observable in other rare-earth systems. The consequences of only one vibration coupled to the rare-earth ion are evident from the detailed derivation of the theory presented here, whereas other formulations of multiphonon theory do not predict this behavior.

The short pulse laser excitation and fast fluorescence measurements necessary to determine multiphonon rates are described, along with an explanation of the particular rare earth decay schemes used in these experiments. Some of the rates were measured directly from fluorescence decays, while others were indirectly determined from the rise and fall of fluorescence from multilevel schemes. Special experimental requirements were necessary in order to extend nonradiative rate measurements to faster rates than have been determined previously. Multiphonon rates are presented for six electronic states in a series of five simple oxide glasses and one complex commercial laser glass. The dependence of the nonradiative rates on energy gap agrees with the predicted behavior. The Raman spectra of these glasses are also presented and shown to correlate with the multiphonon rate measurements. Finally, the temperature dependence of one nonradiative decay rate in all five glasses, combined with the knowledge of the high energy phonons from Raman spectra, gives good agreement with the predictions of the multiphonon theory for glasses. Appendix C is an application of the multiphonon rate measurements to determine conversion efficiencies in a commercially available laser glass.

The second part of this work is concerned with energy transfer mechanisms and rates in Nd:glass. The results of the theory of energy transfer by multipolar coupling are reviewed and specialized to the

Nd ion. A fluorescence decay measurement apparatus is described which recorded Nd decay curves with sufficient accuracy to allow quantitative evaluation of the nonexponential character of the fluorescence function. The long term decay rate exhibits diffusion-limited behavior in agreement with predictions of energy transfer theory. Computer fitting of the observed fluorescence signals to predicted fluorescence decay functions results in good agreement with a model which includes quenching of excitation to unexcited Nd ions and migration of the excitation through the Nd system. These results were applied to a Nd:glass amplifier to determine the effect of nonexponential decay on the peak gain in the amplifier. Finally, the transfer of energy from Ce ions to Nd ions was measured in an effort to sensitize Nd to short wavelength pump light. The last chapter reviews and discusses the results of all these experiments and their importance to understanding rare earths in glass environments.

Chapter II: Multiphonon Relaxation

A. Introduction

Early observations of fluorescence from rare-earth ions in crystals showed that not all electronic levels radiated, in fact only those with a large energy gap to the next lower level exhibited fluorescence.[4] Dieke and others attributed this lack of radiative decay to a fast non-radiative decay by phonon emission. Since the highest energy phonons in these crystals are only a few hundred cm^{-1}, and the energy gaps across which the relaxation occurs are up to 1000 cm^{-1}, the nonradiative process must involve many phonons. Weber,[5] Moos,[6] and others measured these multiphonon decay rates for rare earths in a variety of crystals and for a variety of electronic states. The multiphonon rate was observed to be a decreasing function of energy gap to the next lower electronic state. Kiel[7] attempted to calculate the transition probability for a multiphonon process, and found that the rate for a p phonon process was much less than the rate for a p-1 phonon process:

$$\frac{W_p}{W_{p-1}} \ll 1$$

Riseberg and Moos[8] extended this approximation to show that the multiphonon transition probability is an exponential function of the energy gap across which the decay occurs, independent of which electronic state or which rare-earth ion is involved. The theory outlined in this section follows the general approach of Kiel, although it will be applied to glasses. More of the details of the calculation will be presented than have been published previously, not because any quantitative results are possible, but because the physics of the process becomes apparent in this way. The approximations that are necessary in order to reach a useful result will be evident. Two basic predictions of the theory that are the goals of this derivation are 1) the exponential dependence of the multi-

phonon rate on energy gap, and 2) the temperature dependence of the multiphonon rate which permits identification of the particular phonons involved. Both aspects of the theory have been verified experimentally for rare-earth ions in glasses.

Several other approaches to the theory of multiphonon relaxation have been pursued since Kiel's work. Miyakawa and Dexter[9] use the method of generating functions to calculate multiphonon relaxation, assuming weak coupling of the rare-earth ion to the lattice. Their result predicts both the exponential dependence on energy gap and the temperature dependence that Kiel found, but the formalism of the generating function approach obscures some of the physical aspects of the problem that are of interest. Fischer[10] considered the nonradiative transition probability for strongly coupled systems where the configuration coordinate approach applies. He found an approximately exponential dependence on energy gap, but his model applies to strong coupling only. Fong and coworkers[11] evaluated the multiphonon transition rate for rare-earth ions using a time correlation calculation, arriving at an approximately exponential dependence of the rate on energy gap and a slightly different temperature dependence than Kiel. Struck and Fonger[12] have used the configuration coordinate approach to determine multiphonon emission in a way that can be applied to the weakly coupled rare-earth ions, with results similar to Kiel's. Each of these approaches fails to calculate the actual rate which always involves matrix elements that are not known. For this reason, the simplest approach with the least mathematics is as good as any, and in fact better, since the physical principles are more apparent.

One aspect of the present work is not treated by any of the authors above, and it results from simplifying the model to one harmonic oscillator weakly coupled to a rare-earth ion. The consequences of stimulated

multiphonon emission predicted by this model may be observable in simple systems such as a rare-earth vapor. The extension of multiphonon relaxation theory to glass matrices is also more straightforward using the general approach of Kiel.

Perturbation theory will be employed to calculate the transition probability between electronic levels of rare-earth ions, where the perturbing potential is due to lattice vibrations. The interaction of one phonon will be considered first, the simplest case, but one that includes the basic physics necessary for further calculations. Extension of the model to two, three, and an arbitrary number of phonons involves higher order perturbation calculations where the major additional complication is in considering all possible intermediate states. The difficulty of quantitative calculations will be apparent very early, and approximations will be made and justified in order to simplify the mathematics.

B. Theory

The rare-earth or lanthanide elements have in common a xenon electron core plus N 4f electrons and two 6s electrons. N varies from zero (La) to the closed shell at fourteen (Lu). In chemical compounds, the rare earths are usually trivalent. For the purposes of this work the ions with from one (Ce^{3+}) to thirteen (Yb^{3+}) of the 4f electrons constitute the trivalent rare earths. The 4f orbits lie closer to the nucleus than the 5s, 5p, and 6s radial distributions. The shielding provided by the 5s and 5p orbitals makes the 4f electronic states relatively insensitive to the crystal field, so the effect of the surrounding charges may be treated as a perturbation on the free ion states. L-S coupling is generally a good approximation for these states, and they are characterized by L, S, J, and m_j. The perturbing potential of the static crystal field can be expanded in spherical harmonics in order to

calculate the energy shifts and splittings, and to compute the perturbed wave functions.[1] Group theory reduces the number of terms in the crystal field expansion for a particular crystal symmetry. For the purposes of this derivation, the exact wave functions are not necessary. The electronic part of the total wave function will be identified by S, L, and J, and the Stark splitting will not be explicitly considered.

$$|\psi_{elec}\rangle = |4f^N, S, L, J, \cdots\rangle \tag{1}$$

The wave function for the perturbation calculation is the product of the electronic wave function and the vibrational wave function of the lattice. The vibrational wave function is a product of the individual harmonic oscillator wave functions representing the lattice modes, which are characterized by their phonon occupation numbers.

$$|\chi\rangle = |\psi_{elec}\rangle \prod_{\omega} |n_{\omega}\rangle \tag{2}$$

The lattice part of the wave function is a product over all the vibrational modes that can couple to the ion. The application of multiphonon theory to glasses requires consideration of the concept of a phonon in a glass. According to present theories of glass structure, oxide glasses of the type considered here are formed from networks of glass forming ions such as Si, B, P, Ge, or Te that are strongly bonded to oxygen ions.[13] Distinct structural units such as SiO_4 tetrahedra exist in the glasses, but the orientation of these units lacks any long range symmetry. Network modifiers such as alkali or alkaline earth ions break up the Si-O-Si-O-Si three-dimensional network, introducing non-bridging oxygens that do not link one Si to another. The vibrations of the network modifiers are between two and four times lower in frequency than the vibrations of the network formers.[14] Since multiphonon relaxation involves the high energy vibrations in glasses, the network modifiers

will not be considered here.

The vibrational motion of the network of simple glasses has been calculated by Bell and coworkers[15] and by Su and coworkers.[16] Their technique was to develop a model for the network of ionic masses with appropriate bond strengths and solve for the modes of vibration. These calculations agree well with observed Raman and infrared spectra. The high energy vibrations of the glass network involve localized vibrations of the glass forming units (SiO_4 for example), with frequencies near the Si-O bond stretching vibration. The localized nature of the high energy vibrations makes the exact details of the glass network unimportant to the present case of multiphonon relaxation.

Due to the lack of long range order, the wave vector normally associated with the lattice modes is not simply determined in the glass, so the vibrations will be enumerated by frequency only. The model used here for a glass lattice is that of a large molecule including the rare-earth ion and the surrounding glass-forming units, out to nearest or next-nearest neighbors. For instance, in a silicate glass the rare-earth ion may have six to eight SiO_4 tetrahedra around it. The normal modes of vibration of a tetrahedron will be weakly coupled through the field of the oxygen ions to the rare-earth ion. There are many modes of vibration of this model "molecule," but only the highest energy ones will be important to multiphonon relaxation. While the coupling of the modes and the details of the low frequency modes are uncertain, the high energy vibrations may be identified through Raman or infrared studies, and their importance to multiphonon relaxation is verified by temperature dependence measurements.

The Hamiltonian for the system consists of two parts. H_0 includes the free ion Hamiltonian and the effects of the time averaged crystal field which give the observed energy levels and splittings in the glass.

V is the perturbation caused by the vibrations of the lattice.

$$H = H_0 + V \tag{3}$$

It is convenient to split V into two parts, one which operates on the electronic part of the wave function, and one which operates on the lattice wave function. This is done formally by writing

$$V = \sum_{\omega} \frac{\partial V}{\partial Q_{\omega}} Q_{\omega} \tag{4}$$

where the sum over ω indicates a sum over all the vibrational modes that couple to the ion. Q_{ω} is the normal coordinate or the amplitude of the disturbance of the mode ω. This expression for V is just the first term in a Taylor series expansion of the potential about the equilibrium position of the lattice. The amplitude Q can be referred to several different coordinate systems.

Although the calculations to be described next do not apply to glasses, the physics of the situation will be illustrated for the crystalline case. Even in crystals the problem is too complex for quantitative results.

In a crystal, the expansion of the potential can be simplified by using coordinates that have the symmetry of the ion site. Q_{ω} then refers to one of the normal modes of vibration of the unit cell centered around the ion. Evaluation of the derivatives of the potential with respect to Q_{ω} involves expressing the crystal field in a representation with the same symmetry as the Q coordinate system. Kiel[7] has done a part of this calculation for $LaCl_3$ making use of the symmetry of the rare earth site (a La site). In the calculation of the multiphonon rate below, matrix elements of $\frac{\partial V}{\partial Q_{\omega}}$ must be determined. This can be done, in

principle, if the magnitude of the crystal field and its derivatives can be calculated.

The Q coordinates that operate on the harmonic oscillator states can be expressed in terms of the raising and lowering operators a^+ and a. In general Q will be a linear combination of the lattice modes.

$$Q_\omega = \sum_K b_{\omega K}(a_K^+ + a_K) \tag{5}$$

Van Vleck[17] has done this calculation that relates the point group symmetry of the ion site to the space group symmetry of the lattice for a cubic lattice.

Glasses lack both the point group symmetry of the rare-earth site and the space group symmetry of the periodic crystal lattice. Consistent with the model of a glass described above, the Q coordinate appropriate to a glass is the amplitude of vibration of one of the coupled harmonic oscillators around the rare-earth ion. This amplitude can then be expressed in terms of a^+ and a directly, where the raising and lowering operators are just those of the oscillator at frequency ω.

$$Q_\omega = b_\omega(a_\omega^+ + a_\omega) \tag{6}$$

This choice of coordinates requires no sum over lattice modes to express Q_ω. The question of the appropriate normal mode coordinates for the lattice vibrations will be discussed at length below, after the significance of the choice of coordinates is established. Whatever the choice of Q_ω coordinates, the dependence of the potential on Q_ω, denoted by $\frac{\partial V}{\partial Q_\omega}$, is the electronic part of the perturbation operator, and its matrix element appears in the expressions for transition rates.

To simplify the notation, $\frac{\partial V}{\partial Q_\omega}$ will be V'_ω in the rest of the treatment.

$$V = \sum_\omega V'_\omega Q_\omega = \sum_\omega V'_\omega b_\omega (a^+_\omega + a_\omega) \tag{7}$$

The coefficients b_ω are[18]

$$b_\omega = \left(\frac{\hbar}{2M\omega}\right)^{1/2} \tag{8}$$

where M is normally the mass of the crystal, but is a mass-related coefficient dependent on the choice of Q_ω coordinates. The operators a^+ and a create and annihilate phonons.

$$a^+_\omega |n_\omega> = \sqrt{n_\omega + 1}\, |n_\omega + 1> \tag{9}$$

$$a_\omega |n_\omega> = \sqrt{n_\omega}\, |n_\omega - 1> \tag{10}$$

Using these definitions, the nonzero matrix elements of Q_ω are

$$<n_\omega + 1|Q_\omega|n_\omega> = \sqrt{\frac{\hbar}{2M\omega}}\,(n_\omega + 1) \tag{11}$$

$$<n_\omega - 1|Q_\omega|n_\omega> = \sqrt{\frac{\hbar}{2M\omega}}\, n_\omega \tag{12}$$

Considering a one phonon transition between electronic states a and b, the rate is given by the "golden rule" of time dependent perturbation theory:[19]

$$W = \frac{2\pi}{\hbar} |<\chi_b|V|\chi_a>|^2 \rho(E) \tag{13}$$

$\rho(E)$ is the density of final states. Rather than a density of states, a delta function to conserve energy and a sum over states will be used here. The initial state χ_a has the electronic state ψ_a and the lattice state with the arbitrary initial phonon occupation numbers

$$|\chi_a\rangle = |\psi_a\rangle \prod_{\omega} |n_{\omega'}\rangle \tag{14}$$

In the final state the electronic state has changed to $|\psi_b\rangle$ and one of the phonon states has increased by one.

$$|\chi_b\rangle = |\psi_b\rangle |n_{\omega} + 1\rangle \prod_{\omega' \neq \omega} |n_{\omega'}\rangle \tag{15}$$

The matrix element to be used in (13) is

$$\langle\psi_b|V'_{\omega}|\psi_a\rangle\langle n_{\omega} + 1|\Pi\langle n_{\omega'}|Q_{\omega}|n_{\omega}\rangle\Pi|n_{\omega'}\rangle \tag{16}$$

where ω must be one of the vibrations which conserve energy, $E_a - E_b = \hbar\omega$. Evaluating the matrix element for emission of a phonon from (11) gives

$$\langle\psi_b|V'_{\omega}|\psi_a\rangle\sqrt{\frac{\hbar}{2M\omega}(n_{\omega} + 1)} \tag{17}$$

The total rate will be the sum of the rates for each individual mode:

$$W = \frac{2\pi}{\hbar}\sum_{\omega}{}'|\langle\psi_b|V'_{\omega}|\psi_a\rangle|^2 \frac{\hbar}{2M\omega}(n_{\omega} + 1)\delta(E_a - E_b - \hbar\omega) \tag{18}$$

The matrix elements of V'_{ω} will vary for different initial and final states and for different glass compositions. They cannot be calculated due to the lack of information about the vibrational modes

in the glass and their coupling to rare-earth electronic states.

When the initial and final electronic states are separated in energy by an amount greater than the highest phonon energy in the glass, the perturbation calculation must be done in higher order to allow emission of two or more phonons. For a p phonon process, there are contributions from two terms in the Taylor series expansion of the potential. The first term (7) in the expansion evaluated in a p-order perturbation calculation will be considered next. However, the p^{th} term in the expansion taken in first order perturbation also results in emission of p phonons.

An important aspect of the present theory is the assumption that only the lowest order process that can conserve energy need be considered. This assumption is justified to the extent that the perturbing potential is small, otherwise the perturbation approach to the calculation is invalid. The expressions for multiphonon rates contain matrix elements of the perturbing potential in powers of p, the order of the process. Since these matrix elements are small, their higher powers will be even smaller. This approximation is further supported by the general tendency for the density of phonon states to increase with increasing energy.

Higher order perturbation calculations for the transition probability are given by[20]

$$W = \frac{2\pi}{\hbar} \left| \sum_{m_1 \cdots m_{p-1}} \frac{\langle f|V|m_1\rangle\langle m_1|V|m_2\rangle \cdots \langle m_{p-1}|V|i\rangle}{(E_i - E_{m_1})(E_i - E_{m_2}) \cdots (E_i - E_{m_{p-1}})} \right|^2 \rho(E) \qquad (19)$$

where i and f denote initial and final states and m_1 through m_{p-1} are intermediate states for the p^{th} order process. The sum is over all possible intermediate states m_i. Energy need not be conserved for

intermediate states, only for the initial and final states. The energy denominators, however, decrease the effect of intermediate states with energies very different from the initial state.

To illustrate the enumeration of intermediate states, the two phonon process will be considered first. If only one lattice oscillator is coupled to the ion, with frequency ω such that $E_a - E_b = 2\hbar\omega$, and both the initial and final electronic states are singlet, there are only two terms in the sum (19) over intermediate states.

$$W = \frac{2\pi}{\hbar}\left|\frac{\langle\psi_b|\langle n_\omega + 2|V|\psi_a\rangle|n_\omega + 1\rangle\langle\psi_a|\langle n_\omega + 1|V|\psi_a\rangle|n_\omega\rangle}{E_a - (E_a + \hbar\omega)} + \frac{\langle\psi_b|\langle n_\omega + 2|V|\psi_b\rangle|n_\omega + 1\rangle\langle\psi_b|\langle n_\omega + 1|V|\psi_a\rangle|n_\omega\rangle}{E_a - (E_b + \hbar\omega)}\right|^2 \rho(E) \quad (20)$$

The first term corresponds to an intermediate state with electronic state ψ_a and one phonon emitted into the mode ω. The second term corresponds to an intermediate state with electronic state ψ_b and one phonon emitted. There are two steps required, each with the emission of one phonon, but the electronic state changes only once - either during the first step or the second.

When the phonon creation operator acts twice on the same mode as in this case, the first operation gives $\sqrt{n+1}$ and the second gives $\sqrt{n+1+1}$. In order to conserve energy with two phonons of equal energy, $E_a - E_b$ must be $2\hbar\omega$. Then the rate is

$$W = \frac{2}{\hbar}\left(\frac{\hbar}{2M\omega}\right)^2 (n+1)(n+2)\left|\frac{\langle\psi_b|V'_\omega|\psi_a\rangle\langle\psi_a|V'_\omega|\psi_a\rangle}{-\hbar\omega} + \frac{\langle\psi_b|V'_\omega|\psi_b\rangle\langle\psi_b|V'_\omega|\psi_a\rangle}{\hbar\omega}\right|^2 \delta[E_a - (E_b + 2\hbar\omega)] \quad (21)$$

The rate given by (21) is an approximation because it includes the effects of only one coupled oscillator. In fact the sum which is squared in (21) should include all modes and combinations of modes in pairs - such that $\hbar\omega_i + \hbar\omega_j = E_a - E_b$. Each of these terms will also involve a different matrix element of V'_ω. The matrix elements of Q_{ω_i} and Q_{ω_j} will give $(n_i+1)(n_j+1)$ rather than $(n+1)(n+2)$.

The situation becomes more complicated for three or more phonons. Again assuming singlet initial and final states, there are four possible sequences of electronic states for a three phonon transition, with each step involving emission of one phonon:

$$
\begin{array}{llll}
|a\rangle \xrightarrow{\hbar\omega_1} & |a\rangle \xrightarrow{\hbar\omega_2} & |a\rangle \xrightarrow{\hbar\omega_3} & |b\rangle \\
|a\rangle \longrightarrow & |a\rangle \longrightarrow & |b\rangle \longrightarrow & |b\rangle \\
|a\rangle \longrightarrow & |b\rangle \longrightarrow & |b\rangle \longrightarrow & |b\rangle \\
|a\rangle \longrightarrow & |b\rangle \longrightarrow & |a\rangle \longrightarrow & |b\rangle
\end{array}
\qquad (22)
$$

In the general case of emission of p phonons, there are 2^{p-1} such sequences of electronic states - two possibilities for the first virtual transition, times 2 for the second, ...times 2 for the $p\text{-}1^{th}$, times one for the final step.

The three phonon transition also indicates the nature of the matrix elements of Q_ω for the general case. With m modes of vibration, all of approximately equal energy $\hbar\omega = (E_a - E_b)/3$, the number of intermediate states for each electronic sequence can be counted. There are m possibilities for the emission of all three phonons into the

same vibrational mode, resulting in m terms of the type $(n_\omega + 1)(n_\omega + 2)(n_\omega + 3)$. There are a total of m^3 (m^p in general) combinations of phonons emitted in the three steps, of which m are accounted for as those in which all phonons go into one mode. Of the remaining combinations, $3m(m - 1)$ have two phonons emitted into one mode and the third phonon in another mode, resulting in terms like $(n_i + 1)(n_i + 2)(n_j + 1)$. These are counted as follows: there are m choices for the first two phonons and m - 1 for the third, or there are m places for the first, m - 1 places for the second, and two places for the third--leading to $m(m - 1) + 2m(m - 1)$. The remaining $m^3 - m - 3m(m - 1)$ choices have all three phonons in different modes of vibration. Similar counting may be done for the p phonon process.

To summarize these results in the three phonon case, for each of the four electronic sequences in (22) there are m terms in the sum with $(n_\omega + 1)(n_\omega + 2)(n_\omega + 3)$, $3m(m - 1)$ terms like $(n_{\omega i} + 1)(n_{\omega i} + 2)(n_{\omega j} + 1)$, and the remainder of the form $(n_{\omega i} + 1)(n_{\omega j} + 1)(n_{\omega k} + 1)$, for a total of $4m^3$ terms. Each of the terms will have an electronic matrix element product of the form

$$\langle \psi_b | V'_{\omega_1} | \psi_j \rangle \langle \psi_j | V'_{\omega_2} | \psi_k \rangle \langle \psi_k | V'_{\omega_3} | \psi_a \rangle \tag{23}$$

where j and k can be a or b.

The number of modes m that are important to the multiphonon relaxation may not be large for a glass. It is probable that only the nearest neighbor glass forming units couple strongly to the ion, so that m may by 6 or 8 times the number of high energy modes of the glass forming unit itself. For instance for a silicate, it may be

that only one high frequency normal mode of each tetrahedron couples efficiently to the ion. Then m would be of the order of ten. If the range of the coupling is longer than assumed here, then m may be larger, but numbers from ten to one hundred seem reasonable. Phonon transitions involving $(n_{\omega i}+1)(n_{\omega j}+1)(n_{\omega k}+1)$ will dominate the relaxation for values of m in this range.

The electronic states a and b are split by the static crystal field into at most J + 1 Stark levels. The energy splitting of the Stark manifold are always much smaller than the large energy gaps to which multiphonon theory applies, so these energy differences may be ignored in the energy denominators for the perturbation calculations. The matrix element of V'_ω summed over the Stark levels for any particular step in the sequence of electronic intermediate states is just equal to the matrix element of V'_ω between the original states a and b without considering the crystal field splitting. Thus the Stark levels of a and b need not be included explicitly in counting the intermediate states. The matrix elements are calculated using the unsplit states, which in general include several free ion states mixed in by the crystal field.

The multiphonon transition rate for a p phonon process involving m oscillators of frequency ω is given by

$$W_p = \frac{2\pi}{\hbar}\left|\left(\frac{\hbar}{2M\omega}\right)^{p/2}\sum_{\substack{\omega_i=\omega_1\cdots\omega_m\\ \omega_j=\omega_1\cdots\omega_m\\ \vdots\\ \omega_p=\omega_1\cdots\omega_m}}(n_{\omega_i}+1)^{p/2}\right.$$

$$\left.\times\frac{\langle\psi_b|V'_{\omega_i}|\psi_{a,b}\rangle\langle\psi_{a,b}|V'_{\omega_j}|\psi_{a,b}\rangle\cdots\langle\psi_{a,b}|V'_{\omega_p}|\psi_a\rangle}{(E_a-E_{a,b}-\hbar\omega)(E_a-E_{a,b}-2\hbar\omega)\cdots(E_a-E_{a,b}-(p-1)\hbar\omega)}\right|^2 \quad (24)$$

where the $(n+1)(n+2)\ldots$ terms have been omitted. The subscript a, b on the intermediate states indicates that the 2^{p-1} possible electronic sequences analogous to (22) must be included in the sum. Since the individual terms in the sum are not squared separately, as in the one phonon case, there will be interferences when the sum is squared to give the transition probability. Nevertheless the simplifying assumption will be made that an average matrix element can be defined:

$$W_p = \frac{2\pi}{\hbar}\left(\frac{\hbar}{2M\omega}\right)^p (n_\omega+1)^p \; 2^{2(p-1)} m^{2p} \; \frac{|\langle a|V'_p|b\rangle|^{2p}}{(\hbar\omega)^{2(p-1)}} \qquad (25)$$

The average matrix element $|\langle a|V'_p|b\rangle|$ is essentially a definition obtained by equating (24) and (25), valid for the p phonon process. The sum over electronic sequences when squared gives $2^{2(p-1)}$ terms, and for each of these there are m^{2p} terms from the square of the sum over coupled phonon modes. This expression gives the temperature dependence for a multiphonon transition coupled to m phonon modes, where m is large, through the Bose-Einstein distribution for n(T). As discussed previously, a small number of coupled modes give a contribution with $(n+1)(n+2)\ldots$ and a slower increase with increasing temperature; this will be discussed in the next section. The temperature dependence was one of the two goals of the present derivation.

The higher order derivatives of the potential also make a contribution to the multiphonon rate, as mentioned above. The full expression for the potential in terms of the Q coordinates is

$$V = V_0 + \sum_{i=1}^{m} \frac{\partial V}{\partial Q_i} Q_i + \sum_{i,j=1}^{m} \frac{\partial^2 V}{\partial Q_i \partial Q_j} + \cdots \sum_{i,j,\ldots p}^{m} \frac{\partial^p V}{\partial Q_i \partial Q_j \cdots \partial Q_p} Q_i Q_j \cdots Q_p \qquad (26)$$

where each sum is over the m modes that couple to the ion. The matrix elements of $\frac{\partial^p V}{\partial Q_i \partial Q_j \cdots}$ are not calculable without specific details of the crystal field at the ion site, and even with these details the calculation would be very difficult. The phonon matrix elements however are easily evaluated.

$$\langle n_1, n_2, \cdots n_i + 1 \cdots n_j + 1 \cdots n_m | Q_i Q_j \cdots Q_p | n_1, n_2 \cdots n_i \cdots n_j \cdots n_m \rangle$$

$$= \left(\frac{\hbar}{2M\omega}\right)^{p/2} \sqrt{n_i + 1}\sqrt{n_j + 1} \cdots \sqrt{n_p + 1} \qquad (27)$$

This is exactly the same result as the previous calculation of phonon matrix elements, and when summed over the m coupled modes gives the same factor in the rate. Again there are m terms of the $(n + 1)(n + 2)(n + 3)\ldots(n + p)$ form and m^p total terms. There is not an energy denominator in the rate due to higher order derivatives of the potential, since the perturbation calculation is first order.

Only the first term in the potential expansion taken in p^{th} order perturbation will be considered below. Given the similarity of the phonon terms in the two cases, the physical process is fully represented by the first order term.

The dependence of the multiphonon rate on the energy gap to be bridged results from comparing the rate for a p phonon process with that for a p-1 phonon decay. With the same glass lattice, $\hbar\omega$ and m will be the same for W_p and W_{p-1}; however, the average matrix element $|\langle a|V_p'|b\rangle|$ is not necessarily the same for a p order process as for a p-1 order process, particularly if different initial and final electronic

states are involved. For now, the average matrix element will be assumed to be the same for a p and a p-1 order process. The effect on the final result of the error in this assumption will be discussed below. The ratio of W_p to W_{p-1} is

$$\frac{W_p}{W_{p-1}} = (\hbar/2M\omega)(n_\omega + 1)\ 4m^2\ \frac{|\langle a|V'|b\rangle|^2}{(\hbar\omega)^2} \qquad (28)$$

The dimensions of the average matrix element are energy divided by normal mode displacement, while the quantity $(\hbar/2M\omega)(n_\omega + 1)$ gives the square of the normal mode displacement according to Eq. 11. Thus the ratio of the two rates is physically the square of the energy change caused by the amplitude of the vibration ω divided by the energy of the vibration. The number of modes m and the mass M are related by the choice of normal mode coordinates so that the number of modes that couple is normalized out. This point will be treated in the next section.

If the perturbation V is small, as it must be for perturbation theory to apply, the ratio of W_p to W_{p-1} will be

$$\frac{W_p}{W_{p-1}} = \varepsilon << 1 \qquad (29)$$

This is the result that Kiel found which was extended by Riseberg and Moos [8] in the following manner:

$$\begin{aligned} W_p &= W_{p-1}\ \varepsilon \\ &= W_{p-2}\ \varepsilon^2 \\ &\ \ \vdots \\ &= W_o\ \varepsilon^p \end{aligned} \qquad (30)$$

This may be rewritten as

$$W_p = W_o e^{p \ln(\varepsilon)} \tag{31}$$

Since the number of phonons p is equal to the energy gap ΔE divided by the phonon energy $\hbar\omega$,

$$W_p = W_o \exp\left(\frac{\ln(\varepsilon)}{\hbar\omega} \Delta E\right) \tag{32}$$

This result expresses the exponential dependence of multiphonon relaxation rate on the energy gap across which the decay takes place. The worst approximation in the derivation of this formula is the assumption that the average matrix element $|\langle a|V'|b\rangle|$ is equal for different p and for different electronic states. It is clear that variations of ε should be expected; but ε enters the final result as $\ln(\varepsilon)$, which accounts for the insensitivity of the prediction to the exact nature of the ion-phonon coupling.

The validity of Eq. (32) for crystals has been demonstrated for rare-earth energy levels in many hosts. ε varies from host to host, but for a given host, Eq. (32)is valid to an accuracy of a factor of two or better. The high energy optical phonons also vary from host to host, and this is the primary cause of variations in the observed rates from crystal to crystal. The results of multiphonon decay measurements in glasses reported here confirm that this theory has predictive value in glasses as well as in crystals, in spite of the different concept of a phonon in the two media. In glasses the most important material effect is the maximum phonon energy as in crystals.

C. Relaxation to a Highly Excited Single Mode

As the number of vibrational modes coupled to the rare-earth ion becomes small, the importance of the $(n + 1)(n + 2)(n + 3)...$terms in the relaxation becomes important. The reason for considering the value of m, the number of modes, is that it may be possible to determine experimentally which are more important, the highly excited single mode transitions or the transitions that spread the phonon excitation over many modes of vibration. The temperature dependence of the multiphonon rate results from the Bose-Einstein distribution for n(T):

$$n_{\omega}(T) = \frac{1}{e^{\hbar\omega/kT} - 1} \tag{33}$$

Since $n_{\omega} + 1$ shows a much more rapid percentage increase with temperature than $n_{\omega} + 2$, the transitions to a single mode that is highly excited will contribute very little to the temperature dependence of the total process. However, since the total number of phonon combinations varies with m^p and the number of combinations involving a single highly excited mode varies with m, the number of coupled vibrations would have to be quite small to have an effect greater than the uncertainties in the interpretation and experimental errors in temperature dependent measurements. The origin of the $n_{\omega} + 1$ terms in the expression for the transition rate is Eq. (11) for the matrix elements of the phonon creation operator. The matrix elements depend on the vibrational wave functions for the glass lattice.

The wave functions that are appropriate for the perturbation calculation are determined by the definition of the system under consideration. The simplest case is that of an isolated molecule, where the

"crystal field" perturbations can be expressed directly in terms of the normal modes of vibration of the molecule. In this case it is clear that the number of high energy modes that couple to the rare-earth ion can be quite small for a simple molecule. The terms $(n + 1)(n + 1 + 1)(n + 1 + 1 + 1)$ should dominate the temperature dependence provided that only a few high energy vibrational modes of the molecule couple to the ion. The other extreme is the crystalline environment, where the normal modes of the system involve uniform displacement of N atoms. For the acoustic modes of a crystal lattice, the molecular approximation is clearly not justified. However the highest energy vibrations of a crystal are well approximated as independent Einstein oscillators of frequency ω, corresponding for example to the Si-O stretching vibration in quartz or glass.

The validity of this approximation is indicated by the width of the high energy peak in the Raman spectrum. Shuker[21] has shown that the usual k=0 selection rule for Raman scattering in crystals breaks down in the case of glasses, so that the Raman spectra give information about phonons of all wave vectors. Brawer[14] has taken the approach that it is not useful to consider selection rules for glasses where the wave vector is not defined. In either case, the Raman spectra reflect the properties of the high energy phonons in glasses. The widths in glass are about 100 cm^{-1} for the 1000-cm^{-1} peak, but the approximation is actually better than the ten percent given by $\Delta\omega/\omega$.

The Raman peak in glass is primarily inhomogeneously broadened; that is, the 100-cm^{-1} width is due to different local environments for the individual oscillators - some have alkali ions nearby, some do not, some have non-bridging oxygens, some bridging, etc. This

is not the same as the formation of a band due to strong coupling of the oscillators as in the acoustic phonons. That part of the width due to coupling of the oscillators throughout the solid should be present to an even greater extent in the crystal than in the glass. However the width of the high energy peaks in a crystal of similar composition are $\lesssim 20\ cm^{-1}$ (see Brawer[14]). This narrow width is a good approximation to the delta function expected in the case of perfect Einstein oscillators, but the inhomogeneous broadening in the glass obscures this fact.

An equivalent way of expressing the criterion for the independence of the high frequency oscillators is that they may be considered independent if the excitation remains localized at one oscillator for a time longer than the time required for the ion to make the multiphonon transition.[22] Physically this criterion tests whether the particular vibrational mode excited by the first transition to an intermediate state is still excited when the transition to the second and subsequent intermediate states takes place. If it is not still excited, the (n+1+1) stimulated term is not appropriate, since the excitation diffused away before it could stimulate another phonon. The localization time of the excitation is indeed very short, on the order of one picosecond. ($20\text{-}cm^{-1}$ width of the Raman peak corresponds to a lifetime $T_2 \approx 1 \times 10^{-12}$ sec.) However the time required for the multiphonon transition is considerably shorter. Since energy is not conserved in the intermediate states, these states may not be occupied for a time longer than $\Delta t \approx \hbar/\Delta E$, where ΔE is the error in conserving energy. ΔE is approximately p times the phonon energy since the ion remains in the excited electronic state while emitting p phonons or jumps to the lower electronic state before emitting p phonons. Thus the time that the system remains in an inter-

mediate state must be less than one period of the phonon vibration: $\Delta t \approx \frac{\hbar}{ph\omega} < \frac{1}{\omega}$. For 1000-$cm^{-1}$ vibrations, this corresponds to less than 3×10^{-14} seconds. As before, the oscillators are independent to better than ten percent.

These considerations of the coupling of the oscillators in glass were treated in a different context by Brawer,[14] who developed a theory for calculating the vibrational modes of glasses. He found good agreement between his calculations and experimental observations when he neglected the coupling of one structural unit in the glass to all others. Brawer states that, "Because of the weak-coupling the individual units will execute many vibrations at their resonant frequencies before being damped by motions of their neighbors."[14]

The difference between the molecular and lattice models for the phonon modes can be illustrated for the case of two phonon relaxation. In both cases, the derivative of the potential is taken with respect to the normal coordinates of the "molecule" centered at the rare-earth ion. For simplicity, only the highest energy mode of the molecule will be considered now. ω labels the molecular vibrations. Using the molecular model where the high energy vibrations of the glass are independent Einstein oscillators, only the nearest neighbor oscillators contribute to the motion of the "molecule":

$$Q_\omega = \sum_{\substack{\text{nearest} \\ \text{neighbors}}} c_\omega (a_\omega^+ + a_\omega) \tag{33}$$

Of the total of N oscillators in the glass sample, only six or eight are included in this sum. Then the transition rate is given by

$$W_{mol.} = \frac{2\pi}{\hbar}\left|\sum_{\omega_i,\omega_j}\frac{\langle b|V'_{\omega_i}|a\rangle\langle a|V'_{\omega_j}|a\rangle}{-\hbar\omega}\, C_{\omega_i} C_{\omega_j}\sqrt{n_{\omega_i}+1}\sqrt{n_{\omega_j}+1} + \text{similar terms for other electronic sequences}\right|^2 \quad (34)$$

Since the sum over ω_i and ω_j includes only nearest neighbors, the terms with i=j, which are the stimulated terms, will be a significant portion of the total.

With the lattice model, where the normal modes of the "molecule" surrounding the rare earth are expressed in terms of the normal modes of the entire lattice, Q_ω is given by

$$Q_\omega = \sum_k C_{\omega k}(a_k^+ + a_k) \quad (35)$$

Again ω labels the high energy molecular vibration, but k labels the lattice modes. A superposition of all the lattice modes is necessary to express a localized vibration of the "molecule," so the sum over k has 10^{23} terms in it.[22] The coefficients $c_{\omega k}$ are proportional to $N^{-1/2}$ since the mass involved in the normal mode vibration is the mass of the entire crystal, whereas the c_ω above involves the mass of one ion. This normalization gives the same rate for both models, with the exception of the greater importance of the stimulated terms in the molecular model. The rate for the lattice model is

$$W_{lat.} = \frac{2\pi}{\hbar}\left|\sum_{\omega_i,\omega_j}\frac{\langle b|V'_{\omega_i}|a\rangle\langle a|V'_{\omega_j}|a\rangle}{-\hbar\omega}\sum_{K_i} C_{\omega_i k_i}\sqrt{n_{\omega_i}+1}\sum_{k_j} C_{\omega_j k_j}\sqrt{n_{\omega_j}+1} + \cdots\right|^2 \quad (36)$$

Here the first sum is over six to eight molecular vibrations, but

the sums over k include $m = N = 10^{23}$ terms. The number of stimulated terms is m out of a total of m^2 terms, so the stimulated effects will be negligible.

Multiphonon relaxation involves the highest energy optical phonons, so the molecular model involving independent oscillators is appropriate to describe the ion-lattice system. The experimental observation of the stimulated effects predicted by this model is obscured in glasses by the inhomogeneous nature of the vibrational spectra. (This will be demonstrated in the section describing temperature dependence measurements.) A more definitive experiment might be done with a crystal, particularly one with a relatively isolated high energy vibration that is responsible for multiphonon relaxation. The best candidate for observation of this effect is a hydrated crystal or glass. The O-H vibration at about 3600 cm^{-1} is known to relax rare-earth ions in crystals[4] and glasses[23] (and liquids[24]). For small concentrations of water in a glass, there would be a high probability that only one O-H oscillator is active in multiphonon relaxation of an ion. The expected temperature dependence could then be verified unambiquously. Rare-earth vapors would also be appropriate to observe stimulated multiphonon relaxation, provided that the vapor molecule is sufficiently simple, a rare-earth trihalide for example. In all these cases, the magnitude of the relaxation rate would not be the indication of stimulated vibrations; only the temperature dependence would identify the effect.

Heller[24] has observed nonradiative relaxation of excited rare-earth ions in D_2O caused by small amounts of O-H. His results indicate that a single O-H vibration takes up all the energy, thereby becoming

excited to a vibrational state of $n = 2$ in one case and $n = 5$ in another. Heller did not report the temperature dependence of this effect. Temperature ranges available for such experiments in water are limited by the high vapor pressures (~200 atmospheres at 600 K). Rapp[23] has reported that quenching of rare-earth ions in glasses is linearly proportional to the OH concentration in the glass in an experiment where water was intentionally introduced into the glass melt. This same linear dependence on OH concentration led Heller to his conclusions that a single oscillator was excited to a high vibrational level. The temperature range available for a hydrated glass may be sufficient to observe the expected temperature dependence of $(n+1)(n+2)\ldots$ if the water is not driven off when the glass is heated.

D. Experimental Technique

The following section will describe the experiments to measure multiphonon relaxation of rare-earth ions in glasses. Although details for each individual ion will be described below, the general technique involves the following steps. Some fraction of the ions in the glass are raised from the ground state to an excited electronic state through absorption of a photon from the pump beam (step (1) in Fig. 1). The excited ions emit phonons and relax very quickly ($<<1$ns) from the initial excited state to lower electronic states through a series of closely spaced levels (step 2 in Fig. 1). Although the levels in this series all have some radiative rate, no fluorescence is observed from them because the nonradiative rate is much greater than the radiative rate. This cascade continues until the ions are in a state where the gap to the next lower level is greater than the highest energy phonons $\hbar\omega_{max}$ in the glass; here the relaxation is slowed to tens or

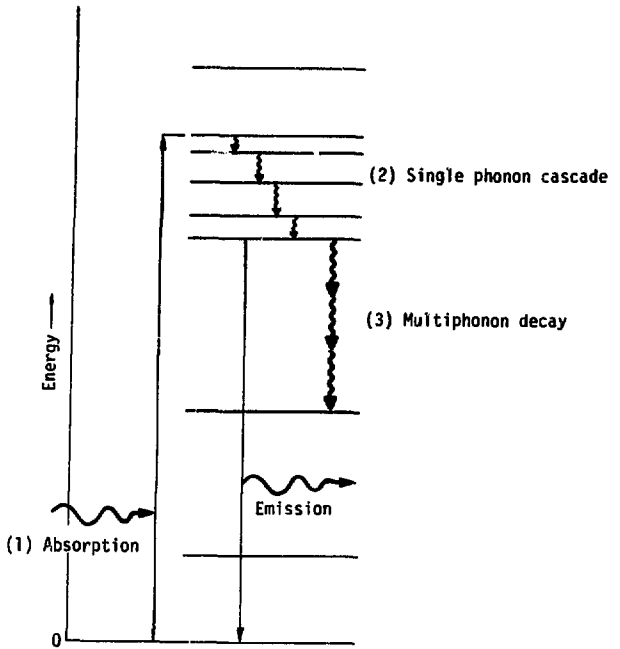

Figure 1 Decay scheme for a rare-earth ion in glass. (1) Absorption of a pump photon raises the ion to an excited state. (2) Emission of low energy phonons rapidly relaxes the ion through a series of closely spaced electronic levels. (3) Relaxation across a large energy gap requires simultaneous emission of several high energy phonons. This multiphonon decay is much slower than the single phonon cascade so the population of the level can be monitored by observing radiative emission.

hundreds of nanoseconds. The population of this longer lived electronic state is then monitored by observing the characteristic fluorescence from those ions which decay radiatively.

The number of fluorescent photons per second from a level is just the radiative rate times the instantaneous number of ions in that state. Since the fluorescent intensity is proportional to the total number of ions, its decay reflects the total decay rate, which is the sum of the radiative and nonradiative rates. In all but two of the measurements in this work, the nonradiative decay rate was much faster than the radiative rate, so the total rate was essentially equal to the nonradiative part. Thus the observed decrease in fluorescence from an excited state was a direct measure of the nonradiative decay.

There are two ways to select the electronic level that is observed. First, selectivity is provided by using a narrow spectral width for the exciting radiation, and second, the desired level can be isolated by narrow optical filters which allow fluorescence from only one level to reach the detector. Combinations of these two techniques were used in the multiphonon experiments.

Measurement of these very fast decays imposed three restraints on the experimental apparatus. First, since almost all the ions decay nonradiatively, the fluorescence intensities were very low, requiring very sensitive detectors. Second, the detectors had to be very fast in order to follow the decays. Finally, the pump pulse requirements were high intensity and very short duration, an application for which pulsed lasers were ideally suited.

Previous studies of multiphonon relaxation in crystals[25] and in glasses[26] were limited to lifetimes greater than about 1 μsec. Be-

cause of the higher energy phonons in glasses, the relaxation rates of interest were faster than in crystals, so the present work required measurements with greater temporal resolution than previous work in this field. Lifetimes as short as 10 nsec were determined with the apparatus developed for these measurements.

These measurements required a carefully chosen combination of a rare-earth ion absorption that matched the wavelength of one of the available short pump pulses. Two pulsed lasers served as the excitation sources for the various decay schemes in this study. A Chromatix 1000E YAG laser produced Q-switched pulses of approximately 200-ns duration at wavelengths of 527 nm, 531 nm, 532 nm, and 473 nm by means of frequency doubling of the Nd:YAG lines in an intracavity second harmonic crystal. These pulses were available at repetition rates of 1 to 50 pulses per second, which made this system ideal for signal averaging. In addition to the fixed wavelengths, tunable pulses were produced by pumping an optical parametric oscillator (O. P. O.), Chromatix Model 1020, with the output of the laser. The $LiNbO_3$ crystal in the O. P. O. was temperature tuned so that with appropriate combinations of pump wavelength, cavity mirrors, and crystal temperature, any wavelength from 0.56 to 3.5 μm was obtainable. The Q-switched oscillator produced about 0.5 mJ at 532 nm, and about ten percent of this energy could be converted to tunable output in the O. P. O. In the experiments reported herein the O. P. O. was used for pumping Tm at about 680 nm, and the 532-nm pulses from the Chromatix laser pumped Nd and Er. Since the pulses were 200 ns long, only the relatively slow decays (Nd $^4F_{3/2}$, Tm $^3F_4$, and Er $^4I_{11/2}$) could be resolved using this convenient repetitive

system.

The second laser excitation source was a 1 ns, 1.06-μm YAG laser with a second harmonic generating crystal and a third harmonic mixing crystal. The laser system is shown in Fig. 2 and a schematic diagram is presented in Fig. 3. The oscillator cavity consists of a 0.64-cm diameter by 9.5-cm Nd:YAG rod in a four flashlamp pump enclosure, a Pockels cell Q-switch, a Glan prism polarizer, and resonant reflectors for both front and rear mirrors.[27] The Pockels cell voltage is maintained at the $\lambda/4$ value (~3k V) to give minimum transmission for light from the rod through the Pockels cell-polarizer to the mirror and back through to the rod. When the rod reaches peak gain, an electrically triggered spark gap shorts the Pockels cell voltage to ground through a 5 ns length of cable. The Pockels cell voltage rings with a 10-ns period causing the Pockels cell-polarizer transmission to peak at the voltage zero-crossing, once every 10 ns. The Pockels cell rise time is such that a 1 ns window every 10 ns results from ringing the Pockels cell voltage. The optical round trip time of the oscillator cavity is exactly matched to the Pockels cell ringing time so that a 1 ns laser pulse builds up in the cavity. The resonant reflectors limit the frequency band-width of the pulse so that it is nearly band-width-limited. The output through the front mirror consists of a train of 1-ns pulses separated by the cavity round trip time of 10 ns.

A single pulse was selected from this train by an optically triggered Pockels cell switch-out[28] that followed the oscillator. Two Nd:YAG and Nd:glass amplifiers built up the pulse energy to a maximum of

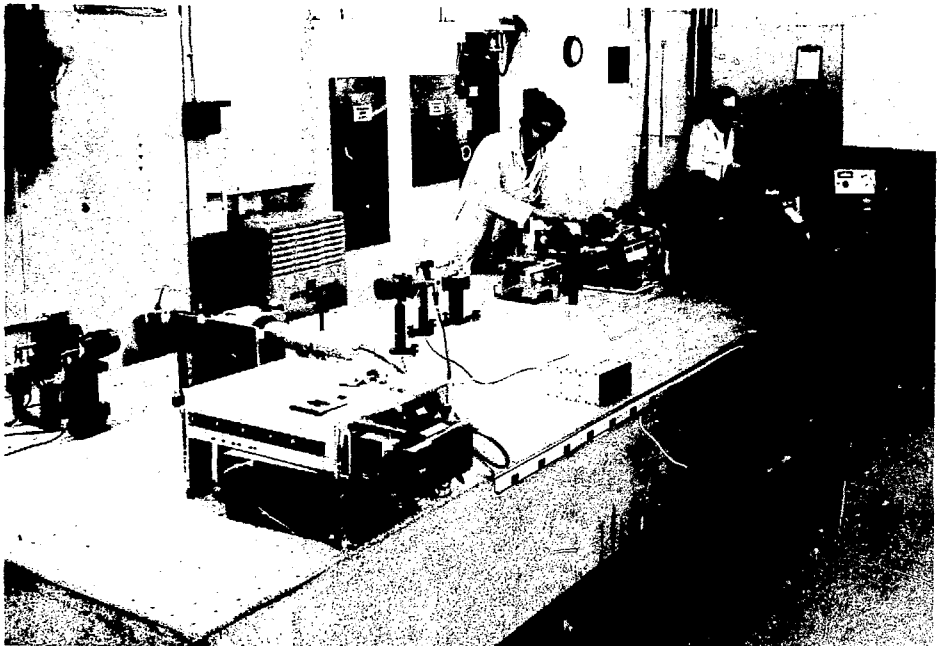

Figure 2 The 1 ns, 1.06 μm Nd laser. D. C. Downs, at right, is touching the 1 ns YAG oscillator while S. C. Roberts aligns one of the three amplifiers. The optical table is an air-mounted granite block.

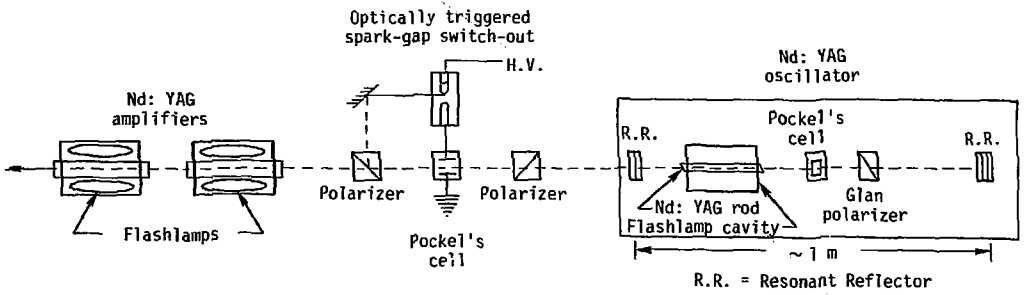

Figure 3 Schematic of 1 ns laser system. The Pockel's cell inside the oscillator cavity is driven sychronously to provide a train of 1 ns pulses.

50 mJ per pulse. The spatial profile of the pulse was about 0.5 cm in diameter and smoothly varying, although no special effort was made to characterize or improve the beam profile.

Following the amplifiers, a Galilean telescope reduced and re-collimated the beam to a diameter of 2 mm in order to increase the beam intensity for higher conversion efficiency to the second and third harmonics. A 2.54 cm long KD*P crystal cut at 41° to the c-axis converted the 1.06 μm pulse to 532 nm with 10 to 20% (energy) efficiency. Following the second harmonic generating (SHG) crystal, another KD*P crystal (cut for Type II phase-matching at 58°) mixed the 1.06-μm and 532-nm light to produce a third harmonic pulse at 355 nm. Thus three different wavelengths were present in the 1 ns pulse out of the laser system: about 30 mJ at 1.06 μm, about 10 mJ at 532 nm, and about 1 mJ at 355 nm (see Fig. 4). One particular pumping pulse was chosen by appropriate filters.

Beam splitters directed a portion of the pump beam to photodiodes which served as energy monitors. The harmonic generating crystals were aligned by optimizing the ratios of green energy to infrared energy, and blue energy to green energy. Adjustment of the laser-amplifier power supply voltage determined the energy in the pump pulses. Because the laser amplifiers required cooling time, the repetition rate of the 1 ns laser system was limited to about once every 30 seconds, making signal averaging a time consuming process.

The basic experimental set-up for multiphonon decay measurements with the 1 ns laser is shown in Fig. 4. The appropriate pump pulse was focused into the sample by a 20-cm focal length lens, creating a line of excited ions near one side of the sample. This side was placed against the entrance slit of a 1/4-m Jarrel Ash monochro-

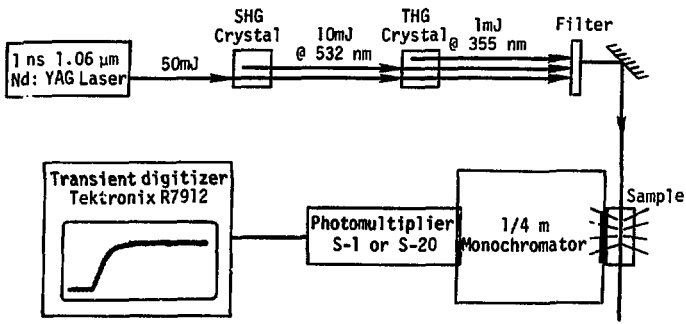

Figure 4 Apparatus for fast fluorescence measurements. The second harmonic generating crystal (SHG) produces 532-nm light from the incident 1.06-μm pulse. The third harmonic generating crystal (THG) mixes 1.06 μm and 532 nm to produce 355 nm. A filter selects either 532 nm or 355 nm to pump the rare-earth ion in the sample.

mator (f/4.5), so that the fluorescent radiation perpendicular to the pump beam was collected. (The samples were all optically thin to both the pump and fluorescence radiation.) At the exit slit of the monochromator, a photomultiplier tube detected the radiation at the desired wavelength. For infrared fluorescence, an Amperex 56CVP tube having an S-1 photocathode was used; for shorter wavelengths, an Amperex 56TUVP with S-20 response was used.

In some cases the fluorescence was too weak for detection through the monochromator, so various filter combinations were used to isolate the desired wavelength. The band-pass and absorption filters were held in the photomultiplier housing against the tube face, and the housing was placed as close as possible to the sample inside a light tight box. The 4-cm diameter photocathode intercepted a large solid angle (~f/1) in this configuration.

When the Chromatix laser served as the pump source, the sample was again placed in a light tight box and the fluorescence collected at right angles. Filters provided wavelength selection, and the same photomultipliers and electronics were used.

The worst experimental problem with both laser pump sources was the intense scattering of the laser pump pulse which at best gave an initial spike on the fluorescence signal, and at worst saturated the photomultiplier. Entrance and exit surface scattering from the samples could be masked by black tape, but bulk scattering was more difficult to avoid. The glass samples were produced in small test melts and were not all of good optical quality, containing index inhomogeneities and inclusions. Absorption filters or the monochromator served to discriminate against scattered pump light, but

fluorescence of the filters themselves when illuminated by intense scattering often buried the desired signal. Careful attention to geometry, filter combinations, and temporal characteristics of the signal was necessary to sort out the fluorescence decay from the more intense scattered laser pulse.

Fluorescence signals from the photomultipliers were processed by a Tektronix transient digitizing system, shown in Fig. 5. A block diagram of the portion of the system used in this work is shown in Fig. 6. The heart of the system is a PDP-11 computer which interfaced to the other components and provided data manipulation capability through both user-written and prepackaged programs. A version of BASIC programming language is used, with variations to control special hardware functions of the system.

The photomultiplier signal is recorded by an R7912 Transient Digitizer, which is similar to a fast oscilloscope in its basic function, but provides a digital output. A 7B92 horizontal sweep plug-in controls the speed of the R7912, with external triggering from a photodiode that looks at the laser pulse. Vertical sensitivity is provided by a 7A19 amplifier plug-in with 50-Ω input impedance. The R7912 is capable of 0.5 ns per division and 10 mV per division with these plug-ins.

The cathode ray tube in the R7912 consists of two parts. A writing beam similar to that in an oscilloscope sweeps across a silicon target with vertical deflection proportional to the applied signal. The target is an array of diode junctions which conduct when struck by the writing beam. On the other side of the target, a reading beam scans the target, producing a current pulse when one of the conducting

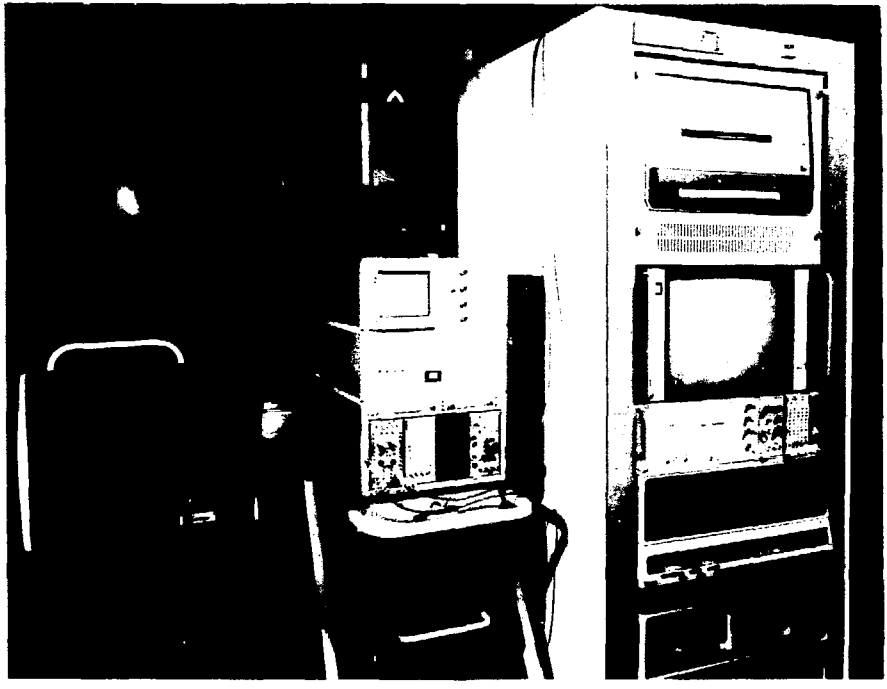

Figure 5 Tektronix digital signal processing equipment. The control console is at left next to the digital processing oscilloscope. In the rack at right are (top to bottom) the hard copy unit, transient signal monitor, R7912 transient digitizer, computer, and tape cassette unit.

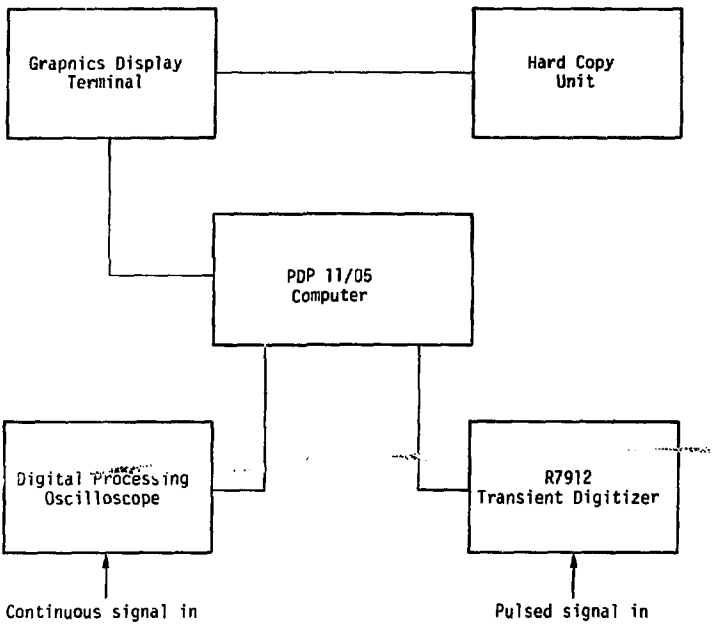

Figure 6 Schematic of the Tektronix system shown in Fig. 5. Use of the digital processing oscilloscope is not described here.

junctions is encountered. This current pulse is processed into the R7912 memory as an array of ones and zeroes. The computer takes this array and converts it into 512 channels, each with a 10-bit number representing signal height.

A computer display terminal (Model 4010-1) inputs instructions to the computer and displays the processed signals and graphs. Permanent copies of the displays are obtained from the 4610 Hard Copy Unit. Simple computer programs were devised to give logarithmic plots of fluorescence decays from which the decay rate was determined as the slope of the log plot. For the Fluorescence rise experiments, a similar program plotted $\ln(I-I_{max})$ from which the slope gave the fluorescence rise time. In most cases the signal that was processed by these simple programs was a result of averaging photomultiplier signals. When the Chromatix laser was used, the high repetition rate made it possible to average as many shots as necessary. Since the signal-to-noise ratio in the slower decay measurements was usually greater than ten to one for a single shot, averaging ten or twenty shots was usually sufficient. With the fast decay measurements involving the 1 ns laser, the signal-to-noise ratio was frequently less than ten, but the very low repetition rate of two pulses per minute discouraged taking more than about ten samples for a given average.

The limiting factor in determining the time resolution of the system was the photomultiplier itself. The R7912 with the plug-ins used is capable of subnanosecond response. With 50-Ω termination at the R7912, the observed rise time when recording the 1-ns pulse

from the laser was about 3 ns, with a slightly longer fall time. With slower decays, a larger load resistor was used on the photomultiplier to increase the signal, but the signal was always checked against the 50-Ω result to insure that it was not distorted by the larger terminator.

E. Rare-Earth Ion Decay Schemes

The rates that could be measured in this work were restricted to those in which the energy gaps across which the decays occur are greater than 1500 cm^{-1} and less than about 4000 cm^{-1}. For gaps less than 1500 cm^{-1}, the multiphonon theory does not apply, since only one or two of the highest energy phonons are involved; also these decays are too fast to measure with the apparatus used. Energy gaps larger than 4000 cm^{-1} in the glasses studied have such small multiphonon rates that the radiative rate is no longer negligible. The radiative rates are not well known, so the accuracy is low for a determination of the nonradiative rate by subtracting the radiative component from the measured total rate. Since the goal of this study was direct measurements of nonradiative rates, these larger energy gaps were avoided.

Judd[29] and Ofelt[30] have developed a method for calculating the dipole transition probabilities for rare-earth ions in crystals. The line strength of the transition can be expressed as the sum of three empirically determined parameters describing the crystal field multiplied by the three appropriate reduced matrix elements of tensor operators. The matrix elements have been calculated for several rare earths, and the Judd-Ofelt approach has been applied to glasses by Krupke[31]

and Reisfeld.[26] Reisfeld's calculations were used to correct for the radiative rates in the two cases where they were not negligible compared to the multiphonon rates.

The energy gaps were determined from absorption spectra of the ions in glasses. Because of the inhomogeneous nature glasses, the assignment of energy gaps was imprecise. Site to site variations of the crystal field result in variations of energy levels, line strengths, and Stark splittings from ion to ion. The absorption spectra reflect a sum over ion sites weighted by the various line strengths. The appropriate energy gap for a multiphonon decay of a given ion is the difference in energy between the lowest Stark component of the upper level and the highest Stark component of the level below. Equilibration among the closely spaced Stark components is very fast compared to multiphonon rates, so the Stark levels will always maintain a thermal distribution within a manifold.[25] The exponential dependence of the multiphonon rate on energy gap will assure that the minimum energy gap from the absorption spectra is somewhat qualitative, resulting in uncertainty of about 100 cm^{-1} in the absolute value and slightly less error in relative values. The gaps did not vary significantly from glass to glass.

Of the thirteen trivalent rare earths, three were chosen to be doped into the glasses for this study. Nd was an obvious choice because of its importance in laser materials, not because it satisfies the criteria outlined above. Er was an ideal choice since three different energy gaps could be studied, all using the same 532 nm pump wavelength. Tm provided a large energy gap which was well suited to temperature dependent measurements.

1. Neodymium

The energy level diagram of Nd^{3+} is shown in Fig. 7. There are two measurable gaps in the cascade down through the Nd Pump bands, one below the $^2P_{3/2}$ level, and one below the $^4G_{7/2}$ level. All the other energy gaps above the $^4F_{3/2}$ are significantly smaller. The decay rates of both the $^2P_{3/2}$ and $^4G_{7/2}$ were determined from the rise of the fluorescence from the $^4F_{3/2}$ metastable level. When the Nd ion is excited by the 355-nm pump pulse, the decay of the $^2P_{3/2}$ is the rate limiting step in the relaxation down to the fluorescing $^4F_{3/2}$ level. The lifetime of the $^4F_{3/2}$ is very long compared to all the steps in the cascade through the pump band. Thus the rise of the emission from the $^4F_{3/2}$ is described by

$$I = (1 - e^{-t/\tau})I_p$$

where τ is the lifetime of the $^2P_{3/2}$ state and I_p the peak intensity. When the ion is exited by 532-nm radiation, the rate limiting step is the decay of the $^4G_{7/2}$ level, which is much faster than the $^2P_{3/2}$ relaxation. Again the rise of the $^4F_{3/2}$ fluorescence is described by the same function with τ being the $^4G_{7/2}$ lifetime. The population in the $^4F_{3/2}$ level can be monitored by observing either the 1.06-μm or the 880-nm radiation. A typical fluorescence rise signal and the associated plot of $\ln(I_p-I)$ are shown in Fig. 8.

The two Nd measurements were the most difficult and least

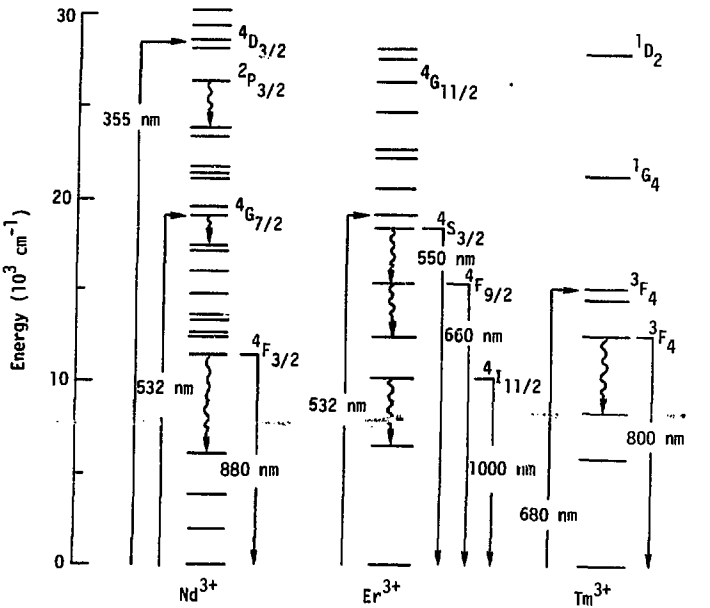

Figure 7 Excitation and fluorescence schemes to study multiphonon relaxation. Wiggly lines indicate the decays measured.

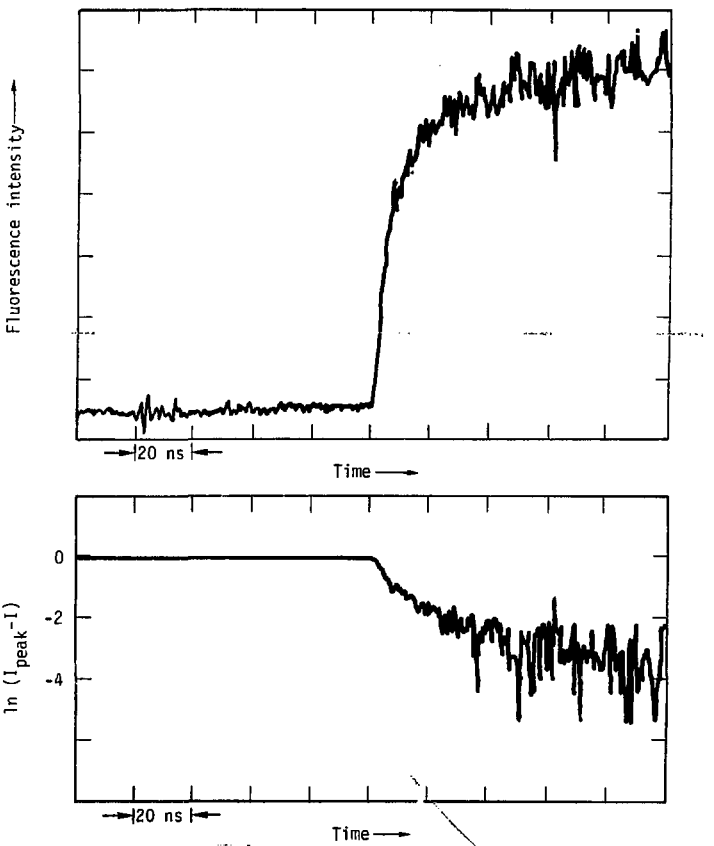

Figure 8 Fluorescence rise signal. The top signal is the Nd $^4F_{3/2}$ fluorescence at 1.06 μm in silicate glass after pumping with 532 nm pulse. The lower trace is ln (Ip - I) from which the slope gives the decay time to the $^4F_{3/2}$ level.

accurate of the multiphonon experiments. The early part of the rise is distorted by the system response (~3 ns) and by any leakage of pump radiation into the photomultiplier. As the signal nears the peak intensity, the noise on the long term signal introduces a large error in $(I_p - I)$. The combination of these sources of uncertainty limited the fastest rates that could be measured with confidence to about 10^8 sec^{-1}. The rates in borate and phosphate glass are not determined since they are greater than 10^8 sec^{-1}. The $^2P_{3/2}$ decay could not be measured in tellurite glass because the glass strongly absorbs 355-nm radiation.

2. Erbium

The three energy gaps that were studied in Er are shown in Fig. 7. After excitation with 532-nm pump radiation, the ion rapidly relaxes to the $^4S_{3/2}$ level, which nonradiatively decays across a gap of about 2800 cm^{-1}, resulting in an exponential decay of the $^4S_{3/2}$ fluorescence (550 nm). The $^4F_{9/2}$ level immediately below the $^4S_{3/2}$ decays faster than the $^4S_{3/2}$ since it has a smaller gap below it (2600 cm^{-1}). Thus the $^4F_{9/2}$ fluorescence signal rises to a peak intensity as it is fed by the $^4S_{3/2}$, and then decays with a rate that approaches that of the $^4S_{3/2}$ at long times. The rate equations for the populations N_1 and N_2 in levels 1 and 2, which decay nonradiatively with rates W_1 and W_2 are

$$\frac{dN_1}{dt} = -N_1W_1 \Rightarrow N_1 = Ne^{-W_1t}$$

where N is the number excited initially.

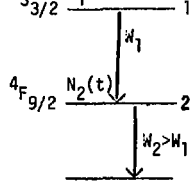

$$\frac{dN_2}{dt} = +N_1W_1 - N_2W_2$$

$$= NW_1 e^{-W_1t} - N_2W_2$$

The solution for N_2 is

$$N_2(t) = \frac{NW_1}{(W_2 - W_1)} (e^{-W_1t} - e^{-W_2t})$$

The peak population in N_2 occurs at t_p given by

$$\left(\frac{dN_2}{dt}\right)_{t_p} = \frac{NW_1}{(W_2 - W_1)} \left(-W_1 e^{-W_1t_p} + W_2 e^{-W_2t_p}\right) = 0$$

$$W_1 e^{-W_1t_p} = W_2 e^{-W_2t_p}$$

$$t_p = \frac{\ln (W_1/W_2)}{(W_1 - W_2)} \qquad (37)$$

After a direct measurement of the $^4S_{3/2}$ lifetime (W_1), and determination of the time to the peak of the $^4F_{9/2}$ signal, the $^4F_{9/2}$ rate (W_2) is determined by the final equation above. This transcendental equation was solved for values of t_p as a function of W_1 and W_2, with the results plotted as contours of constant t_p, as in Fig. 9.

For the two faster levels in Er, the 1-ns laser was used for excitation. The S-20 photomultiplier was appropriate for these emissions at 550 nm and 660 nm. The 550-nm emission from the $^4S_{3/2}$ was too close to the pump wavelength of 532 nm for absorption filters to be effective, so the monochromator was necessary to eliminate scattered pump light. An example of the photomultiplier signal monitoring the $^4F_{3/2}$ is shown in Fig. 10. The emission at 660 nm from the $^4F_{9/2}$ is also shown in the figure, with the peak intensity at about 200 ns after the pump pulse.

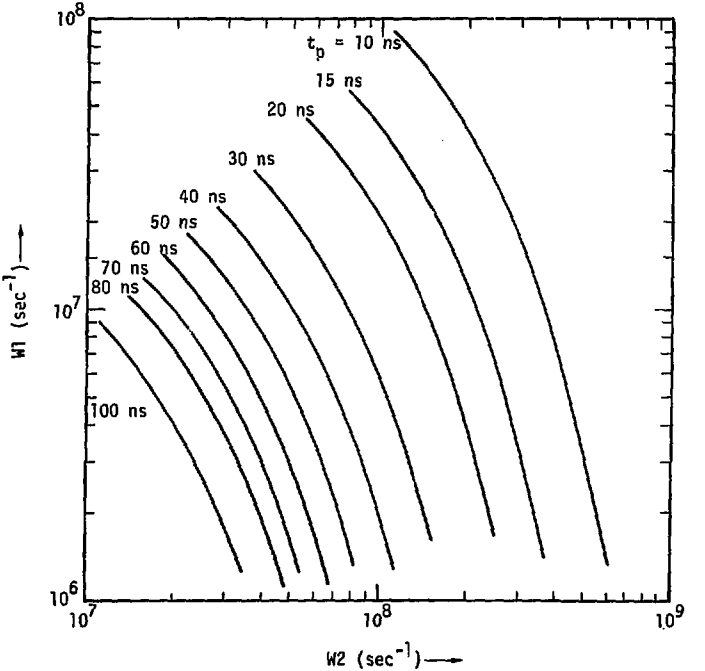

Figure 9 Contours of constant tp from the solutions of Eq. (37), $t_p = \frac{\ln (W1/W2)}{W1 - W2}$. The range of W1 and W2 are appropriate for Er in phosphate glass where t_p = 65 ns and W1 = 2.7 x 10^6 sec^{-1}, giving W2 = 4.6 x 10^7 sec^{-1}.

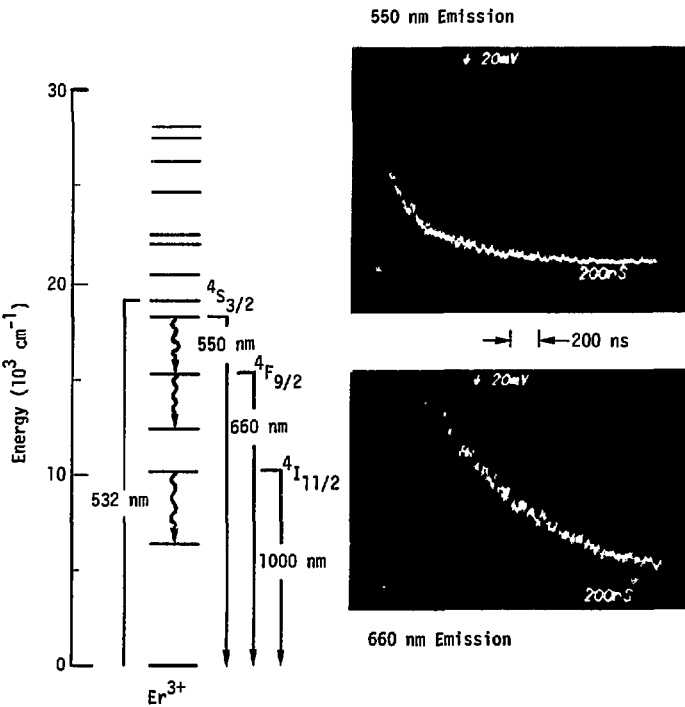

Figure 10 Multiphonon decay rate measurements in Er in silicate glass. The $^4S_{3/2}$ signal is shown at the top, and the $^4F_{9/2}$ below. The fluorescence from the $^4I_{11/2}$ was an exponential decay like the top picture, but much slower.

Errors in the value of the $^4S_{3/2}$ rate will affect the $^4F_{9/2}$ rate, with a high value for the first yielding a low value for second.

The decay of the $^4I_{11/2}$ state in Er across a gap of ~3300 cm^{-1} was slow enough that the rise of the 1-μm fluorescence was effectively instantaneous when recorded on a time scale appropriate to the decay. The Chromatix laser pulses at 532 nm were used to pump in this case, so signal averaging was convenient.

3. Thulium

The largest energy gap in this study was the Tm $^3F_4$ to $^3H_5$ gap of about 3800 cm^{-1}. The Chromatix laser driving the optical parametric oscillator at 680 nm excited Tm into the $^3F_2$ state from which it relaxed rapidly to the $^3F_4$ (see Fig. 7). Emission at 800 nm was observed as a monitor of the $^3F_4$ population. The uncertainty in determining the energy gap for this transition was large, due to the unusually broad (1000 cm^{-1}) absorption bands. Fig. 11 shows the absorption bands due to the two levels of interest in Tm. The broad wing on the short wavelength side of the $^3H_5$ absorption made the assignment of a definite energy gap more ambiguous for Tm than for any of the other gaps. Two possible explanations of the broad lines are 1) unusually large Stark splitting of the level combined with inhomogeneous broadening to smear out the Stark levels or 2) unusually strong vibronic sidebands where photon absorption is accompanied by phonon emission. Tm absorption spectra were recorded for all five glass compositions, and although the phonon spectra differ greatly from glass to glass, the Tm lines were very similar. This fact supports the explanation based on Stark splitting. Vibronic spectra and Stark

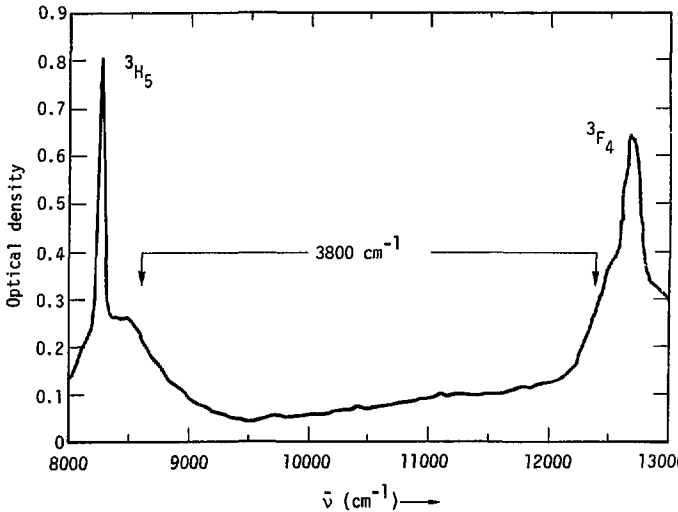

Figure 11 Tm absorption spectrum in silicate glass showing the broad wings on the $^3H_5$ and $^3F_4$ peaks.

spectra would have similar temperature dependences, which rules out an easy resolution of this question by low temperature absorption measurements.

The large energy gap in Tm results in a low nonradiative rate, so the radiative contribution must be subtracted from the observed rate, at least for germanate and tellurite glasses. The nonradiative rate in silicate, phosphate, and borate glasses was greater than 3×10^4 sec^{-1} so the radiative correction was not made for these three.

F. Glass Compositions

The glasses chosen for this study were simple three component oxide glasses in which the network forming complex varied through the series: TeO_2, GeO_2, SiO_2, P_2O_5, B_2O_3. Douglas Blackburn of the National Bureau of Standards supplied these samples. Silicate and phosphate glass were the first choices because of their use in glass lasers. The other three glasses were included after it became apparent that phonon spectra determined nonradiative rates in glasses just as in crystals. Borate glass was known to have higher energy phonons than silicate or phosphate[16,32] while tellurite and germanate have lower phonon cutoffs.[33,26] In addition to the series of five glasses, the same measurements were made on a commercial silicate laser glass, Owens-Illinois ED-4, doped with Nd, Er, Tm, and Pr.

Table I shows the chemical compositions of the five oxide glasses and ED-4. The composition chosen for tellurite glass did not result in a stable glass sample, so a slightly different composition was obtained. This glass is also listed in the table. The five NBS glasses

Compositions in MOL%

	B_2O_3	P_2O_5	SiO_2	GeO_2	TeO_2	Na_2O	BaO	Er_2O_3	Tm_2O_3
Borate	66.6					15	18	0.2	0.2
Phosphate		66.6				15	18	0.2	0.2
Silicate			66.6			15	18	0.2	0.2
Germanate				66.6		15	18	0.2	0.2
Tellurite					66.6	15	18	0.2	0.2

	TeO_2	Al_2O_3	WO_3	Er_2O_3
Improved Tellurite	82	12	6	0.2

ED-2 Composition in wt.%

SiO_2	Al_2O_3	Li_2O	CaO	CeO_2	Nd_2O_3
65	4.7	16.4	10.3	0.5	(0.1 to 6)

Table I: Glass compositions. Note that ED-4 refers to the base glass from which ED-2 is made by the addition of Nd_2O_3.

were doped with both Er and Tm in each sample. This did not greatly complicate the experiments because Tm does not absorb at 532 nm and Er does not absorb significantly at 680 nm. The concentration of rare-earth ion was kept low (0.2 mol%) in order to avoid any ion-ion interactions.

G. Multiphonon Decay Results

The results of the measurements of multiphonon relaxation in ED-4 silicate glass are presented in Fig. 12.[34] The rates are plotted on a logarithmic scale versus the energy gap to the next lower level on a linear scale. The exponential dependence predicted by the theory and observed in crystals is clearly valid for the rare-earth energy levels studied. One datum is presented in Fig. 12 that was not available for the other glass compositions, that is the Pr $^3P_0$ to $^1D_2$ decay across a gap of 3500 cm^{-1}. This decay was observed by pumping with the 473-nm pulses from the Chromatix laser and observing the emission at about 622 nm.

The Nd $^4G_{7/2}$ decay at 1400 cm^{-1} was not included in determining the best line through the data. This energy gap cannot be bridged by a single high energy phonon in silicate glass, but the gap is much less than two high energy phonons; the theory is not expected to apply to it. The Nd $^4F_{3/2}$ decay is indicated on the plot. This is not a measured point; it is an extrapolation of the best line through the other data. This is the Nd laser level which has a radiative rate of 2.5 x 10^3 sec^{-1}, much greater than the nonradiative rate. A limit to the multiphonon rate of the $^4F_{3/2}$ level was determined from the temperature dependence

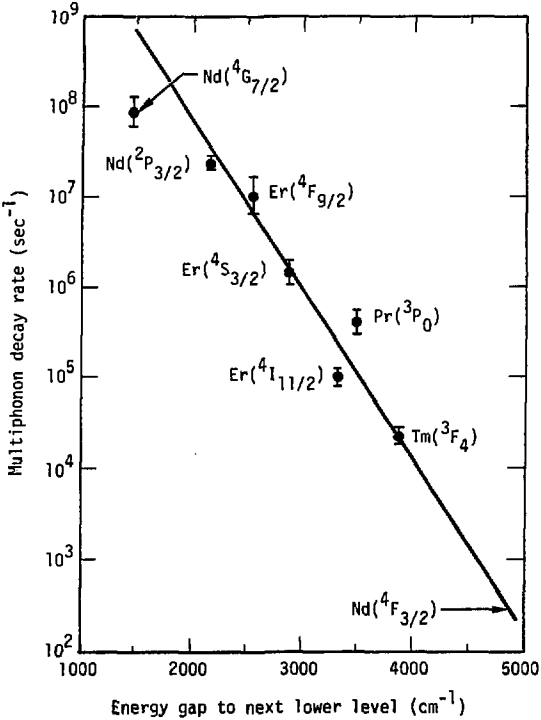

Figure 12 Multiphonon decay rates as a function of energy gap to the next lower level for rare earths in ED-4 silicate glass. The extrapolation to the Nd $^4F_{3/2}$ rate is indicated.

measurements to be described below.

The dependence of the multiphonon rate on glass composition is indicated in Fig. 13.[34] Multiphonon rates for the rare-earth decay schemes described above are shown for the five simple oxide glass compositions of Table I. The particular energy levels are listed at the top of the plot, and the energy gap to the next lower level is the x-axis. The fastest decay rates are those of the borate glass, which fall on a straight line quite well. The phosphate glass is next fastest, followed by the silicate. The silicate rates are equal within experimental error to the rates in the more complex silicate glass, ED-4. The germanate and tellurite glasses do not fit the exponential dependence as well as the other three, but in all cases the multiphonon rate for a given level in the germanate is faster than the rate in the tellurite. The experimental error in these measurements is about twice the size of the data points on the graph, an uncertainty of a little less than a factor of two.

Reisfeld[26] has indirectly measured multiphonon rates for the Er $^4S_{3/2}$ and Er $^4F_{9/2}$ levels in germanate and tellurite glasses, but her results are consistently below the values found here.

Rates from 10^8 to 10^4 sec^{-1} were measured in these experiments. The exponential dependence on energy gap predicted from the theory of multiphonon relaxation is valid to an accuracy of a factor of two in the five glasses studied. The rates for these glasses differ by a factor of 10^3 from the fastest (borate) to the slowest (tellurite), for any particular energy gap. Even the tellurite decays are ten times faster than the fastest measured rates in crystals for similar energy gaps. This large variation with composition and the differences from

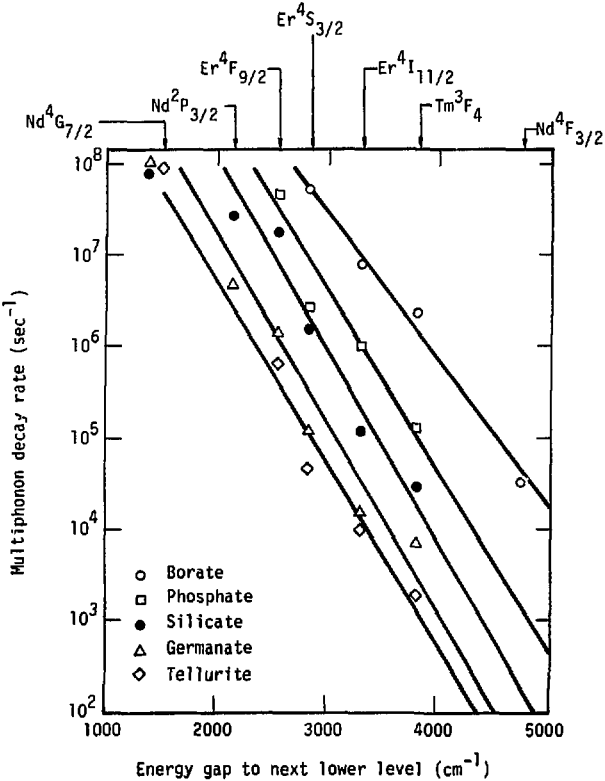

Figure 13 Multiphonon decay rates of rare-earth ions in five oxide glasses as a function of energy gap to next lower level. The ions and energy levels whose decays were measured are indicated at the top of the figure.

glasses to crystals were investigated by means of temperature dependence measurements and their correlation with phonon energies derived from Raman spectra.

H. Raman Spectra

As explained above, the temperature dependence of the multiphonon relaxation rate arises from the Bose-Einstein expression for the occupation numbers of the phonon modes. If the multiphonon relaxation can be accurately represented by a single phonon frequency, such that $p\hbar\omega \approx \Delta E$, then the variation of the rate with temperature will serve to identify the active phonon frequency. The phonons that are present in the glasses were determined by Raman spectra. Identification of the Raman peaks provides a limited number of choices for the frequencies to be tested in the temperature dependence experiments. Thus the combination of the Raman spectra and temperature variations of the multiphonon rates gave a self consistent test of the phonons responsible for the decay.

The theory of vibrational Raman scattering in glasses has been developed in detail.[21, 14] The present work involves only the energies of the various Raman peaks, so only a brief description of Raman scattering will be given. Classically the response of a material to an applied electromagnetic field is given by the polarization P of the medium:

$$P = \alpha E \tag{38}$$

The polarizability of the material is α, and E is the applied field, laser radiation in the present case. The polarization has the time dependence of the incident radiation at frequency ω_0. The Born-

Oppenheimer or adiabatic approximation states that the electrons in the material instantaneously adjust to the changing positions of the nuclei, since the electrons are so much less massive. The polarizability may be expanded in terms of the nuclear coordinates:

$$\alpha = \alpha_o + \frac{\partial \alpha}{\partial q} q + \frac{\partial^2 \alpha_2}{\partial q^2} q^2 + \ldots \tag{39}$$

Taking only the first two terms, the polarization is given by

$$P = \alpha_o E + \frac{\partial \alpha}{\partial q} \quad q \; E \tag{40}$$

The material polarization may be viewed as a dipole field which radiates to give the Raman scattered light. The α_o term gives the unshifted Rayleigh scattering, while the term proportional to a q has frequency components at $\omega_o \pm \omega$.

$$P = \alpha_o E \, e^{i\omega_o t} + \frac{\partial \alpha}{\partial q} \bar{q} \, e^{\pm i\omega t} E \, e^{i\omega_o t}$$

$$= \alpha_o E \, e^{i\omega_o t} + \frac{\partial \alpha}{\partial q} \bar{q} E \, e^{i(\omega_o \pm \omega)t} \tag{41}$$

where ω is the frequency of the nuclear motion, the phonon frequency. Thus the scattered radiation reflects the vibrational frequencies of the material. In crystals, there are selection rules resulting from the translational and point group symmetries that limit which phonon modes can contribute to Raman scattering. These selection rules are generally relaxed in glasses, so that essentially all modes are observed

in Raman spectra, although the relative intensities of Raman peaks vary with glass composition.[35,14,21] For example, the 1100-cm^{-1} peak in silicate glass (Figure 14) is not seen in the Raman spectrum of fused silica.[35] This does not mean that the vibration is not present; it is observed in the infrared spectrum, but selection rules prevent its Raman activity.[16] As network modifying ions are added to fused silica, the selection rule is broken and the peak appears in the Raman spectrum.[35] For the purposes of this work only the energy shifts indicative of the phonon energies are important, so the relative intensities were not considered.

The direction of polarization of the scattered light is an indication of the symmetry of the vibration. Raman scattered light is viewed at right angles to the incident light through a polarizer which passes the polarization that is either parallel or perpendicular to the plane of incidence. The depolarization ratio is defined as the scattered intensity with perpendicular polarization divided by the intensity with parallel polarization. The two extremes for the depolarization ratio are zero for scattering from totally symmetric vibrations and 0.75 for totally asymmetric vibrations.[36] A symmetric vibration is one in which the molecule retains its stationary symmetry throughout the period of the vibration. For example, the breathing mode of a tetrahedral molecule is a symmetric mode.

Figure 14 shows the polarized and depolarized Raman spectra for the simple silicate glass used in these experiments. Clearly the large peak at 1100 cm^{-1} is a highly symmetric vibration, as is the mode at 550 cm^{-1}. In general the polarized spectra were used in identifying

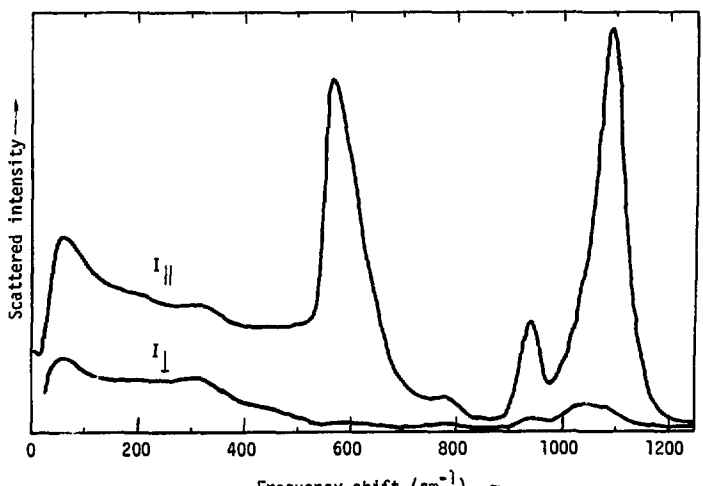

Figure 14 Polarized and depolarized Raman spectra of silicate glass. The top curve records scattered light polarized parallel to the plane of incidence; the bottom curve is perpendicular polarization.

the high energy vibrations of the various glasses. The polarized spectra of the five simple glasses are shown in Fig. 15, and the spectrum for ED-4 is Fig. 16. All spectra were provided by R. C. Harney and F. P. Milanovich, who have published the details of the Raman spectrometer with which these spectra were obtained.[37]

The highest energy peaks in the Raman spectra of the five simple glasses fall in the same order as the multiphonon rates; borate with the highest energy vibration has the fastest rate, followed by phosphate, silicate, germanate, and finally tellurite with the lowest energy phonons and the slowest multiphonon rates. For comparison with crystals, the highest energy phonons in the crystals surveyed by Riseberg and Weber[25] are 600 to 700 cm^{-1}, whereas the tellurite glass has 800-cm^{-1} phonons and the borate spectrum goes up to 1400 cm^{-1}.

I Temperature Dependence

The purpose of the temperature-dependence measurements was to establish that the highest energy glass vibrations are responsible for multiphonon relaxation, a fact that is indicated by the correlation between the high energy cutoffs and the magnitudes of the multiphonon rates in the five glasses. Assuming that the number of oscillators that couple to the ion is greater than ten, so that the terms $(n + 1)(n + 2)\ldots$ are relatively unimportant, the multiphonon theory predicts a temperature dependence of the form

$$W_p = W_0(n + 1)^p \tag{42}$$

The occupation number for a given frequency of phonons is given by

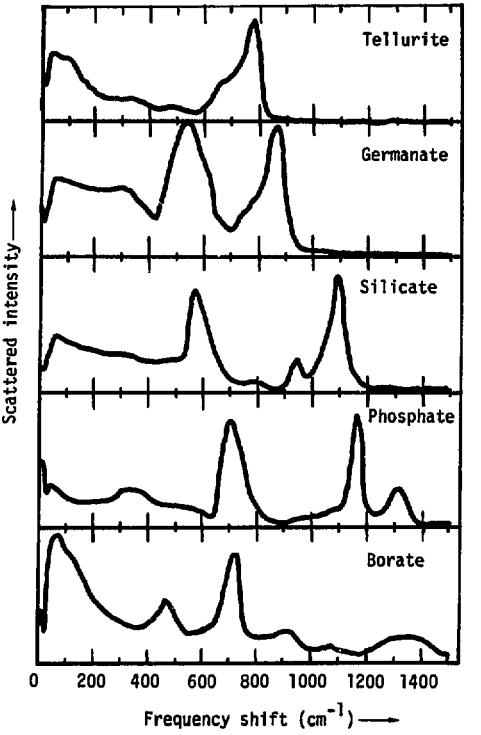

Figure 15 Polarized Raman spectra of five oxide glasses.

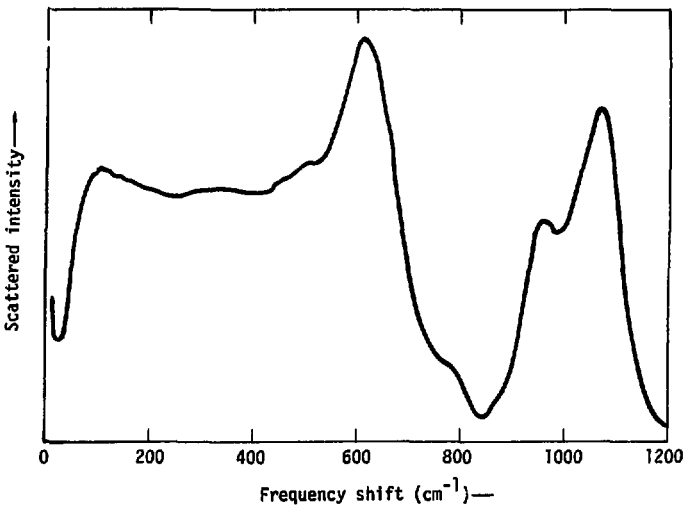

Figure 16 Polarized Raman spectrum of ED-4 silicate glass.

$$n(\omega,T) = \frac{1}{e^{\hbar\omega/kT} - 1} \tag{43}$$

Using (43) in the multiphonon rate expression (42), the resulting temperature dependence is

$$W_p = W_0\left(\frac{1}{1 - e^{-\hbar\omega/kT}}\right)^p \tag{44}$$

where W_0 is the low temperature rate, and p phonons of energy $\hbar\omega$ bridge the gap ΔE. Riseberg,[8] Reed,[38] and others[39] have introduced into the temperature dependence the depletion of the decaying level by thermal population of higher lying levels of arbitrary degeneracy which are assumed to be nondecaying. This latter assumption is not justified in the present case since the energy gap for these thermally populated levels is not significantly greater than for the decaying level itself, and multiphonon theory predicts that the energy gap alone determines the decay rate.

The experimental apparatus for measuring the temperature dependence of multiphonon rates is shown schematically in Fig. 17. An electrically heated "clamshell" oven wrapped with asbestos insulation surrounded the sample. Three holes in the insulation permitted the laser pump pulse to enter and exit and allowed the fluorescence to illuminate the photomultiplier. A thermocouple in contact with the glass sample monitored the temperature. The Chromatix optical parametric oscillator operating at 680 nm pumped the $^3F_2$ level of Tm, and the fluorescence at 800 nm was monitored. This particular energy gap of 3800 to 4000 cm^{-1} was chosen because it was the largest (highest order) gap available

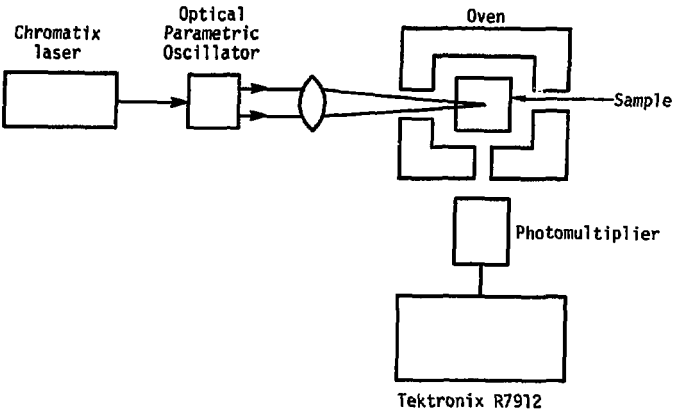

Figure 17 Schematic diagram of apparatus to measure the temperature dependence of multiphonon decay rates.

for which the nonradiative rate dominates the radiative rate. The higher the order of the process, the greater the temperature dependence according to Eq. (44).

As an example of the details of fitting the theoretical temperature dependence to the experimentally determined decay rates, the silicate results are shown in Fig. 18. The curves illustrate the expected temperature dependence for a four phonon decay of 1000-cm^{-1} phonons and a five phonon decay involving 800-cm^{-1} phonons. It is clear that the high energy phonons are active in the decay, but it is not possible to definitely assign the decay to a particular phonon energy. A four phonon decay involving either 900-cm^{-1} or 1100-cm^{-1} phonons fits as well. The restriction of p to integral numbers determines the phonon energy if the energy gap is known; however, the gap may vary from ion to ion, and it is not known accurately. Three phonons of one energy and one of another energy have been fitted, but the results are no more definitive than the single frequency model shown.

The high energy peaks in the Raman spectra consist of more than one type of vibration. In the simple silicate, there is evidence for an unresolved peak at about 1025 cm^{-1} between the two large peaks at 1100 and 950 cm^{-1}. The depolarized Raman spectrum in Fig. 14 shows this peak more clearly, since the strongly polarized peaks at 1100 and 950 cm^{-1} are very weak in the depolarized spectrum. Thus there are at least three high energy peaks in the silicate glass which may be active in multiphonon relaxation, but the energies are too similar to be differentiated by these temperature dependence measurements. In the absence of information about the site occupied by the rare-earth

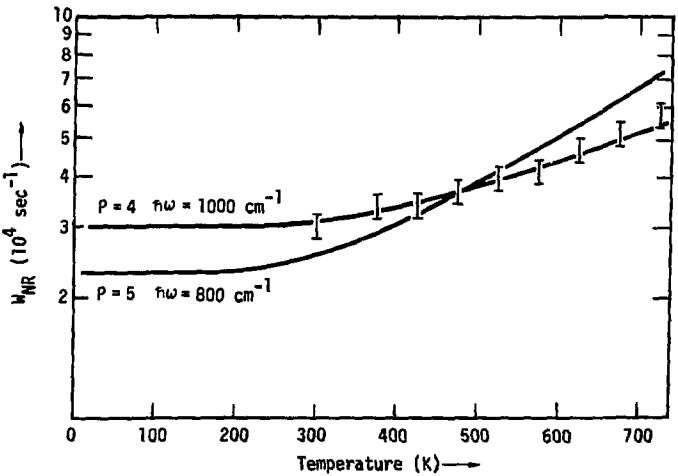

Figure 18 Temperature dependence of the Tm $^3F_4$ to $^3H_5$ decay in silicate glass. The fits to Eq. (44) with four 1000-cm^{-1} phonons and with five 800-cm^{-1} phonons are shown.

ion or the coupling of the ion in glasses, the active vibration cannot be predicted. It is clear from these results that phonons of approximately 1000 cm^{-1} are responsible for the multiphonon decay. The order of the process if not the exact phonon energy is evident from the temperature dependence.

Figure 19 shows the best fits for the Tm decays in phosphate, silicate, germanate, and tellurite glasses. The Tm decay in borate showed variation with temperature that was less than the experimental error, consistent with the low order of the process using 1400-cm^{-1} phonons. In the case of germanate glass, a radiative rate (independent of T) of 10^3 sec^{-1} has been included. This rate was calculated from Reisfeld's value[26] of the oscillator strength of the $^3F_4$ level in germanate glass. The value of 3×10^3 sec^{-1} was estimated for the radiative rate in tellurite glass by comparing the Judd-Ofelt parameters for Er in tellurite and germanate glasses with those of Tm in germanate glass.[26]

In each of the four glasses presented in Fig. 19, the observed rates are consistent with multiphonon decay involving the high energy phonons in the lowest order process subject to energy conservation. The lack of variation with temperature in the borate glass is also consistent with this model.

The number of oscillators available to take up the 4000 cm^{-1} in the Tm decay is probably large enough that the highly excited single mode terms $(n + 1)(n + 2)\ldots$ are less important than the $(n + 1)^p$ terms. However, in order to show the difference in the two temperature dependences, Fig. 20 includes a fit to the silicate temperature dependence for both types of stimulated terms. In the present work

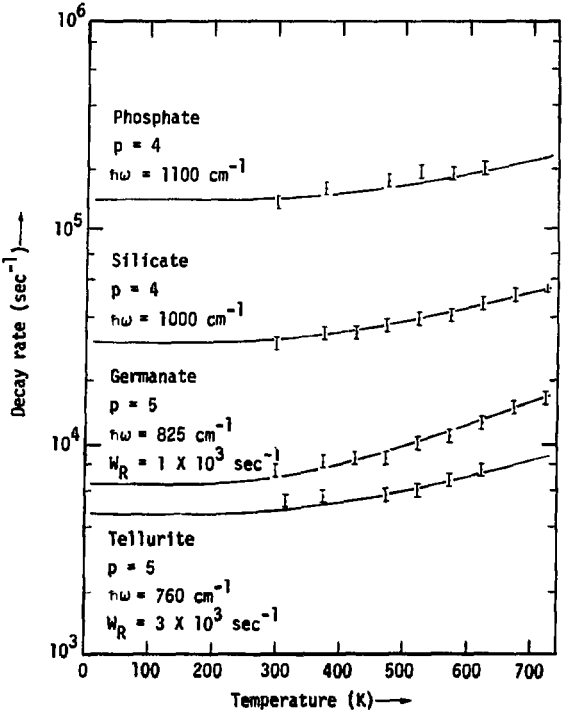

Figure 19 Temperature dependence of the Tm $^3F_4$ to $^3H_5$ decay for four oxide glasses. The number and energy of the phonons in Eq. (44) are indicated. Radiative rates were included for tellurite and germanate glasses.

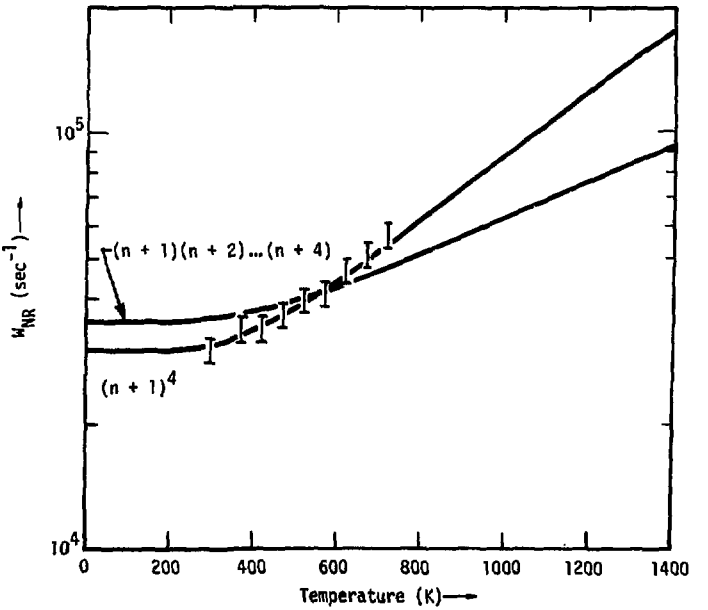

Figure 20 Tm $^3F_4$ to $^3H_5$ decay in silicate glass with temperature dependence for multimode decay, $(n + 1)^4$, and for a single mode receiving all 4 quanta, $(n + 1)(n + 2)(n + 3)(n + 4)$.

the temperature range was limited to values below the melting point of the glasses, about 800 K. The high energy vibrations in glasses are known to persist in the molten state,[40] and it is probable that these measurements could be extended to temperatures above the melting point of the glasses with the appropriate apparatus. A larger temperature range would differentiate more clearly between various phonon relaxation processes, provided that other effects such as changes in the radiative rate are negligible. Since high order processes have a greater increase with temperature, it is possible that lower energy phonons might dominate the relaxation at sufficiently high temperature, where the higher phonon occupation may make up for the small low temperature rate.

The nonradiative component of the Nd $^4F_{3/2}$ decay in laser glasses is of considerable practical importance to understanding and improving glass lasers. It is clear from the results shown in Fig. 13 that a borate glass would have low efficiency due to the high multiphonon decay rate of the laser level. The rate for silicate and phosphate glasses is expected to be less than the rate for borate from the extrapolation of the curves for these glasses in Fig. 13, and both glasses are known to be efficient as Nd laser hosts. It is not known, however, just how efficient these glasses are. The purpose of the experiment to be described below was to determine the nonradiative decay rate for the silicate laser glass ED-4.

In principle the multiphonon rate can be extracted from the observed total rate as a function of temperature, since the multiphonon rate is expected to vary as $(n + 1)^p$. The energy gap below the Nd$^4F_{3/2}$

level is about 4800 cm^{-1}, which makes the decay a fifth order process for the 1000 cm^{-1} phonons in silicate glass. In this case the radiative rate is large compared to the multiphonon rate, so the variation of the radiative rate with temperature must be accounted for. Radiative rates have been calculated[41] for the levels of Nd above the $^4F_{3/2}$, so these values can be substituted in the expression for the total rate:

$$W_R(T) = \frac{\sum g_i W_i e^{-E_i/kT}}{\sum g_i e^{-E_i/kT}} \qquad (45)$$

W_i is the radiative rate of the i^{th} level, at an energy E_i above the $^4F_{3/2}$ with degeneracy $g_i = J + 1/2$. The radiative rate can either increase or decrease with temperature according to whether the thermally populated levels have greater or smaller radiative rates than the $^4F_{3/2}$.

The complication in applying these considerations to Nd in ED-4 is that the fluorescence decay is nonexponential, resulting in a rate that varies throughout the decay, even in very dilute Nd concentrations where ion-ion interactions are negligible. The calculated radiative rates represent an average over the inhomogeneous distribution of ion sites. The observed decays become exponential at very long times, after the ions with faster radiative rates have decayed. This long term decay rate was chosen as the rate to be measured since it is uniquely defined. Using Krupke's values[41] for radiative rates in Eq. (45), the rate at 673 K was found to be 0.94 times the low temperature rate. The absolute value of the calculated radiative rate does not agree with the observed long term rate, but the factor

0.94 is a reasonable approximation to the expected decrease in the long term rate. The total rate at 673 K will be

$$W_t(673) = .94 \left(W_t(300) - W_{nr} \right) + \left(n(673) + 1 \right)^5 W_{nr} \quad (46)$$

where $W_t(300)$ is the observed total rate at 300 K, including W_{nr}, the nonradiative rate at 300 K. The Bose-Einstein occupation number n(673) was calculated for 1000-cm^{-1} phonons at 673 K, resulting in an increase in the nonradiative rate of $(n + 1)^5 = 1.87$. The two experimentally observed rates are accurate to about 5%, they are $W_t(673) = 2.67 \times 10^3$ sec^{-1} and $W_t(300) = 2.35 \times 10^3$ sec^{-1}. The nonradiative rate computed from Eq. (46) is then 600 sec^{-1}, but this result is very sensitive to the errors in the predicted radiative rate at 673 K and to the measured long term rates. For instance, a 2 percent error in the predicted temperature factor 0.94 gives a 20 percent difference in the result for the nonradiative rate. This is the most likely source of error. A 5 percent error in the observed rates contributes 20 percent uncertainty to the final result. The value of about 200 sec^{-1} from extrapolation of the curve in Fig. 13 is probably more accurate than the result derived from the temperature variation of the observed decay.

The results of the multiphonon and temperature dependence measurements provide justification for applying the multiphonon theory developed for crystals to the case of glass hosts as well. The concept of a phonon is valid for glasses, at least for the high energy localized vibrations, consistent with the model used here for a glass lattice.

All the glasses studied in this work were oxide glasses, where the rare-earth ion is coupled to the lattice vibrations through the field of neighboring oxygen ions. Comparisons between the multiphonon rates in oxide glasses are made on the basis of phonon cutoff energy. These same characteristics may not be common to other glass forming systems of interest for rare-earth hosts. Halide glasses have similar structure, but the bonds are more ionic than in oxides.[13] Chalcogenide glasses have very different structural character, and a much wider range of binary glass compositions.[13] While the phonon spectra of these glasses may be found from Raman or infrared measurements, knowledge of the phonon energies compared to oxide glasses does not imply knowledge of the relative multiphonon rates. For example, in BeF_2 glass the highest energy phonons are only about 800 cm^{-1};[15] but until multiphonon rate measurements have determined the coupling of the rare-earth ion to these vibrations, the nonradiative rates in BeF_2 cannot be predicted. Experience with a few compositions of halide or chalcogenide glasses will probably allow predictions of the behavior of other compositions based on phonon spectra.

Chapter III: Energy Transfer

A. Introduction

Ion-ion interactions are important in the operation of rare-earth lasers and fluorescent devices. When an ion is excited into a metastable level, three means are avilable for relaxation to the ground state: the ion can radiate, it can decay nonradiatively by multiphonon emission, or it can transfer its excitation to another ion. It is these latter energy transfer processes that are the subject of this section. The motivation for this work was the need for a better understanding of the interactions among the excited and unexcited Nd ions in a glass laser. Soon after the development of the Nd:glass laser, the Nd lifetime was observed to shorten as the Nd concentration was increased.[42] This is an indication of energy transfer, since the properties of the individual ions are affected by the presence of other ions.

Energy transfer of the type considered here was first encountered in nuclear magnetic resonance experiments where the relaxation time of aligned spins could only be explained by diffusion of the excitation to impurities which quenched the spins.[43] Energy transfer between rare-earth ions finds application today in infrared quantum counters or infrared to visible converters as well as in sensitizing solid state lasers. These energy transfer phenomena can have both good and bad effects on laser materials. In the "alphabet YLF" laser, Ho is the lasing ion, but Er, Tm, and sometimes Yb ions are included in the $YLiF_4$ crystalline host to effectively absorb pump light and transfer excitation to the Ho ions.[44] Concentration quenching is an example

of undesirable effects due to energy transfer.

Forster worked out the theory of fluorescence quenching for organic dyes where the excited dye molecules interact with nearby quenching molecules by a dipole-dipole interaction.[45] Dexter later applied this theory to sensitized luminescence in solids.[46] Since then, many workers have contributed to the experimental and theoretical treatment of energy transfer, so many in fact, that only those aspects of energy transfer that are relevant to the goals of this work will be mentioned here. A recent comprehensive review of energy transfer theory, experiment, and application is given by Watts.[47] Glass hosts are not ideal for experiments designed to study fundamental energy transfer processes in solids because of the inhomogeneous ion environments. The results derived from the study of crystals will be applied to glasses and particularly to silicate and phosphate laser glasses.

Energy transfer between ions in a solid can be accomplished either radiatively or nonradiatively. Only the nonradiative processes will be of interest here. Radiative transfer is easily treated by measuring the absorption and emission characteristics of the ions involved and allowing for the geometry of the experiment. Radiative transfer rates depend on the number of ions between the excited volume and the observer and their emission or absorption strength. Nonradiative transfer on the other hand is dependent on the density of ions, not on the total number.[46] In radiative transfer, the lifetime of the excited ion, as indicated by its fluorescence decay, is not affected by the presence of other ions. The other ions absorb the photons, but the rate at which the photons are emitted is not changed. The individual ion does not

"know" that other ions are present. This is not the case in nonradiative transfer, where transfer is accomplished by a coupling mechanism between the ions. For transfer to be significant, the rate of transfer from one ion to another must be comparable to the rate at which the ion radiatively decays. If the excited ion gives up its energy to an ion that does not radiate, the observed decay rate will be greater than the radiative rate, since the number of radiating ions is decreased. If the transfer occurs between like ions, the excitation is not lost, and the decay rate does not change.

In the systems of interest here, the ions are weakly coupled to each other, so that proper basis states are the isolated ion wave functions. Kenkre and Knox have discussed the difference between this weak coupling which is treated by perturbation theory and strong coupling in which the state of the system is a mixed state.[48] In this latter model, the excitation effectively oscillates between the two ions, whereas with weak coupling there is a monotonically increasing probability that the excitation will transfer.

B. Theory

The rate of energy transfer between ions is calculated here from Fermi's Golden Rule, where the coupling between the ions is treated as a small perturbation. The wave function for the calculation is the product wave function of the two ions, each in its ground or excited electronic state. For the transfer of excitation from ion A initially in excited state χ_A^* to ion B initially in its ground state χ_B, the matrix element is

$$M = \langle \chi_A | \langle \chi_B^* | H_{int} | \chi_A^* \rangle | \chi_B \rangle \tag{47}$$

The final state with A in its ground state χ_A and B in its excited state χ_B^* represents the transfer of the excitation from A to B. The rate is given by

$$W = \frac{2\pi}{\hbar} |M|^2 \rho(E) \tag{48}$$

The perturbation H_{int} can be one of several coupling mechanisms. Exchange coupling results from the overlap of the wave functions of A and B, and is consequently a very short range interaction falling off exponentially with the distance between ions. Calculation of the exchange transfer probability requires antisymmetrized wave functions, not just the products used above.[46] Although exchange interactions are identified by some authors as the effective coupling for energy transfer in systems with high concentrations of ions,[49] the low concentrations of interest here make exchange coupling a very unlikely mechanism. A second proposed transfer mechanism that will not be considered here is virtual-phonon exchange formulated by Orbach and Tachiki[50] and later extended by DeLosh and Grant.[51] The latter work predicts the same dependence of the rate on ion-ion separation as in the dipole-dipole case to be discussed below. There is at present no experimental evidence supporting the virtual-phonon interaction.

The Coulomb interaction between two ions separated by relatively large distances (~3 nm) provides sufficient coupling to bring about transfer of excitation. The expansion of the electric field of one ion gives dipole, quadrupole, etc., contributions. (The charge of the ion is compensated by the neighboring ions in the material, so

the material is electrically neutral over distances of interest here.) The energy of interaction of one dipole in the field of another dipole varies as R^{-3}, where R is the distance between the ions. A dipole-quadrupole interaction energy varies as R^{-4}, and quadrupole-quadrupole interactions as R^{-5}, etc. When this electrostatic interaction is used in the Golden Rule calculation of the rate for energy transfer, the rate varies as R^{-6} for dipole-dipole, R^{-8} for dipole-quadrupole, R^{-10} for quadrupole-quadrupole, etc., since the interaction matrix element is squared.

Dexter has shown that the dipole-dipole interaction between two ions can be expressed in a straightforward way in terms of the dipole matrix elements connecting the ground and excited states of the individual ions.[46] Since these same dipole matrix elements cause electric dipole radiation and absorption, they are easily evaluated from optical data. For ion A with normalized emission line shape $f_A(E)$ and radiative lifetime τ_A, transferring its energy to ion B with integrated absorbance Q_B and normalized lineshape $f_B(E)$, the rate of transfer is

$$W_{DD} = \frac{3\hbar^4 c^4}{4\pi n^4} \frac{1}{R^6} \frac{Q_B}{\tau_A} C_k \int \frac{f_B(E) f_A(E)}{E^4} dE \qquad (49)$$

The constant C_k is the local field correction to the dielectric constant and is generally taken to be 1. The dependence of the rate on the sixth power of the separation is evident. Qualitatively, the rate also depends on the strength of the dipole transitions of the two ions and the extent to which the energies are resonant The integral of the lineshapes, an overlap integral, gives the necessary energy con-

servation. Similar expressions for the dipole-quadrupole and higher order interactions could be derived, but the matr' elements are not available from absorption and emission data as they are for dipole-dipole transfer. Watts[47] indicates the procedure for calculating the dipole-quadrupole transition probability from known radial integrals of rare earths.

With this understanding of the interaction between two ions at a distance R from each other, the effects of these interactions among all the ions on the macroscopic properties of the system of ions will be examined. Transfer can occur between like ions, hereafter referred to as diffusion, or between unlike ions, referred to as quenching. The possibility of back transfer (A→B→A) will be neglected. In the cases of interest here, the B ion rapidly relaxes from the resonant state to a lower nonresonant level that cannot transfer back to the A ion. Diffusion does involve back transfer.

Diffusion alone in a system of excited ions is not observable in a fluorescence decay experiment, since the decay rate is not changed by the diffusion of the excitation among the ions. Quenching of excited ions of one variety to unexcited ions of a second variety is observable either as an increase in the decay rate of the initially excited ions or as characteristic fluorescence from the previously unexcited quenching ions. The effects of diffusion become observable through the combination of quenching and diffusion, so quenching will be treated first.

When a random distribution of ions of type A are excited into a metastable electronic state, each ion has the same probability for

radiative decay, resulting in a purely exponential fluorescence decay for the ensemble of ions. If quenching ions of type B are also present and randomly distributed in the material, some of the excited A ions will be sufficiently close to a B ion for energy transfer (quenching) of the excitation from A to B. Since the transfer probability varies inversely with the distance between ions, some A ions will be so far from the nearest B ion that they will only decay radiatively. The rate of decay for any ion is just the sum of the radiative rate and the transfer rate, so the decay rate of individual A ions will vary as the distances to nearby B ions varies in a random way. Only ions with identical environments will have identical decay rates. The observed decay of the collection of A ions will no longer be determined by a single rate, but by a sum of exponential decays with some distribution of decay rates. Those ions which are near quenching centers will decay rapidly, so the decay rate at short times after excitation will be large; after these ions have decayed, only those ions with no quenching ion nearby will remain excited and the decay rate will be just the radiative rate. Therefore quenching in the absence of energy migration among the A ions will be characterized by a nonexponential fluorescence decay with the rate approaching the purely radiative rate at long times.

Forster developed the theory of quenching, assuming dipole-dipole interactions between dye molecules.[45] He showed that for a uniform distribution of quenching ions the spatial average of the quenching transitions gives a decay function following short pulse

excitation of the form

$$\phi(t) = \exp\left\{-\frac{t}{\tau} - CN_q t^{1/2}\right\} \tag{50}$$

where τ is the radiative lifetime, and N_q is the concentration of quenching ions. A more general derivation of the quenching rate in the absence of diffusion gives[49]

$$\phi(t) = \exp\left\{-\frac{t}{\tau} - \Gamma\left(1-\frac{3}{s}\right)\frac{N_q}{N_0}\left(\frac{t}{\tau}\right)^{3/s}\right\} \tag{51}$$

where $s = 6$ for dipole-dipole, $s = 8$ for dipole-quadrupole, and $s = 10$ for quadrupole-quadrupole interactions. $\Gamma(x)$ is the gamma function, and N_0 is the critical concentration at which the probability for quenching is equal to the radiative probability. Several authors have attempted to use this fluorescence decay function to determine which multipole term is responsible for quenching in various systems.[52] Inokuti and Hirayama have given a similar nonexponential function for exchange coupling.[49] It is difficult to distinquish between an initial decay that varies as $t^{1/2}$ (dipole-dipole) and one that varies as $t^{3/8}$ (di; -quadrupole), since these dependences hold only at very early times after excitation. When diffusion among the excited ions is taken into account, it becomes even more difficult t- determine s from fluorescence decay curves.

A series of theoretical decay curves for different concentrations of quenching ion are shown in Fig. 21 where Eq.(50) for dipole-dipole interactions was used. It is important to note that at very long times the slope of the decay curves on a semi-logarithmic plot

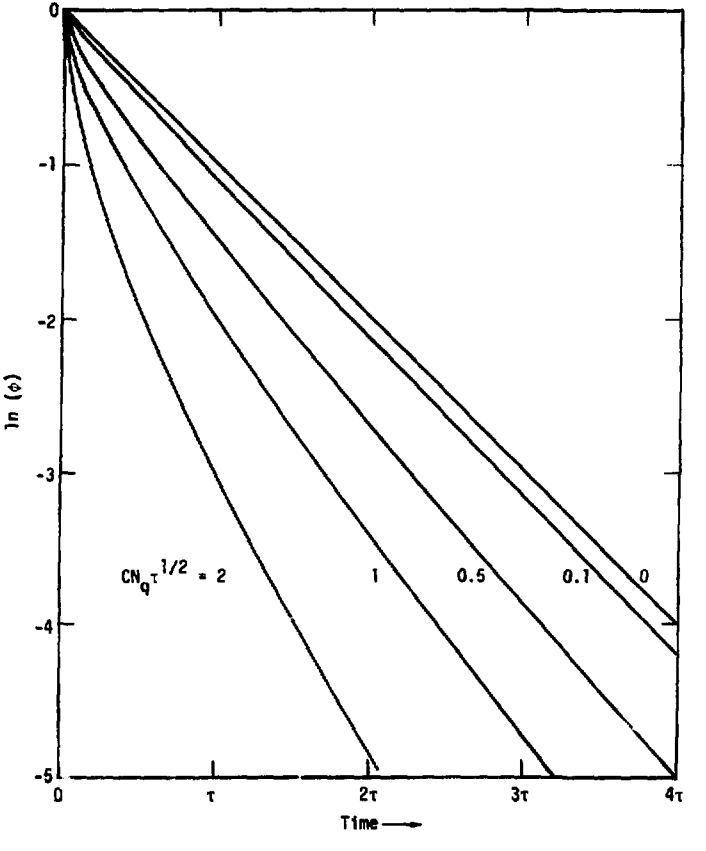

Figure 21 Fluorescence decay with dipole-dipole quenching. The log of the fluorescence from Eq. (50) is plotted as a function of time in units of the radiative lifetime τ, for $CN_q = 0$, $.1/\tau^{1/2}$, $.5/\tau^{1/2}$, and $2/\tau^{1/2}$.

all become equal to the radiative rate, indicating that all ions near quenching centers have already decayed.

It is common to approach the problem of energy transfer experimentally by measuring quantum efficiencies. Quantum efficiency is defined as the ratio of the number of ions that decay radiatively to the number of ions initially excited. These experiments are difficult, since geometry, excitation density, absorption, or other changes from sample to sample affect the measured values of quantum efficiency. Studying the time dependence of the fluorescence decay is independent of geometry and in this way is less subject to error. Quantum efficiency measurements give the integral of the decay function over time, with proper allowance required for pulsed or continuous excitation.[53]

Diffusion of the energy among the ions of type A, the active ions, may be faster than the quenching interaction since diffusion is generally a resonant process. For rare-earth ions there is no Stokes shift, so the transition from the metastable level of an excited ion to its ground state is exactly resonant with the transition from the ground state of an identical ion nearby to its excited metastable level. This assumes that all ions of type A have the same energy levels, which is not the case for the inhomogeneously broadened levels found in rare-earth ions in glass. The decrease in the transfer rate between ions in different crystal field environments results from a decrease in the overlap integral in Eq.(49) when $f_A(E)$ and $f_{A'}(E)$ are shifted in energy.

The diffusion of excitation among ions in a solid is different from the case of diffusion of a gas, since the excitation is moving from one discrete site (ion) to another and not moving along a continuous path as a molecule in a gas moves. This discontinuous hopping of the excitation can be approximated as classical diffusion, although Artamonova et al.[54] find that the diffusion in the Nd: glass system is best described by a stepwise rather than continuous theory. The evidence for a distinction between the two descriptions is not compelling, and the simpler case of classical diffusion will be used here.

Although diffusion is a spatial process, in the case of inhomogeneous ion systems, it may be manifest as spectral diffusion. Recently fluorescence line narrowing experiments have exhibited spectral diffusion directly. With narrow bandwidth laser excitation it is possible to excite only those ions in an inhomogeneous distribution which have local environments that give rise to an energy level that is resonant with the laser line. Other ions in different sites are not excited since they have no energy level resonant with the laser. The emission from the selectively excited ions is characteristically narrow, reflecting the homogeneous linewidth of the ions. After a short laser pump pulse, diffusion of the excitation from the selectively excited ions to all the other ions in the inhomogeneous distribution will cause the initial narrow fluorescence to gradually broaden until the full inhomogeneous line is observed. The characteristic time of this spectral diffusion is the same as the spatial diffusion time. Both types of diffusion will be temperature dependent, since phonon energy is required to make up the difference between nonresonant ions.

Spectral migration has been observed in Eu^{3+} in glass in fluorescence line narrowing experiments,[55] and this technique represents the best prospective method for directly measuring the diffusion rate in Nd:glass.

Forster's treatment of quenching was in the limit of no diffusion of the excitation in the A molecules. The other extreme, quenching with very fast diffusion, gives a particularly simple result, namely exponential decay. In between the extremes of no diffusion and fast diffusion, the theory is more complicated. In fast diffusion, the initially uniform distribution of excited ions remains uniform, since as soon as an ion is quenched or radiates, the diffusion process re-distributes the remaining excitation uniformly throughout the medium. This is not the case with no diffusion where quenching ions are surrounded by an ever increasing sphere within which there are no excited ions. The total decay with fast diffusion will be determined by those ions which are closest to quenching centers and thus have the fastest decay rates, but the rate will be independent of time since the distribution of excitation is always the same. A decay rate that is independent of time leads to a pure exponential fluorescence decay.

Matnematically the number of excited ions as a function of time is given by

$$\frac{\partial N^*}{\partial t} = -\frac{N^*}{\tau} - N^* N_q W_M \tag{52}$$

$$N^*(t) = \exp\left\{-\frac{1}{\tau} - N_q W_M\right\} \tag{53}$$

W_m is the quenching rate for those ions that are closest to quenching ions. This is the same result as the Stern-Volmer model for energy transfer that is independent of the distance between ions.[49] The details of the configuration averages that lead to Eq. (53) have been worked out by Grant[56] who pointed out that the form of the decay is independent of the model for ion-ion interaction when fast diffusion is active.

Figure 22 shows the expected fluorescence decays for various concentrations of quenching ions, again plotted on a semi-logarithmic scale, assuming fast diffusion.

Yokota and Tanimoto have worked out the expected fluorescence decay when both quenching and diffusion are active and diffusion is not fast enough to maintain the initial distribution of excitation.[57] The differential equation that describes the interaction of quenching, diffusion, and radiative decay is[57]

$$\frac{\partial N^*}{\partial t} = -\frac{N^*}{\tau} + D\nabla^2 N^* - \sum_i W[R_i(t)]\, N^* \qquad (54)$$

$W[R_i(t)]$ is the interaction rate between A and B ions separated by R which is a function of time, since the distribution of excited ions changes with time as those near quenching centers decay. Assuming dipole-dipole interaction between A and B ions, $W_{AB} = CR_{AB}^{-6}$, the decay is described by

$$\phi(t) = \exp\left\{-\frac{t}{\tau} - \frac{4}{3}\pi^{3/2} N_B C^{1/2} t^{1/2} \left(\frac{1 + 10.87\,x + 15.50x^2}{1 + 8.743\,x}\right)^{3/4}\right\} \qquad (55)$$

where $x = DC^{-1/3}t^{2/3}$, and D is the diffusion constant for A to A transfer. N_B is the concentration of quenching ions.

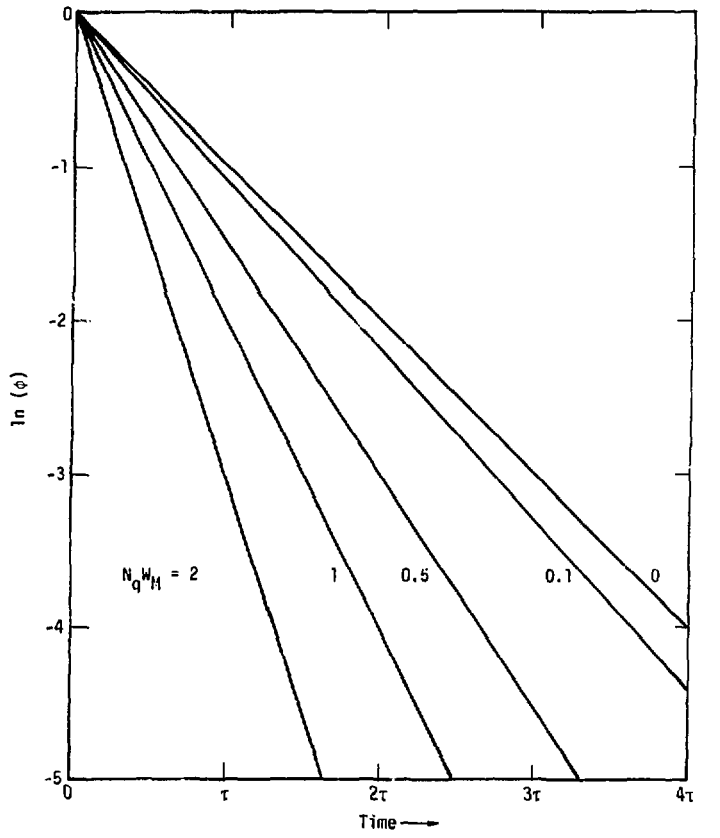

Figure 22 Fluorescence decays with fast diffusion. Equation (53) is plotted for values of NqW_M from 0 to $2/\tau$.

The previous expression for quenching in the absence of diffusion follows from Eq. (55) with D = 0. The fast diffusion limit described earlier does not follow directly from this expression. The most interesting characteristic of Eq. (55) is its behavior at long times, a regime that is most easily investigated experimentally. After all the excited A ions that are situated near quenching B ions have given up their excitation, the rate of quenching is limited by the diffusion of excitation to those A ions that are near B ions. This long time behavior is referred to as diffusion-limited relaxation, and is characterized by exponential decay at long times.[58] In the limit as t goes to infinity, the fluorescence decay function becomes

$$\phi(t) = \exp\left\{-\frac{t}{\tau} - \frac{t}{\tau_D}\right\} \tag{56}$$

$$\frac{1}{\tau_D} = 0.51\ (4\pi N_B C^{1/4} D^{3/4}) \tag{57}$$

The decay rate at long times is proportional to the concentration of quenching ions and to the diffusion coefficient to the 3/4 power. C in this equation is the coefficient of A to B transfer from $W = C_{AB}R^{-6}$. The diffusion coefficient is related to the rate of energy transfer from A ion to nearest neighbor A ion:[43]

$$D = WR_0^2 \tag{58}$$

For dipole-dipole interactions between the A ions, D is proportional to R^{-4} and thus to the concentration of A ions to the 4/3 power:

$$D \propto \frac{C_{AA}}{R^6} R^2 = \frac{C_{AA}}{R^4} \propto N_A^{4/3} \text{ since } N_A \simeq \frac{1}{R^3} \tag{59}$$

The diffusion-limited decay as a function of the concentrations of both A and B ions is

$$\phi(t) = \exp\left\{-\frac{t}{\tau} - k_2 N_A N_B t\right\} \tag{60}$$

where k_2 is a constant proportional to C_{AA} and C_{AB}.

In summary, the complete expression for diffusion and quenching through dipole-dipole interactions shows $\exp(-k_1 N_B t^{1/2})$ dependence at short times after excitation and exponential decay at long times with a decay rate of $1/\tau + k_2 N_A N_B$. The transfer rate can be calculated at least approximately for a particular ion system, so the constants k_1 and k_2 or the constants C and D in the complete expression can be approximated from optical absorption and emission data through Eq. (49).

The results of energy transfer theory will be applied to the Nd:glass system, first to analyze the fluorescence decay of Nd and then to consider the possibilities of improving Nd laser efficiency by adding sensitizing ions such as Ce^{3+}. The effect of multiphonon decay of the Nd $^4F_{3/2}$ will be neglected in the following. Since this relaxation was found to be a small effect, it may be considered as a small addition to the radiative rate.

C. Nd Fluorescence Decay Measurements

The basic experimental technique for studying energy transfer in Nd:glass was recording the Nd fluorescence intensity as a function of time. This was accomplished by pumping the sample with a short (300-ns) laser pulse, and monitoring the fluorescence with a photomultiplier

and oscilloscope that were fast enough to follow the decay. The differences between exponential and nonexponential decay are very slight, so very small experimental errors are essential in order to be able to characterize such subtle effects as quenching and diffusion.

The Nd fluorescence experiments were begun before the Tektronix signal-averaging system described earlier was available. Initially, the fluorescence decay curves were photographed from an oscilloscope face and hand plotted on a semi-logarithmic scale. The distortions on the oscilloscope face were larger than the effects of nonexponential decay, so an improved method was developed. Figure 23 shows the experimental setup for fluorescence measurements using the transient digitizer to record the Nd fluroescence. The Chromatix YAG laser operating at 532 nm excited the Nd ions in the sample, and the fluorescence was monitored with a photomultiplier (56CVP S-1 response). A Biomation Model 802 transient recorder captured the signal in digital storage. After one shot, the signal was clocked out of the transient recorder to an X-Y-Y' recorder. The X channel on the recorder plotted time, the Y channel was the signal intensity, and the Y' channel was the logarithm of the intensity obtained from an electronic log converter (Hewlett-Packard 7562A).

The log converter was used for preliminary measurements, but baseline drift made it inaccurate for precise fluorescence studies. Logarithmic plots were generated from the linear plots either by hand plotting or after the data had been stored in the computer.

A more detailed schematic of the fluorescence decay apparatus is shown in Fig. 24. The system is triggered to receive a signal by a PIN diode into which a portion of the laser pulse is directed.

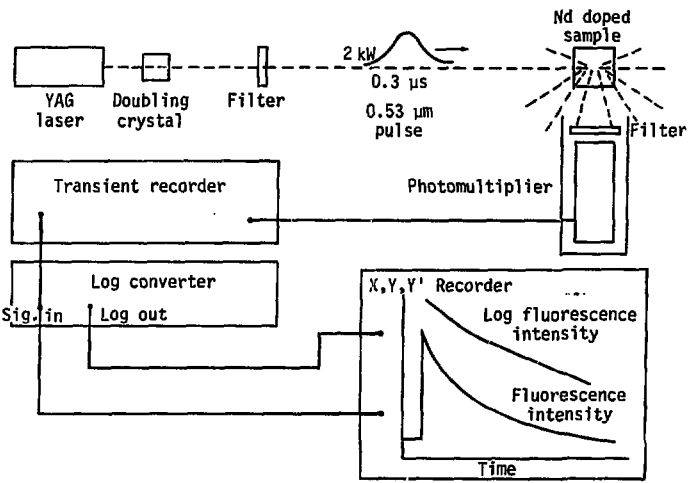

Figure 23 Schematic diagram of the apparatus to record Nd fluorescence decays.

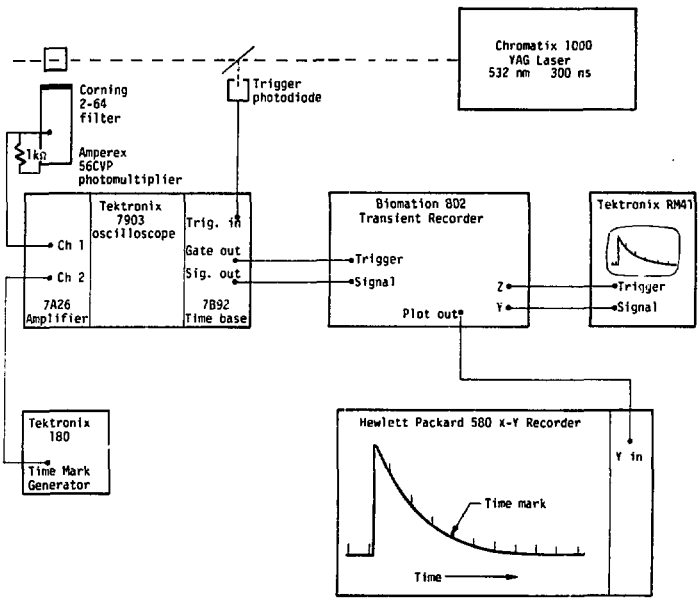

Figure 24 Details of the fluorescence decay experiment electronics.

The signal from the photomultiplier and the time marks are added in the 7A26 amplifier, and the sum provides the signal input to the Biomation transient recorder. An enable switch on the transient recorder resets its trigger to receive one shot. After triggering, the fluorescence signal is digitized into 1000 channels, corresponding to 0.5 or 2 μsec per channel, depending on the time base selected. The amplitude resolution of the transient recorder is 0.4%. After one shot is recorded, the stored signal is displayed on the RM 41 oscilloscope for visual inspection. If the amplitude and timing are appropriate, the plot switch on the Biomation recorder is actuated manually and the signal is plotted out on the X-Y plotter.

The time marks provided a check of the time linearity and calibration, but amplitude linearity was more difficult to verify. The eventual solution was to record the fluorescence decay of a Nd doped sample which had a very pure exponential decay. After several dilute samples were evaluated, Nd in glass was rejected as a standard for calibration since the inhomogeneous distribution of ion sites in glasses gave a nonexponential decay even at the lowest concentrations available. A sample of 0.1 weight percent Nd in $YAlO_3$ showed a pure exponential decay with 182-μsec lifetime over four lifetimes, and so was chosen as the linearity check.

The large plot of the fluorescence decay was either hand plotted on a semi-logarithmic scale or converted on a computer interfaced digitizing table to computer cards with time and relative intensity. The card decks were input to the computer system and stored as a data file.

Several alternative experimental setups were tried, but none of the others gave adequate linearity in amplitude to allow accurate description of the decay over three or four lifetimes. Phase sensitive detection was not effective, because of variations in the laser output intensity during the time required to scan a decay. The same problem plagued the boxcar averager, even when a second channel to normalize the laser intensity was included. Signal averaging with exisiting commercially available equipment was unsuccessful because the initial portion of the decay requires fast detection, and the signal averagers could not follow the signal. An arrangement with the Biomation signal averager capturing a signal and clocking the signal out slowly to a signal averager permitted averaging of as many decays as necessary. However, the signal to noise ratio was so high for a single shot with the transient recorder that additional averaging was unnecessary. The limitation was the amplitude resolution of the transient recorder. By taking one shot with the signal peak on scale and a second shot with the same timing but a more sensitive amplitude scale, a curve could be pieced together over four or more lifetimes (down to $e^{-4} = 0.02$ or less).

It was very important to accurately record the initial portion of the decay where the $\exp(-kt^{1/2})$ behavior is expected. With the 300-ns pulse and proper geometry and filtering, the apparatus used here gave a reliable signal within about 2 μsec after the pump pulse. Subsequent experiments with the new fast transient recorder described in the section on multiphonon decay have shown no detectable

errors in the fluorescence decay results.

The relaxation processes for Nd^{3+} in glass are shown in Figure 25. At very low concentrations, less than one weight percent, practically all the excited ions fluoresce from the metastable $^4F_{3/2}$ level to one of the ^4I levels. The ^4I levels relax nonradiatively to the ground $^4I_{9/2}$ level by multiphonon emission. The $^4F_{3/2}$ multiphonon emission may be ignored, consistent with the earlier estimate of this rate. At higher concentrations, the energy transfer processes shown in Fig. 25 take place. Energy migration between an excited Nd ion and a nearby ground state Nd results in no loss of excitation; but the quenching process, this time between two Nd ions, results in a loss of excitation. This mechanism for concentration quenching was proposed by Peterson and Bridenbaugh[59] for Nd in $NaWO_4$, and Snitzer proposed that it is responsible for similar quenching in Nd:glass.[42] Since the coupling between the Nd ions is weak, the rates of transfer are small and transfer cannot compete with multiphonon decay for any levels except the metastable $^4F_{3/2}$.[59] The quenching process that is active in Nd glass is described by the previous theory with the only change being the replacement of the quenching B ions with some constant fraction of the A ions.

Due to the inhomogeneous nature of the glass environment, the Nd fluorescence decay is nonexponential even in the limit of zero concentration. Maurer attempted to account for this behavior by assuming a distribution of radiative rates, weighted by the fraction of ions with these rates.[60] Although this is possible in principle, it would require experimental accuracy much better than was achieved

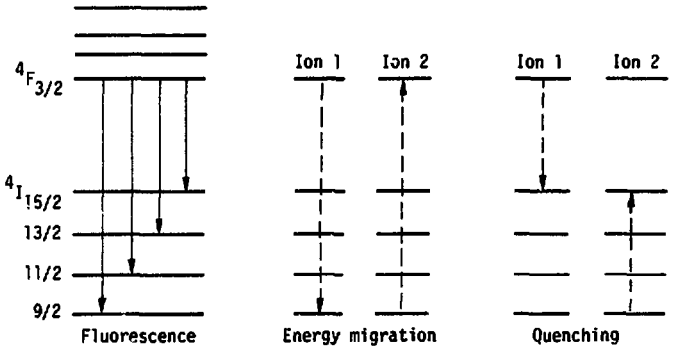

Figure 25 Decay modes of Nd^{3+} in glass.

in these experiments to uniquely determine the range of radiative rates and the weighting function that gives the fraction of ions with a particular rate.

Experiments using narrow-band excitation of fluorescence in glasses could determine the range of radiative rates and the weighting, since only ions in a particular environment are excited. Preliminary observation of radiative rate variation with excitation wavelength at low temperatures indicates 100% variation of the rate with site variations.[61] In order to determine how many ions are in a particular site, both the radiative rate and the absorption coefficient of the exciting radiation must be recorded. The absorption coefficient is proportional to the number of ions and to the spontaneous transition rate. The primary difficulty in performing these experiments is the requirement for a tunable narrow-band laser operating at about 880 nm, the pump wavelength from the ground state to the $^4F_{3/2}$ level.

The fluorescence curve of 0.1 weight percent Nd_2O_3 in ED-2 glass demonstrates the nonexponential nature of the decay. Figure 26 shows the observed fluorescence signal and the semi-logarithmic plot showing the deviation from a pure exponential. The decay rate is the slope of the semi-logarithmic plot. The decay approaches an asymptotic rate of 2.27×10^3 sec^{-1}, but the initial rate is approximately 3×10^3 sec^{-1}. Determination of the initial rate is more ambiguous than finding the final rate, since the rate is changing rapidly early in the decay but reaches a constant value at long times (when the signal is $<e^{-3}$ of the initial value). This inhomogeneous quality of rare-earth ions in glasses has several consequences for

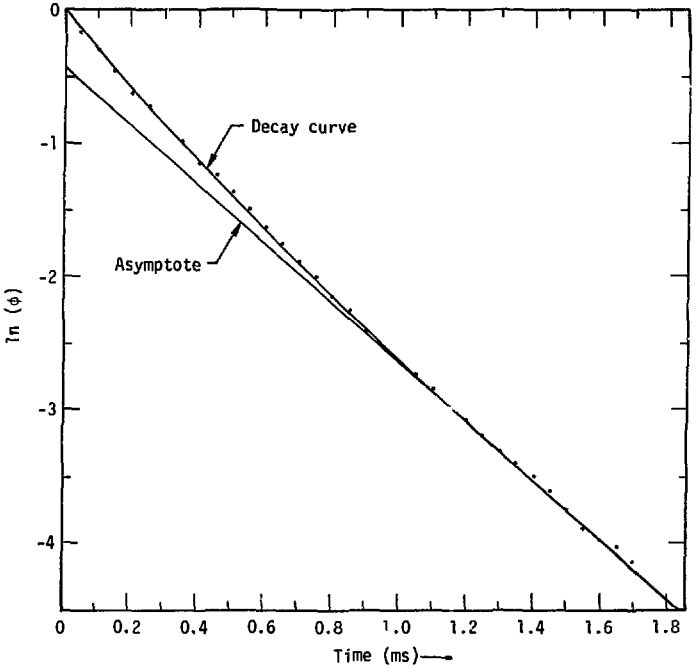

Figure 26 Fluorescence decay of 0.1 wt.% Nd_2O_3 in ED-2 glass. The asymptote is the long term decay rate.

experiments on glasses; in the present case it makes quantitative experiments on energy transfer difficult. Similar behavior was found in every glass for which a very low concentration sample was available, although the initial and final rates varied from glass to glass. The Judd-Ofelt calculations of the radiative rate of Nd in glasses are based on absorption spectra which characterize the weighted distribution of ion sites, and the resulting rate represents that of an average ion. For example, the calculated rate for Nd in ED-2 glass is 2.7×10^3 sec^{-1}, in between the initial and long term rates observed.[31] The question of what rate should be used in laser design calculations will be examined in detail in a later section.

The decay curves for the concentration series 1, 2, 3, and 6 wt.% Nd_2O_3 in ED-2 laser glass are shown in Fig. 27. The overall rate of decay increases as the concentration of Nd ions increases, and the deviation from a pure exponential decay increases as well. Very similar families of curves were plotted for LSG-91H silicate glass and for LHG-5 phosphate glass. Both of these glasses are commercially available laser glasses, as is ED-2, but the exact compositions are proprietary information. It is clear from these fluorescence curves that the average rate of decay of the excited Nd ions increases to more than twice the low concentration value when the Nd concentration increases to 6 weight percent. This indicates a quantum efficiency of only 50% at the high concentration, whereas it is near 100% at very low Nd concentration.

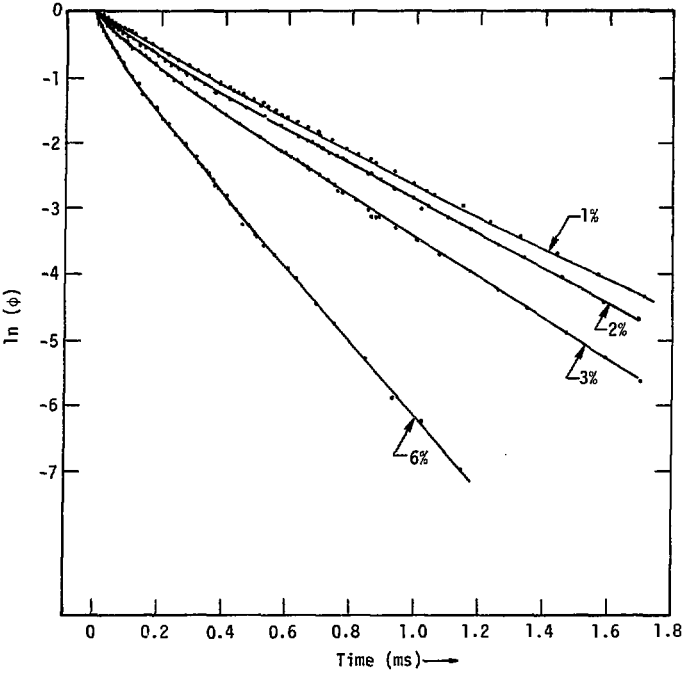

Figure 27 Fluorescence decay curves for 1-, 2-, 3-, and 6- wt.% Nd_2O_3 in ED-2 silicate laser glass.

D. Diffusion-Limited Decay

The behavior of the fluorescence decays at long times is consistent with diffusion-limited decay described by Eq. 56. Since the Nd ions are both the diffusing and quenching species in the present case, the diffusion-limited decay should be given by

$$\Phi(t) = \exp\left\{-\frac{t}{\tau} - k_2 N^2 t\right\} = e^{-(\frac{1}{\tau} + W_D)t} \qquad (61)$$

where N is the Nd concentration in ions per cm^3. This assumes dipole-dipole coupling between the ions. Diffusion-limited decay has not been solved for the dipole-quadrupole case, but the dependence on concentration should be greater. Substituting R^{-8} dependence for the diffusion constant, the diffusion-limited rate would vary as $N^{5/2}$. This is not strictly correct, since it still assumes dipole-dipole coupling for the quenching transition, but it gives a minimum dependence on N for dipole-quadrupole coupling. Dipole-quadrupole coupling is forbidden for both the diffusion and quenching transitions in Nd by the $\Delta J \leq 2$ selection rule for reduced matrix elements for dipole-quadrupole transitions.[47] Crystal field mixing of other J states will break this selection rule, but this will be a small effect compared to the allowed dipole-dipole transition rates.

Taking the long term rate for the low concentration as the radiative rate $1/\tau$, the diffusion-limited rate was obtained from the final decay rate for ED-2. These results are displayed on a log-log plot in Fig. 28, where diffusion-limited rate $W_D = W_{final} - 1/\tau$ is plotted versus N. The slope of a curve on this plot gives the

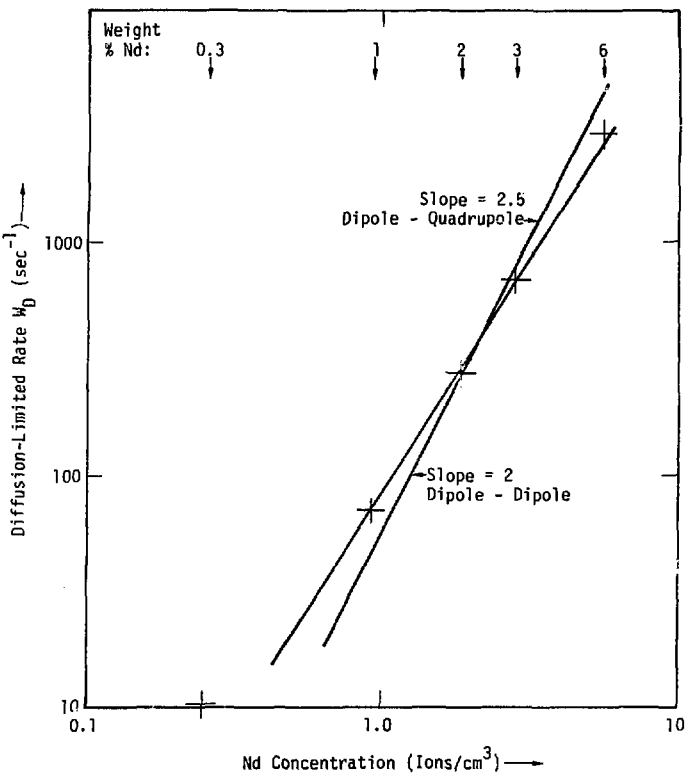

Figure 28 *Log-log plot of the diffusion-limited rates in ED-2 glass. The Nd concentrations in wt.% are shown at top. A slope of 2 on this plot indicates* $W_D \propto N^2$.

power of the dependence on N. A line with slope of 2 and one with slope of 5/2 are shown for comparison. The first low concentration point is very sensitive to the value chosen for the radiative rate, but the concentrations above 1 wt.% are well described by a rate proportional to N^2.

Concentrations are conveniently expressed in weight percent for the purpose of mixing the constituents of a glass, but ions per cm^3 are more appropriate for energy transfer experiments. The relation between ions per cm^3 and wt.% is

$$N(cm^{-3}) = \frac{\text{wt \% } Nd_2O_3 \times 100 \times \text{glass density}(g/cm^3) \times 2 \times 6.02 \times 10^{23}}{\text{molecular weight of } Nd_2O_3 \text{ (g)}}$$

Figure 29 shows the long term decay rates as functions of Nd concentration squared for several glass compositions. On this type of plot, a straight line indicates dependence on N^2 and the slope of the line is k_2 in Eq. (61). Only one glass was found to deviate markedly from N^2 dependence of the long term rate. The phosphate glass series P-107 showed a more nearly linear dependence on concentration. This result is uncertain because the glass composition from one sample to the next in the series was not uniform. Phosphate glasses melted in small experimental quantities, as in the P-107 series, have shown variable composition in several cases. Since the commercially developed phosphate glasses showed the same N^2 dependence as the silicate glasses, it is unlikely that the P-107 series indicates a fundamental difference; this is most likely a spurious result. Kraevskii et al. report a linear dependence for energy transfer in

phosphate glasses, but the citations given are incorrect so the original results could not be located.[62] The relative Nd concentrations within each glass series were checked by optical absorption measurements. Due to the changes in absorption strength with glass composition, one series could not be checked against another.

The results of all the long term decay rate experiments support the conclusion that Nd ions are themselves the quenching centers for Nd excitation, and that the energy migrates through the Nd system by dipole-dipole interactions until a quenching Nd is encountered. It is not clear from these results whether a Nd ion in a particular crystal field environment is always a quenching center or that any Nd ion can exchange energy by both quenching and diffusion with different probabilities. It is clear that the quenching centers are not Nd pairs, because the number of quenching centers would be proportional to N^2 in that case, resulting in a long term rate varying with N^3. ($N_B \propto N_{Nd}^2$ and $D^{3/4} \propto N_{Nd}$ so $W_D \propto N_{Nd}^3$ for quenching by pairs.)

Other possible explanations of the observed quenching behavior include quenching to impurities introduced with the addition of Nd_2O_3 to the glass. While this would lead to the number of quenching centers proportional to Nd concentration, the careful chemical analysis of commercial laser glasses carried out at this laboratory and elsewhere show no evidence of impurities. Rare earths are difficult to isolate from other rare earths, but the development of efficient rare-earth lasers has depended on high purity chemical components.

The y-intercepts of the curves in Fig. 29 give the long term radiative rates in the glasses, and the slopes of the lines give

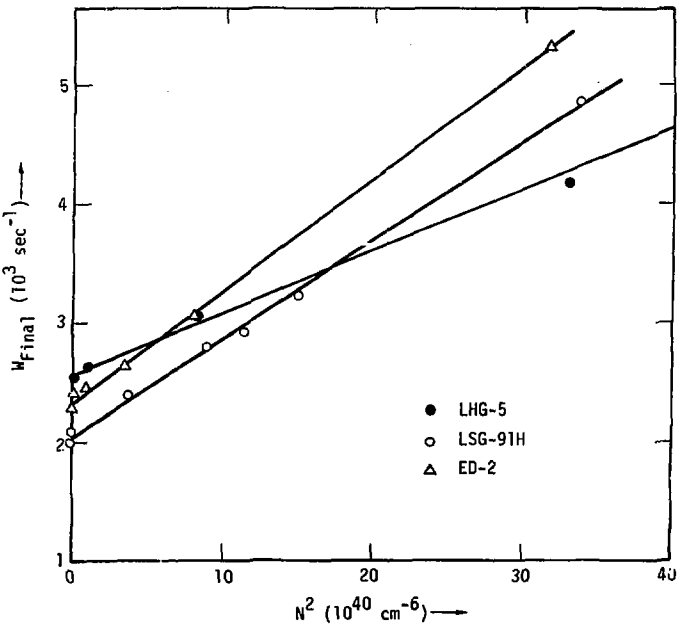

Figure 29 Long term Nd fluorescence decay rate as a function of concentration squared for ED-2 and LSG-91H silicate glasses and LHG-5 phosphate glass.

the constant k_2. From Eqs. (57) and (59), k_2 is proportional to $C_{AB}^{1/4}$ and to $C_{AA}^{3/4}$:

$$k_2 \propto N_B\, C_{AB}^{1/4}\, D^{3/4} \propto N_B\, N_A\, C_{AB}^{1/4}\, C_{AA}^{3/4} \tag{62}$$

C_{AB} is the coefficient of energy transfer for the quenching interaction, and C_{AA} is the coefficient for the diffusion interaction. From Eq. 49 they reflect the strength of the transition and the overlap integral for absorption and emission:

$$C_{AB} \propto W_A Q_B \int \frac{f_B(E)\, f_A(E)}{E^4}\, dE \tag{63}$$

$$C_{AA} \propto W_A Q_A \int \frac{f_A(E)\, f_A(E)}{E^4}\, dE \tag{64}$$

where $W_A = 1/\tau_A$. Since k_2 is a stronger function of C_{AA}, it is likely that the resonant overlap integral would have the major effect on determining the slopes in Fig. 29. Only LHG-5 has a significantly different slope. This may result from a lower value of C_{AB} that is a consequence of energy mismatch (low value of the overlap integral) for the quenching transition. Although narrow line widths increase the resonant overlap integral, they would have the opposite effect on slightly offset lines, where the high energy tail of one line overlaps the low energy tail of the other.

The line widths of Nd in glass are a combination of the Stark splittings of the electronic levels and the inhomogeneous displacements of the Stark components for ions in different crystal field environments.

The overlap integral for a given pair of ions in different environments is not the integral of the absorption and emission line shapes observed in the bulk sample; it is the overlap of the narrow Stark levels of one ion with those of the other. The homogeneous linewidths of the Stark levels may change from site to site, and the Stark splitting certainly changes. The expression for the transfer rate in Eq.(49) overestimates the probability for transfer in an inhomogeneous material if the observed absorption and emission spectra are used in the overlap integral, whether for the resonant process (diffusion) or for the quenching transition. Measurements of the diffusion-limited rates do not allow separation of quenching and diffusion terms, since the product $C_{AA}^{3/4}\, C_{AB}^{1/4}$ enters along with a fraction giving the number of Nd ions that are effective as quenching centers.

E. Complete Decay Function

The full fluorescence decay of Nd in glass should follow the expression for quenching and diffusion developed by Yokota and Tanimoto[57] for the case of dipole-dipole coupling, since the diffusion-limited results are consistent with this coupling mechanism. Equation 55 modified for the case of Nd ions as both quenchers and fluorescing ions becomes

$$\Phi(t) = \exp\left\{-\frac{t}{\tau} - \frac{4\pi^{3/2}}{3} NC^{1/2} t^{1/2} \left(\frac{1 + 10.87x + 15.50x^2}{1 + 8.743x}\right)^{3/4}\right\} \quad (65)$$

$$x = DC^{-1/3} t^{2/3}$$

N is the number of Nd ions per cm^3, C is the coefficient for the quenching process from $W_{AB} = C\ R^{-6}$, and D is the diffusion coefficient which should be proportional to $N^{4/3}$.

E. J. Goodwin and J. B. Trenholme created a computer program to fit the experimentally observed fluorescence decays to the function in Eq. (65), hereafter referred to as the Y-T expression. The computer program was designed to run on the CDC 7600 computer system at the Lawrence Livermore Laboratory, and was named NURD. The procedure for fitting the Y-T expression was first to compute the value of the function at the times for which data points were input, using initial guesses for the parameters C, D, and τ. The square of the deviation of the function from each data point was then summed, with appropriate weights for each point; this sum was called χ^2. A subroutine then minimized χ^2 by a method known as a creeping simplex technique.[63] Simply stated, the creeping simplex routine searches for the minimum of a function by varying the parameters of the function according to set rules. The functional form of the Y-T expression, the parameters, and the limits within which the parameters could vary were inputs for NURD.

The fitting routine could provide excellent fits of the Y-T expression to the data points for a particular concentration of Nd; this was not a verification of the theory, but an indication that two or three parameters were adequate to fit such smooth curves. The test of the theory was the equivalence of the values C, D, and τ from one concentration to the next. In this regard the program was only partially successful.

A typical fit of the Y-T expression to the fluorescence curve of ED-2 with 3 wt.% Nd_2O_3 is shown in Fig. 30. A linear and a semi-logarithmic plot are provided by NURD, as well as contour plots showing the minimum of χ^2 as a function of each pair of parameters. In the case shown, the radiative rate $1/\tau$ was constrained to be between 2.32 and 2.33 x 10^3 sec $^{-1}$, while C and D and the intensity at $t = 0$ were allowed to vary. The fit is very good, but that is to be expected for a three parameter fit to a smooth curve, even if the functional form were not exactly correct. Similar fits for a wide range of choices of constraints and relative weights failed to give systematic agreement for the values of C and D. C should be constant for all concentrations of Nd, and D should be proportional to $N^{4/3}$ if the Y-T expression correctly describes the decay.

The best results for the Y-T expression obtained for the ED-2 concentration series are shown in Table II. C varies from 1 to 2 x 10^{-40} sec^{-1} cm^6 and $D/N^{4/3}$ varies from 0.6 to 1.7 x 10^{-39} sec^{-1} cm^6. Similar values and variations were found for the LSG-91H concentration series. In spite of the variation by a factor of two or three in the parameters, the results of the computer fitting indicate the strengths of the diffusion and quenching interactions. Using these values, the rates for quenching and diffusion between an excited Nd ion and a neighboring ground state ion separated by the average interion distance in 3% ED-2 glass (1.5 nm) are

$$W_{QUENCH} = \frac{C}{R_{AV}^6} = \frac{1.5 \times 10^{-40}\ sec^{-1}\ cm^6}{(1.5 \times 10^{-7}\ cm)^6} = 13\ sec^{-1} \qquad (66)$$

$$W_{DIFF} = \frac{D}{R_{AV}^6} = \frac{1 \times 10^{-39}\ sec^{-1}\ cm^6}{(1.5 \times 10^{-7}\ cm)^6} = 88\ sec^{-1} \qquad (67)$$

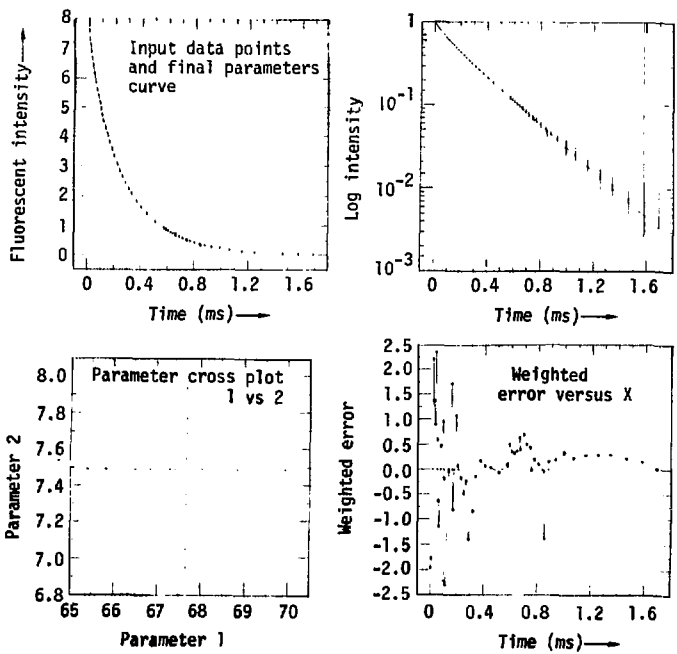

Figure 30 Plots generated by the computer program NURD. Top left is a linear plot of the fluorescence decay data and the fit to the Y-T expression. Top right is the semi-log plot of the same data and fit (note that this is base-10 log rather than natural log used previously). Bottom left is a typical parameter cross plot showing contours of χ^2 as function of two parameters. Bottom right shows the deviation of the data points from the computed Y-T curve.

Sample	N (10^{20} cm^{-3})	C (10^{-40} sec^{-1} cm^{6})	D (10^{-12} cm^{2} sec^{-1})	$D/N^{4/3}$ (10^{-39} sec^{-1} cm^{6})
ED-2.1	0.93	2.02	0.375	0.87
ED-2.2	1.82	1.44	1.07	1.04
ED-2.3	2.82	1.02	2.81	0.58
ED-2.6	5.47	1.52	7.37	1.65

Table II: Best-fit parameters C and D for the Y-T expression, Eq. (65), for ED-2 glasses. The radiative lifetime was constrained to be between 420 and 440 μsec. C and $D/N^{4/3}$ should be constants for perfect agreement with the Y-T expression.

These rates are small compared to the radiative rate of about 2.7 x 10^3 sec^{-1}, but they represent the rates for ions at the average separation. Since the rates are such strong functions of R the rates will be much larger for ions that are closer together. On the average the diffusion transition is almost ten times more probable than quenching, but this will change from pair to pair as the crystal field environments change.

The assumption that the lowest concentration (0.1%) in ED-2 should be free of diffusion or quenching is justified by the values of C and D above. The average diffusion transition rate is only .007 sec^{-1} at 0.1 wt.% Nd. However, the fluorescence decay curve for this low concentration is nonexponential, resulting from site to site variations in the radiative rates. This is the probable cause for the inadequacy of the Y-T expression to fit the series of decay curves with the same C and D parameters. The Y-T expression includes a radiative rate ($1/\tau$) which was taken to be the long term rate in the fitting procedure. This rate is not correct at early times, and the error is large. In order for the Y-T expression to take this time varying rate into account, a distribution function for the radiative rate would be necessary and a much more complicated expression would result.

In Appendix A, the average diffusion rate is calculated from Eq. (49) for comparison with the result of the fitting program. Spectral data for the low lying Nd ^4I levels are not available, so the calculation of the rate for the quenching transition was not performed. The rate for the diffusion transition is found to be $3.8 \times 10^{-39} / R^6$

sec^{-1} cm^{-6} using the room temperature absorption and emission spectra for ED-2 glass. This is about four times the value obtained from fitting the Y-T expression, but as explained above the inhomogeneous nature of the glass spectra is expected to lead to an overestimate for the rate calculated from Eq. (49). This result indicates that the overlap integral of an average pair of ions is reduced by a factor of 4 from the overlap of the observed emission and absorption spectra due to the shifts of the energy levels in different crystal field environments. The oscillator strengths also change from site to site, so the observed diffusion rate is a weighted average of these two effects.

F. Application to Nd:glass Amplifier

The quantum efficiency after short pulse excitation of a particular Nd concentration may be calculated by integrating the Y-T expression with the correct C and D parameters. The rate of emission of photons from the excited Nd ions is equal to the radiative rate times the instantaneous number of excited ions, and the total number of photons emitted is the time integral of this rate.

$$n = \int_0^\infty \frac{1}{\tau} \Phi(t)\, dt \tag{68}$$

For a purely radiative decay, $\Phi(t) = e^{-t/\tau}$, this integral is equal to one, so the fraction of ions that radiatively decay is given by Eq. (68) with the appropriate decay function (the Y-T expression in this case).

For a nonexponential decay, the quantum efficiency for short pulse exictation is not equal to the quantum efficiency for continuous or long pulse excitation.[53] The actual pumping conditions for a

Nd:glass laser usually produce an excitation pulse of approximately the same duration as the fluorescence lifetime of the Nd. The quantum efficiency given by Eq. (68) above does not apply under these conditions. In order to numerically evaluate the effect of nonexponential decay on realistic laser amplifiers, a function that was simpler than the Y-T expression was used to approximate the nonexponential decays. This simplified decay function has terms for radiative decay, quenching, and long term diffusion-limited behavior, with the appropriate concentration dependence:

$$\Phi(t) = \exp\left\{-\frac{t}{\tau} - QNt^{1/2} - D'N^2t\right\} \qquad (69)$$

When this "Q-D" expression was substituted into NURD, the fits to the data for the ED-2 and LSG-91H series were about as good as the Y-T fits, and the function was much easier to handle in the pump efficiency calculations. For the purposes of these calculations any good approximation to the decay functions was adequate, whether or not it reflected the physics of the energy transfer explicitly.

NURD was modified to fit all the decay curves simultaneously with the same Q and D' parameters. Figure 31 shows the family of curves for the ED-2 concentration series, with the fits described by Eq. (69). The values of Q and D' are shown in Table III for ED-2 and LSG-91H laser glasses. These parameters do not provide a good fit over the entire fluorescence decay for all concentrations, but for the early part of the decay, which most strongly affects laser performance, the Q-D expression is a good approximation.

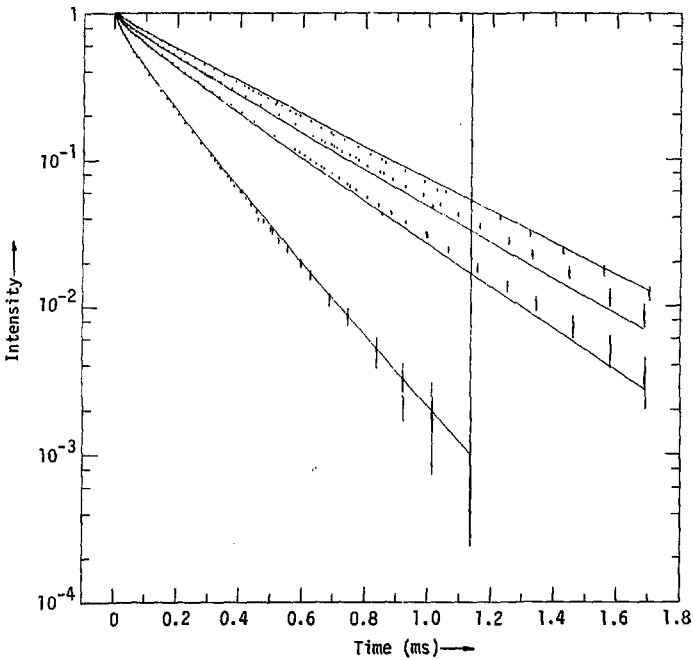

Figure 31 Simultaneous fits of 1-, 2-, 3-, and 6- wt.% Nd_2O_3 decay curves to the Q-D' expression.

Glass	τ	Q (10^{-23} cm^3 $sec^{-1/2}$)	D' (10^{-45} cm^6 sec^{-1})
ED-2	461 μsec	6.75	9.33
LSG-91H	500	8.45	7.06

Table III: Best fit parameters for the Q-D' expression, Eq. (69), for simultaneous fitting of four Nd concentrations in ED-2 and LSG-91H glasses.

The figure of merit for a laser amplifier in the present context is the peak gain achieved during flashlamp excitation with a given flashlamp pumping circuit. Gain here refers to gain coefficient expressed in cm^{-1}, so the energy gain of a laser amplifier of length L is exp(g L) where g is the gain coefficient. The peak gain is proportional to the number of excited ions; for the present purposes only relative gains are of interest so the constant of proportionality will be ignored. A small computer program for a Hewlett Packard 9830 computer was developed to solve the differential equation for the flashlamp pumping circuit of a typical laser amplifier and then to perform the convolution of the pump pulse with the decay function of the Nd in glass. The light output from a flashlamp changes its spectral content and hence its effectiveness in pumping Nd:glass as a function of the current density through the lamp. A phenomenological correction to the flashlamp current density has been determined that gives the effective pumping power for the particular amplifier considered here.[64] This correction was applied to the solutions of the flashlamp driving circuit in the computer program. Appendix B gives the flashlamp circuit parameters, the pumping efficiency correction, and a description of the "B" size disk laser amplifier for which these calculations were performed.[65]

Figure 32 shows the flashlamp current pulse, the effective pump pulse, and two gain curves, all as a function of time. The higher gain curve was calculated for a pure exponential decay with a lifetime of 290 μsec. The lower curve is the gain with the Q-D' nonexponential decay function for ED-2 with 3 wt.% Nd_2O_3. Subsequent calculations

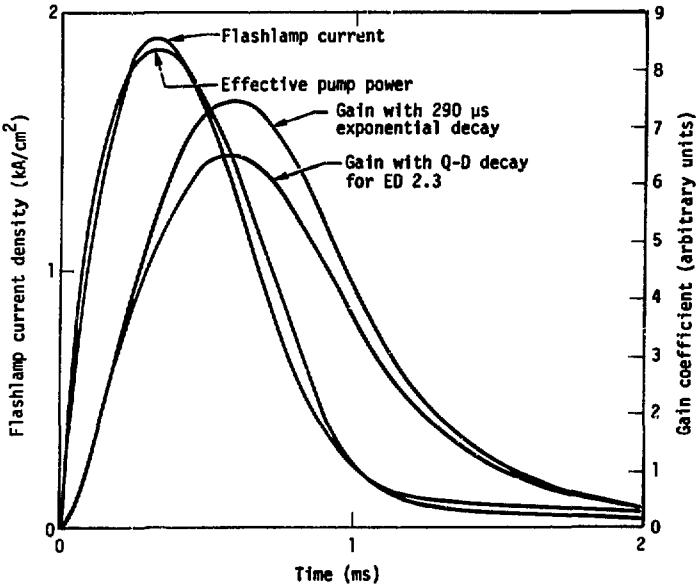

Figure 32 Gain as a function of time for a "B" disk amplifier with 3-wt.% Nd_2O_3 in ED-2 glass disks. The flashlamp current and effective pump power are shown along with the gain curves for a 290 μsec pure exponential decay and for the Q-D' decay of ED-2.3. The gain curves result from convolution of the effective pump pulse with the fluorescence decay function.

have shown that an effective lifetime for ED-2 with 3 wt.% doping is 234 μsec; that is, the same peak gain results from a pure exponential decay with this effective lifetime as when the actual nonexponential decay is used in the calculations. This effective lifetime is considerably shorter than the commonly accepted values for ED-2.3, leading to lower gains than would be calculated using the usual value of 290 μsec.[66] In the case shown in Fig. 32 the peak gain was ~13% lower than that calculated with a pure exponential decay with 290 μsec lifetime.

The effective lifetime quoted above will be a weak function of the flashlamp pump parameters, since the convolution of the actual decay and the pump pulse will vary as the pump pulse becomes shorter or longer. This effect is small over the range of pumping parameters used in the "B" disk amplifier, but for significantly shorter pump pulses, the full calculation should be performed to specify the effective lifetime which could then be used over a small range of pumping parameters. The significance of the effective lifetime is that it allows a much simpler calculation of the gain from the pump pulse characteristics. An actual convolution of the decay function and the pump pulse is not necessary for a pure exponential decay. The decay can be included in the differential equation for the flashlamp pumping circuit and solved simultaneously. The nonexponential decay cannot be described by terms in the differential equation for the flashlamp circuit, and must be included in a convolution integral that is done separately.

Application of the energy transfer results to the case of a

disk laser amplifier have shown that concentration quenching does in fact reduce the laser's efficiency and that the nonexponential character of the decay complicates the quantitative determination of the efficiency. A single value for quantum efficiency has previously been applied to laser design calculations, but these results show that no single parameter will serve to specify efficiency under all pump pulse conditions. The effective Nd lifetime (234 μsec) for the particular pump pulse investigated here was slightly less than the 1/e time (~245 μsec) and considerably less than the generally accepted "average" lifetime (290 μsec) for ED-2 laser glass with 3 wt.% Nd_2O_3.

G. Ce - Nd Energy Transfer

The transfer of energy from an A ion to a B ion is not always detrimental as it is in the case of fluorescence quenching. Sensitization is often used to increase the efficiency of a laser material. Sensitized Nd:glass has been investigated previously but has not proved to be of sufficient value to be manufactured commercially.[67] With increased emphasis on improvements in Nd:glass for laser-fusion applications, and with the increased understanding of energy transfer in rare-earth ions in glass, it is worth reconsidering the possibility of including a second ion to absorb pump energy and transfer it to the Nd.

A good candidate for sensitizing Nd is already included in ED-2 laser glass, but not for that purpose. Ce^{3+} is doped into ED-2 glass at a concentration of 4.4×10^{19} cm^{-3} in order to inhibit glass damage due to ultraviolet light absorption. The absorption of Ce

in ED-2 is so strong that wavelengths below about 350 nm are absorbed in a thin layer (~ 1 mm) of glass at the entrance surface. For efficient sensitization, the glass should be optically thin to the radiation that excites the Ce, in order for the excitation to be spread through the bulk of the laser rod or disk. An experimental glass series with lower Ce concentration was produced by Owens-Illinois in order to investigate the problems of ultraviolet damage with less Ce. These samples were obtained for the present Ce - Nd energy transfer experiments.

Trivalent cerium has only two levels in the 4f electronic configuration, the ground state and a level about 2000 cm^{-1} above it. The 5d levels in glass are at about 28000 cm^{-1}, and they absorb strongly since the 4f to 5d transition is electric dipole allowed. The emission band for the 5d to 4f transition is Stokes shifted, as shown in Fig. 33. This emission band overlaps the Nd absorption into the $^4D_{3/2}$ level, providing the possibility of energy transfer from the excited Ce to the Nd. No back transfer would be expected since the Nd ion would decay rapidly by multiphonon emission to lower, nonresonant levels.

Previous measurements[67] of Ce to Nd transfer have used the quantum efficiency approach, where the number of photons emitted by Nd ions is compared to the number of pump photons absorbed by the Ce ions. As discussed earlier, this technique is subject to greater uncertainty than measurements of the change in decay rate of the Ce ion. Although radiative transfer is possible in the present case, the concentration of Nd was low enough that the samples were all optically thin to the Ce emission, so radiative transfer was negligible. Radiation trapping

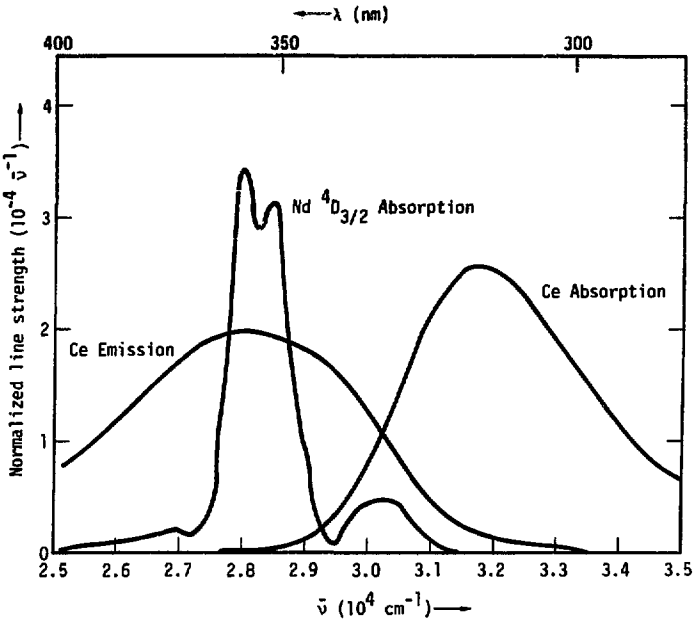

Figure 33 Normalized room temperature Ce emission and absorption spectra and Nd $^4D_{3/2}$ absorption curve. The Ce emission and Nd absorption overlap, giving rise to energy transfer from Ce to Nd.

can distort the observed lifetime in some fluorescing systems, but experimental checks revealed no trapping and re-emission of Ce fluorescence by Ce ions.

Ce^{3+} was excited to the 5d band by the 355-nm pulses from the third harmonic of the 1-ns laser. The emission was sufficiently intense to give a signal on a vacuum photodiode (ITT F-4000) which was processed in the Tektronix transient digitizing system described earlier. A Corning 3-75 filter eliminated the scattered pump radiation. The samples contained varying amounts of Nd, and the two series had different Ce concentrations. A family of decay curves for the lower Ce concentration are shown in Fig. 34. The decays for both Ce concentration were observed to be purely exponential for all Nd concentrations, within the accuracy of these experiments. Figure 35 shows the log plot of the decay from the low concentration Ce sample with 4×10^{20} Nd ions per cm^3. The slope of the log plot is also shown, indicating no deviation from a purely exponential decay over at least three e-folding times. Scattered light limited the observations at early times so that the first 3 ns were not resolved.

The decay rates for both Ce concentrations are displayed as functions of the Nd concentrations in Fig. 36. Within the experimental errors, the data all lie on a straight line, independent of the Ce concentration. This linear dependence of the rate on the Nd concentration has been observed previously at this laboratory by R. R. Jacobs, who used a nitrogen laser to excite these same samples. The 20-ns pulses from the nitrogen laser limited the observation of fluorescence to late times in the decay.

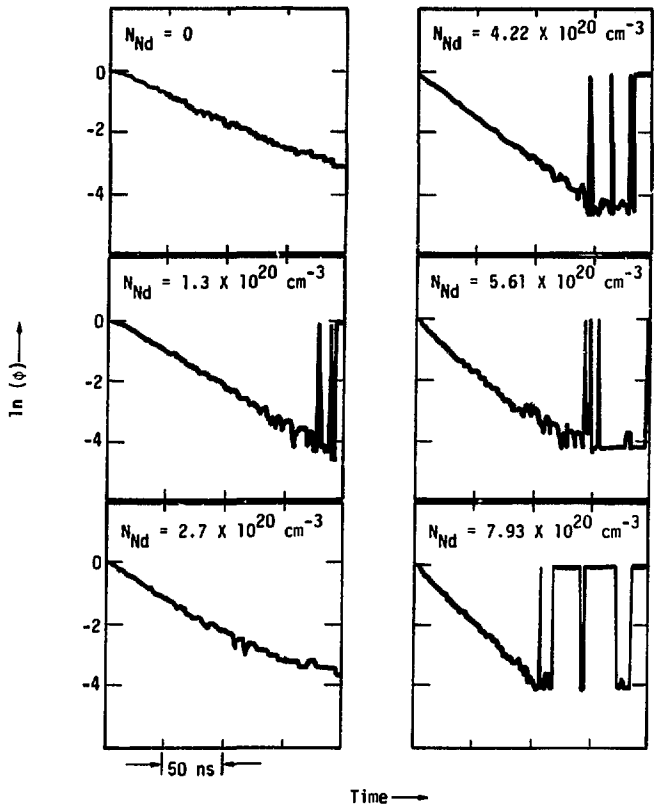

Figure 34 Ce fluorescence decays in presence of varying amounts of Nd. The G-S 115 glass series has 1.53 x 10^{18} Ce ions per cm^3.

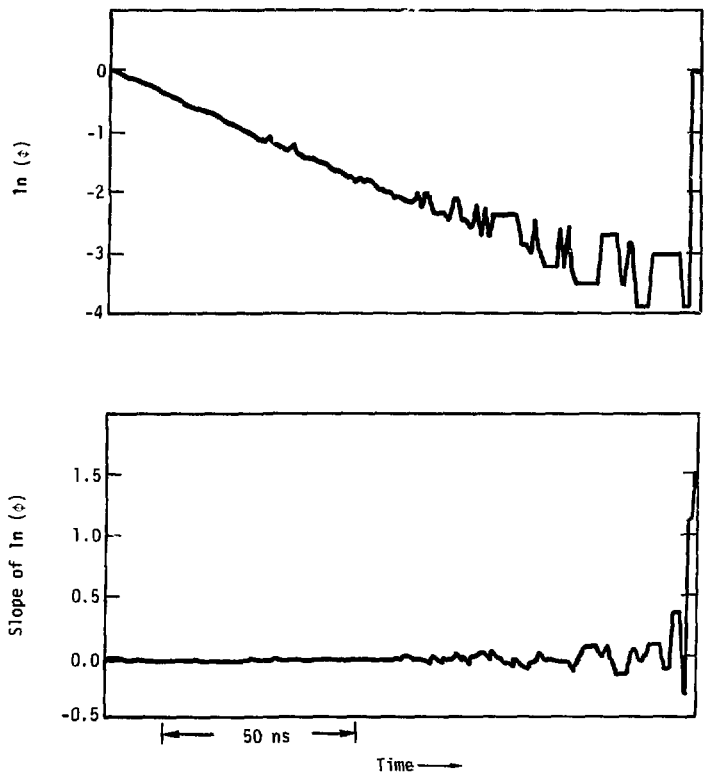

Figure 35 Natural log of Ce fluorescence decay and the variation of the rate with time. The sample has 1.53×10^{18} Ce ions and 4.22×10^{20} Nd ions per cm^3. The constant value of the slope indicates a purely exponential decay; that is, a constant decay rate.

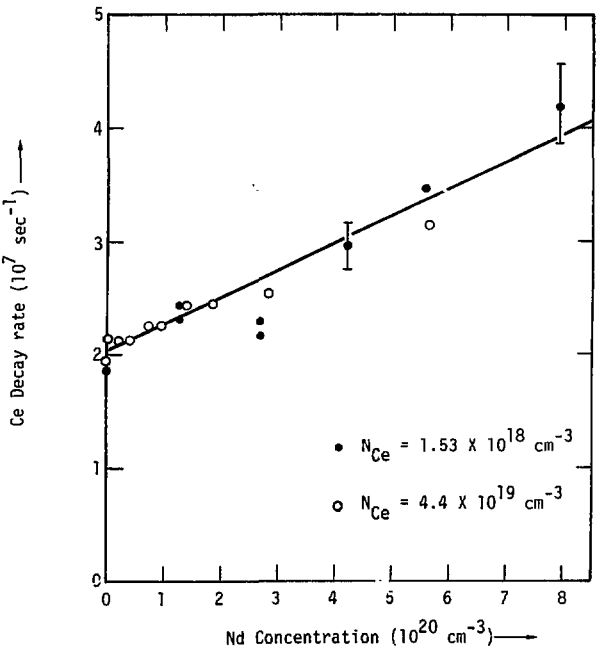

Figure 36 Ce decay rate as a function of Nd concentration for both values of Ce concentration.

The decay rate of Ce^{3+} increases to twice the radiative rate at the highest Nd concentration in these experiments. This indicates that half of the pump photons absorbed by the Ce are effective in pumping Nd. At the Nd concentrations normally found in laser glasses, the effect is smaller, but may be significant in improving pump efficiency. At 3 wt.% Nd_2O_3 (2.85×10^{20} cm^{-3}) the Ce decay rate is 2.6×10^7 sec^{-1} as compared to the radiative rate of 1.9×10^7 sec^{-1}. The fraction of Ce that decays by transfer to Nd at 3 wt.% is given by $1 - W_{rad}/W_{tot} = 0.27$, an amount that could produce a significant increase in Nd excitation. Much of the energy output of a flashlamp is in short wavelengths, depending on the current through the lamp. With the transfer efficiency for a given Nd concentration, the spectral profile of the flashlamp output, and the absorption spectrum of Ce in a sensitized laser glass, the additional pumping due to Ce absorption can be evaluated. Problems of glass damage and color center formation when the Ce concentration is reduced must be solved before Ce will be useful as a sensitizer.

The Ce decay curves are identical to those shown in Fig. 22 for fast diffusion decays; they are pure exponentials and the rate is proportional to the concentration of quenching ions (Nd). For a quenching transition that is dependent on the distance between A and B ions, a nonexponential decay should result unless the diffusion of the excitation is fast compared to the quenching rate. Otherwise, there will be a distribution of rates caused by the variations in the distance between pairs of ions. A model that gives exponential decay without diffusion, the Stern-Volmer model, assumes a transfer rate

that is independent of the distance between ions; no such transition mechanism is known.

The average diffusion rate for Ce to Ce transfer is calculated in Appendix A from Eq. (49). The rate is found to be ~400 sec^{-1}, much too slow to explain the observed fast diffusion behavior of the Ce system. Although this contradiction is not understood at present, further investigation of the Ce - Nd system is planned. Short wavelength excitation is known to produce Ce^{4+} in glass doped with Ce^{3+},[67] and it is possible that the 355-nm pulses produced Ce^{4+}, introducing either a permanent or transient change in the Ce - Nd system.

Chapter IV: Conclusion

The theory of multiphonon relaxation developed originally for rare-earth ions in crystals has been applied to glasses. The expected exponential dependence of the multiphonon rates on energy gaps has been verified for five oxide glass compositions, independent of the particular rare earth or electronic state involved. The phonons active in relaxing excited rare-earth ions across large energy gaps are the high energy molecular vibrations of the network forming ions. Raman spectra combined with the temperature dependence of the multiphonon rates verified this identification of the active phonons.

The relative multiphonon rates in these glasses are determined by the highest energies in the phonon spectra, with the rates in borate glasses being 10^3 times the rates in tellurite glasses for the same energy gaps. All the rates measured here were much faster than those for comparable gaps in crystals. The coupling of the rare earth to the phonons is relatively constant in the oxide glasses, but halide or chalcogenide glasses may have different coupling strengths. The knowledge of phonon energies in non-oxide glasses is not sufficient to predict nonradiative rates until experiments similar to these have measured a few rates to determine the coupling strength. Since the coupling of the lattice to the electronic states enters the expression for the energy gap law as the argument of a logarithm, the coupling must change radically in order for the rates to change significantly for glasses with the same phonon energies.

The molecular nature of the high energy vibrations in glasses leads to the consideration of multiphonon decay to a single highly

excited mode. The temperature dependence of nonradiative rates in the glasses studied here do not indicate relaxation to a single vibration, but the predicted behavior may be observable in hydrated glasses or simple rare-earth molecules. Vibrational deactivation of rare earths in D_2O with small amounts of H_2O has been shown to involve only one O-H oscillator,[24] but the temperature dependence has not yet been investigated.

Another aspect of multiphonon decay that should be explored is the variation in coupling between different ions in the same glass. The inhomogeneous nature of the glass environment that leads to nonexponential radiative decay should result in nonexponential multiphonon decay as well. The experiments described here did not address this question.

The application of multiphonon theory to a specific rare earth in glass is given in Appendix C, where the influence of nonradiative rates on the performance of a Nd:glass laser is assessed. The verification of the theory for glasses assures that a few rate measurements in new glasses can be extrapolated to give the nonradiative rates of interest for new laser materials.

Energy transfer in Nd:glass accounts for the observed nonexponential fluorescence decay of excited Nd ions. Quenching of the excitation of one Nd to a nearby unexcited Nd leads to a decrease in lifetime with increasing Nd concentration. Diffusion among the Nd ions redistributes the excitation after quenching takes place, leading to a nonexponential decay of the excited population. At long times the decay is diffusion-limited, with a rate that varies with N^2. The

coupling between Nd ions is due to dipole-dipole interaction, and the decay was found to follow the expression derived by Yokota and Tanimoto[57] except for deviations caused by the variation of the radiative rate in glass.

A more direct study of diffusion in the Nd:glass system is possible using the techniques of fluorescence line narrowing experiments. Selected types of sites can be separately observed in these experiments rather than the weighted sum of the entire distribution that was studied here. It is not understood whether some Nd ions are always quenching centers for Ndexcitation or whether the same ions can take part in both diffusion and quenching, with different probabilities. It may be possible to address this question with fluorescence line narrowing techniques.

With the decay function and its dependence on concentration, it is now possible to predict the fluorescent behavior of new laser glasses at various Nd concentrations given a measurement at one (high) concentration and a radiative rate, either from a calculation or from a low concentration measurement. This will be useful in optimizing the concentration to be used for laser amplifiers consistent with other constraints, such as the available flashlamp pump pulse. The application of the fluorescence decay function to determining the peak gain of a typical amplifier shows that the nonexponential character of the decays has an impact on laser design calculations. For a limited range of pumping pulse characteristics, an effective exponential lifetime may be chosen to simplify the calculations. A single number to specify

quantum efficiency will not suffice for all conditions however.

Energy transfer from Ce to Nd in laser glass was observed, and the dependence on Nd concentration was established. This information will be useful for calculations to assess the advantages of sensitizing Nd with Ce. The purely exponential decay of Ce in the presence of quenching by Nd is not understood, but the general understanding of energy transfer in glass will help in interpreting experiments designed to resolve this question.

ACKNOWLEDGMENTS

I am grateful for assistance from several people during the course of this work. Marvin J. Weber directed my research and helped out in each phase of my progress. Marv's wisdom and keen interest in this area contributed greatly to my completion of this work. In the multiphonon measurement, Howard Lowdermilk worked closely with me over months of experimental frustrations and gratifying breakthroughs. Consequently Howard deserves credit and my thanks for his efforts. The experiments involved quite sophisticated electronic devices and no less sophisticated electronic technicians; I am grateful for the excellent technical assistance of Dennis Downs and Dick Morgret. Also supporting this work were Stan Roberts, Jeanne Lynch and Champe Dobler, my thanks to them also. I appreciate the time and effort that Ed Goodwin expended in computer programming to support this work.

Many technical discussions with Jeff Paisner were helpful, and a day discussing this work with Professor R. Orbach was very useful. I thank Jeanne Shrode for proofreading and coordinating the typing and John Emmett for providing support and incentive for this work.

Finally, thanks to Celeste for her understanding when this work served as an excuse for not doing a thousand jobs at home.

Appendix A: Dipole-Dipole Transition Rates

Dexter's formula for the transition probability from an excited ion A to ion B at a distance R is

$$W_{DD} = \frac{3h^4c^4}{4\pi n^4}\frac{1}{R^6}\frac{Q_B}{\tau_A}C_k\int\frac{f_B(E)f_A(E)}{E^4}\,dE \qquad (49)$$

where τ_A is the radiative lifetime of A and Q_B is the integrated absorbance of B. C_k is the local field correction, taken to be 1 here. The overlap integral involves the normalized lineshape functions:

$$\int f(E)\,dE = 1.$$

It is convenient to express energy in terms of wave numbers (cm^{-1}) for these calculations, $E = hc\bar{\nu}$. The integrated absorbance was calculated from the absorption spectra converted to wave numbers:

$$Q_B = \int\sigma(E)\,dE$$

$$= \frac{1}{N}\int\alpha(E)\,dE$$

$$= \frac{hc}{N}\int\alpha(\bar{\nu})\,d\bar{\nu}$$

The cross section for the transition is $\sigma(cm^2)$, and the measured absorption coefficient is $\alpha(cm^{-1})$. N is the number of ions per cm^3. When Eq. (49) is expressed in terms of wave numbers, the rate is

$$W_{DD} = \frac{3}{2(2\pi)^5n^4hc}\frac{1}{R^6}\frac{Q_B}{\tau_A}\int\frac{f_B(\bar{\nu})f_A(\bar{\nu})\,d\bar{\nu}}{\bar{\nu}^4}$$

$$W_{DD} = \frac{1.3 \times 10^{11}}{R^6} \frac{Q_B}{\tau_A} \int \frac{f_B(\bar{\nu}) f_A(\bar{\nu})\, d\bar{\nu}}{\bar{\nu}^4}$$

where the index of refraction of ED-2 was used (n = 1.556). The absorption curve for the appropriate transition was obtained from a spectrophotometer plot which gave the optical density as a function of wavelength for a sample of Nd in glass or Ce in glass. The optical density plots were digitized on a Hewlett-Packard 9830 computer and converted to absorption coefficient versus wave number and stored in an array for further manipulation. From the absorption array, Q was determined from the equation above. The absorption array was then integrated in order to normalize to $f(\bar{\nu})$. Emission spectra for Ce and Nd were similarly stored in a computer array as a function of wave number, integrated, and normalized. The Ce emission spectrum was taken from Rapp's data,[67] and the Nd emission spectrum was taken in this laboratory. All emission and absorption spectra were at room temperature.

For the calculation of the Nd-Nd diffusion rate, the absorption and emission spectra for Nd around 880 nm were used. These normalized spectra are shown in Fig. 37. The value of Q was found to be 4.38×10^{-34} $cm^2 erg$. For the radiative lifetime, the reciprocal of the radiative rate for the $^4F_{3/2}$ to $^4I_{9/2}$ was derived from Krupke's value[41] for the branching ratio and the long term radiative rate found previously.

$$\beta\left(^4F_{3/2} - {}^4I_{9/2}\right) = \frac{W\left(^4F_{3/2} - {}^4I_{9/2}\right)}{\left(W\ {}^4F_{3/2\,TOTAL}\right)} = 0.4$$

$$\frac{1}{\tau_A} = W\left(^4F_{3/2} - {}^4I_{9/2}\right) = 0.4 \times 2.32 \times 10^3\ sec^{-1} = 928\ sec^{-1}$$

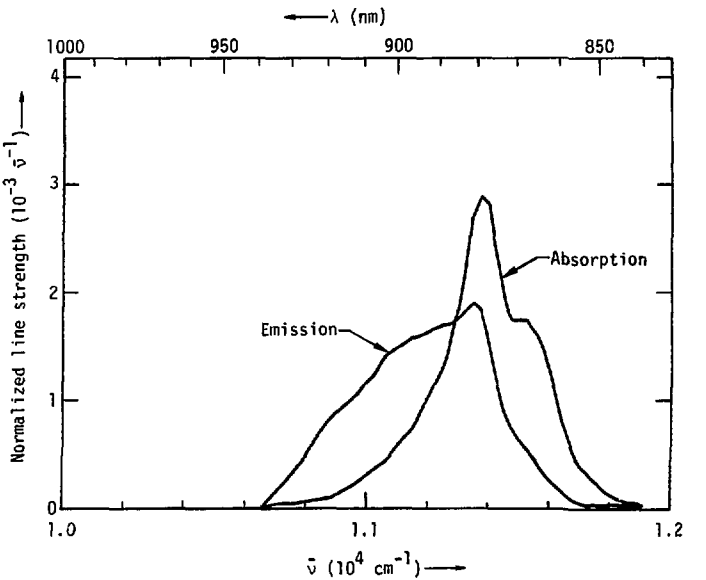

Figure 37 Room temperature absorption and emission spectra for Nd $^4F_{3/2}$ to $^4I_{9/2}$ transition, normalized to unit area.

The overlap integral was found to be 7.17×10^{-20} cm^5 (the units are the reciprocal of wave numbers to the fifth power). The resulting dipole-dipole transition rate for the diffusion transition in Nd was

$$W_{DD} = \frac{3.8 \times 10^{-30}}{R^6} \text{ sec}^{-1} \quad (R \text{ in cm})$$

The calculation for Ce was performed in the same way. Normalized Ce emission and absorption spectra are shown in Fig. 33. The radiative rate for Ce was taken to be the observed rate in Ce in glass with no Nd, $1/\tau = 2 \times 10^7$ sec^{-1}, that is, the Y intercept of Fig. 36. The value of Q was found to be 1.845×10^{-30} $cm^2 erg$, and the overlap integral was 3.32×10^{-23} cm^5. Thus, the transition strength was greater than Nd, but the overlap was decreased. The resulting diffusion transition rate in Ce was

$$W_{DD} = \frac{1.6 \times 10^{-34}}{R^6} \text{ sec}^{-1}$$

For comparison with the transfer rates, the average separation of Ce ions can be substituted for R.

$$R = (N)^{-1/3} = (1.53 \times 10^{18} \text{ cm}^{-3})^{-1/3} = 8.7 \times 10^{-7} \text{ cm}$$

Then the diffusion transition rate between an average pair of Ce ions in ED-2 glass is $W_{DD} = 3.7 \times 10^2$ sec^{-1}.

Appendix B: Calculation of Effective Pumping in a Disk Amplifier

The amplifier chosen for this application is the "B" size disk amplifier designed at the Lawrence Livermore Laboratory for use in large target irradiation lasers. The active medium in the amplifier consists of six elliptical laser disks, each 2.35 cm thick, with 10 x 18.4-cm minor and major axes. The disks are pumped by 24 linear flashlamps each with a 1-cm bore and 112-cm arc length. The flashlamps are connected in pairs to 12 capacitor banks with 72.5 μF capacitance and 1050 μH inductance in a single mesh circuit. In a single mesh circuit, the inductor is in series with the lamp, and both are connected across the capacitor.

The differential equation for the flashlamp circuit is[68]

$$\frac{dI}{d\tau} + IR \pm \alpha |I|^{1/2} + \int_0^{\tau} I \, d\tau' = 1$$

where normalized units are used. For inductance L, capacitance C, current i, and initial voltage V, the following substitutions have been made:

$$\tau = \frac{t}{\sqrt{LC}}$$

$$Z = \sqrt{\frac{L}{C}}$$

$$I = \frac{Z}{V} i$$

The constant α is related to the length ℓ and diameter d of the flashlamp:

$$\alpha = \frac{0.3 \, \ell/d}{(VZ)^{1/2}}$$

R is the resistive loss of the circuit, and was taken to be 0.35 Ω. The differential equation was solved by a Runge-Kutta technique with the circuit parameters given above. To convert current density in the lamp to effective pump power, the following correction was applied to the current pulse:

$$P_{effective} = \frac{10(1 - e^{-J/350})}{J^{0.8}} J$$

where J is the current density in A/cm^2 and P is the effective pump power.

Figure 32 shows the flashlamp current pulse, the effective pump pulse, and the gain for the circuit described here. The gain was computed as the convolution of the effective pump pulse and the decay function (the Q-D' expression). Because of the nonexponential nature of the decay function, the decay could not be included in the program loop that solved the flashlamp equation and computed effective pump power. A pure exponential decay could be included as a multiplicative constant in a sum to integrate the effective pump power. At each point of time, the effective pump power could be added to the sum over the previous pump powers multiplied by $\exp(-\Delta t/\tau)$. For the nonexponential decay the entire sum of previous pump powers must be recalculated at each new time.

NONRADIATIVE RELAXATION OF RARE-EARTH IONS IN SILICATE LASER GLASS*

C. B. Layne, W. H. Lowdermilk, and M. J. Weber

Lawrence Livermore Laboratory
University of California
Livermore, California 94550

· ABSTRACT ·

Rates for nonradiative decay by multiphoton emission are measured for rare-earth ions in silicate laser glass and used to estimate quantum efficiencies.

* This work was performed under the auspices of the U.S. Energy Research and Development Administration.

NONRADIATIVE RELAXATION OF RARE-EARTH IONS IN SILICATE LASER GLASS

C. B. Layne, W. H. Lowdermilk, and M. J. Weber

Lawrence Livermore Laboratory
University of California
Livermore, California 94550

Three important properties of lasers doped with rare-earth ions are determined by the nonradiative decay rates of the excited states of these ions. First, the pump conversion efficiency [1] is large when the nonradiative decay rate from the pump band to the upper laser level is much greater than the rate for radiative decay from the pump band. Second, for a high radiative quantum efficiency, the nonradiative decay rate from the upper laser level should be small compared to the radiative rate. And third, for a four-level laser system, the relaxation rate of the terminal laser level is important in determining the saturation flux for a laser pulse of given duration. We have determined the nonradiative decay rates for rare-earth ions doped into Owens-Illinois ED-4 glass in order to estimate these properties. ED-4, a widely used commercial laser glass, is a silicate glass modified by the addition of LiO_2, CaO, and Al_2O_3. When doped with Nd^{3+}, this glass is designated as ED-2.

The lifetime of an excited state is determined by all the competing radiative and nonradiative decay processes; the latter include decay by both ion-ion interactions and the emission of phonons. To reduce the probability of nonradiative decay by ion pair interactions in this work, the rare-earth concentrations of our samples were less than 1 mol%. When the energy gap between the excited ionic energy level and the next lower

level is greater than the energy of the most energetic lattice vibration, the nonradiative decay must involve the emission of several phonons. The multiphonon relaxation rates among the $4f^n$ levels of rare-earth ions have been investigated in many crystals including several laser materials [2]. These studies have shown that in these high-order processes, the detailed features of the electronic states and phonon modes involved in the transition average out. Thus the multiphonon decay is adequately described in many cases by the stimulated emission of phonons, all of a single frequency ω, leading to a decay rate of the form

$$W_{NR} = Ce^{-\alpha\Delta E}[n(\omega,T) + 1]^p \quad , \tag{1}$$

where C and α are constants characteristic of the host material, ΔE is the energy gap to the next-lower ionic level, and $p = \Delta E/\hbar\omega$ is the number of phonons which must be emitted in order to conserve energy in the transition. The explicit temperature dependence of W_{NR}, through the Bose-Einstein occupation number $n = (e^{\hbar\omega/kT} - 1)^{-1}$, provides a way to determine experimentally the number and energy of the phonons involved in the decay process.

It has been established that the nonradiative decay of rare-earth ions in crystals involves emission of the highest energy phonons in the lowest order, and therefore most probable, process consistent with energy conservation and the lattice vibrational spectrum [2]. The highest energy vibrations of a lattice are, in general, the most localized modes characterized by the short range order of the material. This statement is born out by the similarity of the infrared and Raman spectra of vitreous materials and their crystalline polymorphs. One would expect that the nonradiative decay of rare-earth ions in glasses should also be dominated

by these highest energy lattice vibrations. The glass lattice vibrational frequencies of ED-4 may be obtained from the Raman spectrum [3]. The highest frequency band at 900-1100 cm^{-1} is attributed to the Si-O-Si stretching mode of the silicate lattice network. Based on a fit to our measurements of the temperature dependence of W_{NR} using Eq. (1), we conclude that this highest frequency vibrational mode plays the dominant role in the nonradiative decay. We have found in addition that the strength of ion-lattice coupling in glasses is about the same as it is in crystals. Consequently, since the highest vibrational frequencies of the glass lattice are much greater than the highest phonon frequencies of most crystals, the multiphonon decay rates in glasses are much greater than in crystals.

In order to establish the dependence of the nonradiative decay rate on the energy gap, the rates for eight excited states of four different trivalent rare-earth ions in ED-4 glass were measured. The decay rates were determined from measurements of the transient fluorescence following pulsed selective excitation. Two different laser sources were used to excite the various ionic energy levels. One source was a Nd:YAG laser which produced a 100 mj pulse at 1.06 μm with a duration of 1 nsec. This pulse was used to produce pulses at the second and third harmonic frequencies by frequency doubling and mixing in KD*P. The second source was a tunable $LiNbO_3$ optical parametric oscillator which was pumped by the frequency doubled output of a Chromatix Nd:YAG laser with a pulse duration of 200 nsec. (Details of the experimental apparatus and techniques used will be published elsewhere). The total fluorescence decay rate measured in this experiment consists of a radiative and nonradiative contribution. Fortunately, the measured rates in ED-4 were much larger than the estimated radiative rates, and thus the latter were neglected.

The measured nonradiative decay rates for the various ionic energy levels are plotted in Figure 1 as a function of the energy gap to the next lower level. An approximate exponential dependence on the energy gap, independent of the rare-earth ion or electronic level, is obtained. This systematic dependence can be used to estimate the nonradiative decay rates from other rare-earth energy levels of interest in ED-4. The exponential dependence of the decay rate should not, however, be extrapolated to values of the energy gap corresponding to the excitation of less than approximately two quanta of the highest frequency lattice vibrational mode. For relaxation processes involving only one or two vibrational quanta, the averaging effect of high-order processes is not present, and in this case the decay rate is expected to depend on the details of the electronic state and vibrational mode excited in the decay. This effect is apparent in the deviation from the exponential fit of the decay rate for the $^4G_{7/2}$ level of Nd^{3+} with an energy gap of 1400 cm^{-1}. The results shown in Figure 1 of course apply only to the silicate glass. The characteristic vibrational frequencies of other glasses are significantly different, leading to large variations of the nonradiative decay rates [4].

We conclude by applying the results of this experiment to the Nd^{3+} doped ED-2 glass to estimate the pump conversion efficiency, the radiative quantum efficiency of the $^4F_{3/2}$ upper laser level, and the lifetime of the $^4I_{11/2}$ terminal laser level. Since the nonradiative rate depends exponentially on the energy gap, the decay time from the optical pump bands to the $^4F_{3/2}$ level is determined by the largest energy gap encountered in the cascade. The largest gap, of approximately 2300 cm^{-1} occurs below the $^2P_{3/2}$ level. The fluorescence lifetime of this level was measured to be 50 nsec. The radiative lifetimes of all the excited states in the pump bands have been calculated using the Judd-Ofelt intensity parameters

for ED-2 [5]. These lifetimes are all longer than 10^{-5} sec. Thus, since ion pair interactions are believed to be negligible, the pump conversion efficiency is found to be greater than 99%. The nonradiative decay rate for the $^4F_{3/2}$ level, based on the extrapolation shown in Figure 1 to an energy gap of 4800 cm^{-1}, is estimated to be 200 sec^{-1}. The radiative decay rate for this level is about 3×10^3 sec^{-1} leading to a radiative quantum efficiency of approximately 95% in the absence of concentration quenching. An estimate of the radiative quantum efficiency which is in agreement with this value was obtained from measurements of the temperature dependence of the fluorescence lifetime of the $^4F_{3/2}$ level. This temperature dependence arises from thermal population and decay of levels above the $^4F_{3/2}$ in addition to the temperature dependence of W_{NR} shown in Eq. (1). This result is, however, less accurate since the change in the measured rate over the available temperature range is small compared to the uncertainty in the measurement. Finally the lifetime of the $^4I_{11/2}$ terminal level with a gap of 1500 cm^{-1} is predicted to be approximately 10 nsec. This value is in good agreement with estimates based on attempts to measure this lifetime directly [6].

REFERENCES:

[1] Our definitions of pump conversion efficiency and radiative quantum efficiency differ from conventions used by other authors. We separate the total efficiency into two parts: pump conversion efficiency is defined as the number of ions in the upper laser level divided by the number of absorbed pump photons, and radiative quantum efficiency is defined as the fraction of ions in the upper laser level which decay radiatively. Both concentration quenching and multiphonon relaxation may decrease radiative quantum efficiency. The present measurements pertain only to the multiphonon contribution, while previous measurements determined the product of pump conversion efficiency and radiative quantum efficiency including concentration quenching.

a) L.G. DeShazer and L.G. Komai, "Fluorescence Conversion Efficiency of Neodymium Glass", J. Opt. Soc. Am. 55, 940-944, August 1965.

b) R.A. Brandewie and C.L. Telk, "Quantum Efficiency of Nd^{3+} in Glass, Calcium Tungstate, and Yttrium Aluminum Garnet", J. Opt. Soc. Am. 57, 1221-1225, October 1967.

[2] L.A. Riseberg and M.J. Weber, "Relaxation Phenomena in Rare-Earth Luminescence", Progress in Optics, XIV (North Holland Publishing, Amsterdam, 1975). In press.

[3] R.W. Hellwarth, J. Cherlow, and T. Yang, "Origin and Frequency Dependence of Nonlinear Optical Susceptibilities of Glasses", Phys. Rev. 11, B964-B967, January 1975.

[4] W.H. Lowdermilk, C.B. Layne, and M.J. Weber, "Nonradiative Relaxation of Rare Earth Ions in Glasses: (II) Dependence on Vibrational Spectrum", Bull. Am. Phys. Soc., Series II, 20, 448, March 1975.

[5] W.F. Krupke, "Optical Properties of ED-2 Laser Glass", Internal Report UCIR-714, Univ. of Calif., Lawrence Livermore Laboratory, December 1973.

[6] a) D.K. Duston, "Factors Influencing the Gain in Neodymium Doped Laser Glass", Ph.D. Thesis, Rensselaer Polytech. Inst., Troy, New York, May 1969.

REFERENCES: (cont'd)

[6] b) V.V. Grigoryants, et al., "Determination of τ_{21} Relaxation Time of $^4I_{11/2}$ Level of Neodymium Ions in Glass", Zh. Prikl. Spektr., 14, 73-77, January 1971.

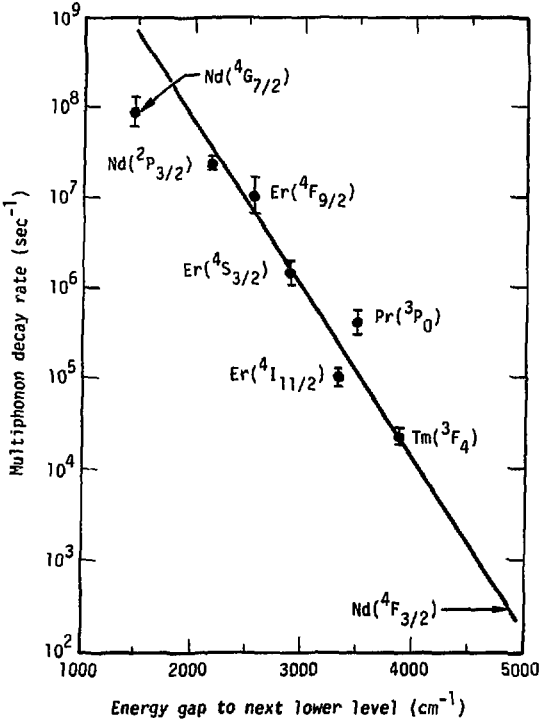

Figure 1 Multiphonon decay rates as a function of energy gap to the next lower level for rare earths in ED-4 silicate glass. The extrapolation to the Nd $^4F_{3/2}$ rate is indicated.

References

1. G. H. Dieke, Spectra and Energy Levels of Rare Earth Ions in Crystals (Interscience Publishers, New York, 1968), pp.1-17, 80-103.

2. E. Snitzer, "Optical Maser Action of Nd^{3+} in a Barium Crown Glass", Phys. Rev. Lett. 7, 444 (1961).

3. J. L. Emmett, J. Nuckolls, and L. Wood, "Fusion Power by Laser Implosion", Sci. Am. 230, 24 (1974).

4. G. H. Dieke, "Energy Levels of and Energy Transfer in Rare Earth Salts", in Paramagnetic Resonance, W. Low, Ed. (Academic Press, New York, 1963), Vol. I, pp. 237-252.

5. M. J. Weber, "Radiative and Nonradiative Transitions of Rare-Earth Ions: Er^{3+} in LaF_3", in Physics of Quantum Electronics, P. L. Kelley et al., Eds. (McGraw-Hill Co., New York, 1966), pp. 350-360.

6. W. D. Partlow, and H. W. Moos, "Multiphonon Relaxation in $LaCl_3:Nd^{3+}$", Phy. Rev. 157, 252 (1967).

7. A. Kiel, The Interaction of Paramagnetic Ions with Lattice Vibrations, Ph. D. thesis, Johns Hopkins University, Baltimore, Md. (1962).

8. L. A. Riseberg and H. W. Moos, "Multiphonon Orbit-lattice Relaxation of Excited States of Rare-Earth Ions in Crystals",

Phys. Rev. 174, 429 (1968).

9. T. Miyakawa and D. L. Dexter, "Phonon Sidebands, Multiphonon Relaxation of Excited States, and Phonon-Assisted Energy Transfer between Ions in Solids", Phys. Rev. B 1, 2961 (1970).

10. S. Fischer, "Correlation Function Approach to Radiationless Transitions", J. Chem. Phys. 53, 3195 (1970).

11. F. K. Fong, S. L. Naberhuis, and M. M. Miller, "Theory of Radiationless Relaxation of Rare-Earth Ions in Crystals", J. Chem. Phys. 56, 4020 (1972).

12. C. W. Struck and W. H. Fonger, "Unified Model of the Temperature Quenching of Narrow-Line and Broad-Band Emmissions", J. Lumin. 10, 1 (1975).

13. H. Rawson, Inorganic Glass-Forming Systems, (Academic Press, New York, 1967), pp. 11-23.

14. S. Brawer, "Theory of the Vibrational Spectra of Some Network and Molecular Glasses", Phys. Rev. B 11, 3173 (1975).

15. R. J. Bell and P. Dean, "Properties of Vitreous Silica: Analysis of Random Network Models", Nature (Lond.) 212, 1354 (1966).
R. J. Bell, N. F. Bird, and P. Dean, "The Vibrational Spectra of Vitreous Silica, Germania, and Beryllium Fluoride", J. Phys. C 1, 299 (1968).
R. J. Bell and D. C. Hibbins-Butler, "Accoustic and Optical Modes

in Vitreous Silica, Germania, and Beryllium Fluoride", J. Phys. C 8, 787 (1975).

16. J. Bock and G-J. Su, "Interpretation of the Infrared Spectra of fused Silica", J. Am. Ceram. Soc. 53, 69 (1970).
N. F. Borrelli and G-J. Su, "An Interpretation of the Infrared Spectra of Vitreous Boron Oxide", Phys. Chem. Glasses 4, 206 (1963).

17. J. H. Van Vleck, "The Jahn Teller Effect and Crystalline Stark Splitting for Clusters of the Form XY_6", J. Chem. Phys. 7, 72 (1939).

18. A. Yariv, Quantum Electronics (John Wiley & Sons, Inc., New York 1967), p. 73.

19. L. I. Schiff, Quantum Mechanics (McGraw-Hill Book Co., Inc., New York, 1949), pp. 189-199.

20. W. Heitler, The Quantum Theory of Radiation, (Clarendon Press, Oxford, 1954), 3rd ed., pp. 136-145.

21. R. Shuker, Raman Scattering: Density of States in Amorphous Materials, Ph. D. thesis, Catholic University of America, Washington, D. C. (1971).

22. K. K. Rebane, Impurity Spectra of Solids (Plenum Press, New York, 1970). p. 17.

23. P. J. Vergano, K. D. Pohl, and C. F. Rapp, private communication.

24. A. Heller, "Formation of Hot OH Bonds in the Radiationless Relaxations

of Excited Rare Earth Ions in Aqueous Solutions", J. Am. Chem. Soc. 88, 2058 (1966).

25. L. A. Riseberg and M. J. Weber, "Relaxation Phenomena in Rare Earth Luminescence", in Progress in Optics, E. Wolf, Ed., Vol. 14, in press.

26. R. Reisfeld and Y. Eckstein, "Intensity Parameters of Tm^{3+} and Er^{3+} in Borate, Phosphate, and Germanate Glasses", Solid State Commun. 13, 265 (1973).
R. Reisfeld and Y. Eckstein, "Radiative and Non-Radiative Transition Probabilities and Quantum Yields for Excited States of Er^{3+} in Germanate and Tellurite Glasses", J. Non-Cryst. Solids 15, 125 (1974).

27. R. L. Carman, B. C. Johnson, and L. L. Steinmetz, "A Self-Driven Laser Oscillator for Directly Producing Bandwidth-Limited Pulses of about 1 Nsec", Opt. Commun. 7, 169 (1973).

28. G. I. Kachon, L. L. Steinmetz, and J. Kysilka, "Selection and Amplification of a Single Mode-Locked Optical Pulse", Appl. Phys. Lett. 13, 229 (1968).

29. B. R. Judd, "Optical Absorption Intensities of Rare-Earth Ions", Phys. Rev. 127, 750 (1962).

30. G. S. Ofelt, "Intensities of Crystal Spectra of Rare-Earth Ions", J. Chem. Phys. 37, 511 (1962).

31. W. F. Krupke, "Induced-Emission Cross Sections in Neodymium Laser Glasses", IEEE J. Quantum Electron. QE-10, 450 (1974).

32. Y. S. Bobovich, "An Investigation of the Structure of Glassy Phosphates Using Raman Spectra", Opt. Spectrosc. 13, 274 (1962).

33. V. V. Obukhov-Denisov, N. N. Sobolev, and V. P. Cheremisinov, "Vibrational Spectra of the Modifications of Germanium Dioxide", Opt. Spectrosc. 8, 267 (1960).

34. C. B. Layne, W. H. Lowdermilk, and M. J. Weber, "Nonradiative Relaxation of Rare-Earth Ions in Silicate Laser Glass", IEEE J. Quantum. Electron. Sept. 1975, in press. Included as Appendix C.

35. I. Simon, "Infra-Red Studies of Glass", in Modern Aspects of the Vitreous State, J. D. MacKenzie, Ed. (Butterworths, London, 1960), pp. 120-151.

36. G. Herzberg, Molecular Spectra and Molecular Structure II. Infrared and Raman Spectra of Polyatimic Molecules, (Van Nostrand Reinhold Co., New York, 1945), pp. 269-271.

37. R. C. Harney and F. P. Milanovich, "An Automated Photon-Counting Raman Spectrometer", to be published in August, 1975, Rev. Sci. Instrum.

38. E. D. Reed, Multiphonon Relaxation of Excited States of Rare Earth Ions in YVO_4, $YAsO_4$, and YPO_4, Ph. D. thesis, Johns Hopkins University, Baltimore, Md. (1972).

39. W. D. Partlow and H. W. Moos, "Multiphonon Relaxation in $LaCl_3:Nd^{3+}$", Phys. Rev. 157, (1967).

40. S. K. Sharma, "Raman Study of Ferric Chloride Hexahydrate and Ferric Chloride Hexadeutrate in Crystalline, Molten, and Glassy States," J. Non-Cryst. Solids 15, 83 (1974).

41. W. F. Krupke, Optical Properties of ED-2 Laser Glass, Lawrence Livermore Laboratory Rept. UCIR-741 (1973).

42. E. Snitzer, "Glass Lasers," Appl. Opt. 5, 1487 (1966).

43. N. Bloembergen, "On the Interaction of Nuclear Spins in a Crystalline Lattice," Physica (Utr.) 15, 386 (1949).

44. E. P. Chiklis, C. S. Naiman, R. C. Folweiler, D. R. Gabbe, H. P. Jenssen, and A. Linz, "High-Efficiency Room-Temperature 2.06-um Laser Using Sensitized Ho^{3+}:YLF," Appl. Phys. Lett. 19, (1971).

45. T. Forster, "Experimental and Theoretical Investigation of the Intermolecular Transfer of Electronic Excitation Energy," Z. Naturforsch. 4a, 321 (1949).

46. D. L. Dexter, "A Theory of Sensitized Luminescence in Solids," J. Chem. Phys. 21, 836 (1953).

47. R. K. Watt, "Energy Transfer Phenomena," in Optical Properties of Ions in Solids, Proceedings of the NATO summer school at Erice, Italy, 1974. To be published by Plenum Press, 1975.

48. V. M. Kenkre and R. S. Knox, "Theory of Fast and Slow Excitation Transfer Rates," Phys. Rev. Lett. 33, 803 (1974).

49. M. Inokuti and F. Hirayama, "Influence of Energy Transfer by the Exchange Mechanism on Donor Luminescence," J. Chem. Phys. 43, 1978 (1965).

50. R. Orbach and M. Tachiki, "Phonon-Induced Ion-Ion Coupling in Paramagnetic Salts," Phys. Rev. 158, 524 (1967).

51. R. G. DeLosh and W. J. C. Grant, "Electronic Energy Transfer via Virtual-Phonon Processes," Phys. Rev. B 1, 1754 (1970).

52. J. Chrysochoos, "Nature of the Interaction Forces Associated with the Concentration Fluorescence Quenching of Nd^{3+} in Silicate Glasses," J. Chem. Phys. 61, 4596 (1974).

53. K. B. Eisenthal and S. Siegel, "Influence of Resonance Transfer on Luminescence Decay," J. Chem. Phys. 41, 652 (1964).

54. M. V. Artamonova, Ch. M. Briskina, A. I. Burshtein, L. D. Zusman, and A. G. Skleznev, "Time Variation of Nd^{3+} Ion Luminescence and an Estimation of Electron Excitation Migration Along the Ions in Glass," Sov. Phys. JETP 35, 457 (1972).
S. I. Golubov and Yu. V. Konobeev, "Effects of Diffusion on Energy Transfer by Resonance in Solids," Phys. Status Solidi B 56, 69 (1973).

55. W. M. Yen, S. S. Sussman, J. A. Paisner, and M. J. Weber, Fluorescence Line Narrowing and Energy Migration in Upconverted Transitions; Eu^{3+} Glass, Lawrence Livermore Laboratory, Rept. UCRL-76481 (1975), to be published in Phys. Rev. Lett.

56. W. J. C. Grant, "Role of Rate Equations in the Theory of Luminescent Energy Transfer," Phys. Rev. B 4, 648 (1971).

57. M. Yokota and O. Tanimoto, "Effects of Diffusion on Energy Transfer by Resonance," J. Phys. Soc. Jap. 22, 779 (1967).

58. M. J. Weber, "Luminescence Decay by Energy Migration and Transfer: Observation of Diffusion-Limited Relaxation," Phys. Rev. B 4, 2932 (1971).
R. K. Watts and H. J. Richter, "Diffusion and Transfer of Optical Excitation in YF_3:Yb,Ho" Phys. Rev. B 6, 1584 (1972).

59. G. E. Peterson and P. M. Bridenbaugh, "Study of Relaxation Processes in Nd Using Pulsed Excitation," J. Opt. Soc. Am. 54, 644 (1964).

60. R. D. Maurer, "Nd^{3+} Fluorescence and Stimulated Emission in Oxide Glasses," Proceedings of the Symposium on Optical Lasers, J., Fox Ed. (Polytechnic Press, Brooklyn, N. Y., 1963), pp. 435-447.

61. J. A. Paisner, private communication.

62. S. L. Kraevskii, Yu. P. Rudnitskii, and E. I. Sverchkov, "nonradiative Energy Transfer in Phosphate Glasses Activated with Rare Earth Ions," Opt. Spectrosc. 36, 662 (1974).

63. S. L. S. Jacoby, J. S. Kowalik, and J. T. Pizzo, Iterative Methods for Nonlinear Optimization Problems (Prentice-Hall, Inc., Englewood Cliffs, N. J., 1972), pp. 79-83.

64. J. B. Trenholme, Laser-Fusion Program Semiannual Report - July-December 1973, Lawrence Livermore Laboratory Rpt. UCRL-50021-73-2, p. 45.

65. W. F. Hagen, Laser-Fusion Program Semiannual Report - July-December 1973, Larence Livermore Laboratory Rept. UCRL-50021-73-2, pp. 15-16.

66. C. F. Rapp, ED-2 and ED-8 Laser Glass Characterization and Optimization, Owens-Illinois Co. Technical Report, March 29, 1974.

67. C. F. Rapp, Solarization and Ce^{3+} Sensitization Studies on the ED-2 Laser Glass, Owens-Illinois Co. Technical Report, October 30, 1974.

68. J. P. Markiewicz and J. L. Emmett, "Design of Flashlamp Driving Circuits," IEEE J. Quantum Electron. QE-2, 707 (1966).